ISSN: 2408-2384 (Online)
ISSN: 1686-5456 (Print)

Environment and Natural Resources Journal

Volume 19, Number 6, November-December 2021

Environment and Natural Resources Journal (EnNRJ)
Volume 19, Number 6, November - December 2021 ISSN: 1686-5456 (Print)
ISSN: 2408-2384 (Online)

AIMS AND SCOPE

The Environment and Natural Resources Journal is a peer-reviewed journal, which provides insight scientific knowledge into the diverse dimensions of integrated environmental and natural resource management. The journal aims to provide a platform for exchange and distribution of the knowledge and cutting-edge research in the fields of environmental science and natural resource management to academicians, scientists and researchers. The journal accepts a varied array of manuscripts on all aspects of environmental science and natural resource management. The journal scope covers the integration of multidisciplinary sciences for prevention, control, treatment, environmental clean-up and restoration. The study of the existing or emerging problems of environment and natural resources in the region of Southeast Asia and the creation of novel knowledge and/or recommendations of mitigation measures for sustainable development policies are emphasized.

The subject areas are diverse, but specific topics of interest include:

- Biodiversity
- Climate change
- Detection and monitoring of polluted sources e.g., industry, mining
- Disaster e.g., forest fire, flooding, earthquake, tsunami, or tidal wave
- Ecological/Environmental modelling
- Emerging contaminants/hazardous wastes investigation and remediation
- Environmental dynamics e.g., coastal erosion, sea level rise
- Environmental assessment tools, policy and management e.g., GIS, remote sensing, Environmental Management System (EMS)
- Environmental pollution and other novel solutions to pollution
- Remediation technology of contaminated environments
- Transboundary pollution
- Waste and wastewater treatments and disposal technology

Schedule
Environment and Natural Resources Journal (EnNRJ) is published 6 issues per year in January-February, March-April, May-June, July-August, September-October, and November-December.

Publication Fees
There is no cost of the article-processing and publication.

Ethics in publishing
EnNRJ follows closely a set of guidelines and recommendations published by Committee on Publication Ethics (COPE).

Environment and Natural Resources Journal (EnNRJ)

Volume 19, Number 6, November - December 2021
ISSN: 1686-5456 (Print)
ISSN: 2408-2384 (Online)

Editorial Office Address
Research Management and Administration Section,
Faculty of Environment and Resource Studies, Mahidol University
999, Phutthamonthon Sai 4 Road, Salaya, Phutthamonthon, Nakhon Pathom, Thailand, 73170
Phone +662 441 5000 ext. 2108 Fax. +662 441 9509-10
Website: https://ph02.tci-thaijo.org/index.php/ennrj/index
E-mail: ennrjournal@gmail.com

Environment and Natural Resources Journal (EnNRJ)

Volume 19, Number 6, November - December 2021 ISSN: 1686-5456 (Print)
ISSN: 2408-2384 (Online)

CONTENT

Environment and Natural Resources Journal 2021; 19(6): 427-434

The Removal of Heavy Metals from the Leachate of Aged Landfill: The Application of the Fenton Process and Nanosilica Absorbent

Kamran Taghavi, Dariush Naghipour, Seyed Davoud Ashrafi, and Malihe Salehi*

Department of Environmental Health Engineering, School of Health, Guilan University of Medical Sciences, Rasht, Iran

ARTICLE INFO

Received: 31 Mar 2021
Received in revised: 23 Jun 2021
Accepted: 28 Jun 2021
Published online: 5 Aug 2021
DOI: 10.32526/ennrj/19/202100051

Keywords:
Fenton process/ Heavy metals/ Leachate/ Nanosilica absorbent/ Waste

*** Corresponding author:**
E-mail: salehiml@yahoo.com

ABSTRACT

Since leachate is typically composed of numerous constituents, its management requires special attention. After the raw leachate of Saravan in Rasht (Guilan Province, Iran) was transferred to a laboratory and its specifications were determined, it was subjected to experiments by the bench-scale method. The analyses of pH and heavy metals were performed in the main and control anaerobic reactors at time zero, before precipitation, and two hours after precipitation. After the anaerobic process was over and the optimal retention time was identified in the anaerobic reactor, the removal of heavy metals was analyzed by the Fenton process and nanosilica absorbent in leachate treatment. In the primary anaerobic reactor, the highest and lowest removal rates were 59 and 39% for Ni and Cu, respectively. In the Fenton process with optimal H_2O_2/Fe^{+2} ratio, Cu and Hg showed the lowest and highest removal rates of 22.4 and 54.54%, respectively. At the optimal rate of nanosilica absorbent and the retention time of 15 min, As was removed maximally with an efficiency of 38% and Cu was removed minimally. The results revealed that the integration of the anaerobic process with the Fenton process and nanosilica absorbent was very effective in removing heavy metals from the aged landfill leachate.

1. INTRODUCTION

The growth of industries and the development of technology over the past few decades have increased the production of solid waste (Sheng and Chih, 2000). There are various ways to dispose or use municipal waste including separation, hygienic disposal, incineration, and composting. Hygienic disposal is the simplest and least expensive method of waste disposal that is most commonly used in Iran and even the world. However, hygienic disposal has a major problem - the generation of leachate, which is very harmful to health and the environment (Ghasemi and Hagalifard, 2014). The Rasht city is one of the most important cities in the north of Iran. The Rasht area is 136 km^2 and generates about 500 tons of waste per day (Pirouz et al., 2010). The Saravan landfill is the largest dumpsite in the north of Iran. The Saravan landfill is located in the south of Rasht city, Iran (Karimpour-Fard et al., 2020).

Biological reactors are capable of decomposing or removing the compounds of waste to the extent that the toxic compounds of the waste leachate are reduced to below the acceptable standards for drinking water or groundwater (Taghipour, 2009; Kiani et al., 2015).

After years in different cells and parts of the landfill, different phases of decomposition may be in progress. Leachate production is significantly reduced by replacing the final coating. In evaluating the long-term sustainability of a landfill, it should be considered that the coverage of the landfill will shrink. When the landfill coverage vanishes, the amount of leachate will increase even long after the landfill is closed (Taghipour, 2009).

The variations of the leachate compounds and the quantity of pollutants removed from the waste often depend on the age of a landfill expressed as the time of waste decomposition or the calculation of the time of the first leachate emergence. The landfill age obviously plays an important role in leachate characterization, which is a function of the type of waste stabilization processes. It should be emphasized that any changes in composition depend on the amount of water leaked into the landfill, too. Leachate contamination load generally maximizes in the first

Citation: Taghavi K, Naghipour D, Ashrafi SD, Salehi M. The removal of heavy metals from the leachate of aged landfill: The application of the fenton process and nanosilica absorbent. Environ. Nat. Resour. J. 2021;19(6):427-434. (https://doi.org/10.32526/ennrj/19/202100051)

years of landfill use and then, it decreases after several years. This trend generally applies to the main indices of pollution (TOC, BOD, and COD), microbial population, and major inorganic ions (heavy metals, Cl, and SO_4) (Saadatmand, 2012).

One of the most important parameters is the organic component of waste, which is biodegradable. Furthermore, the organic component of waste has a significant effect on landfill decomposition and therefore affects the quality of leachate. In the next step, the presence of substances that have a toxic or inhibitory effect on bacterial growth and disrupt the biodegradation process is of importance. Also, metals are released from the waste mass into the leachate in acidic conditions. When water seeps from decomposing wastes, both biological materials and chemicals penetrate the leachate. Since numerous components constitute the leachate, special attention should be paid to its management (Saadatmand, 2012).

Leachate treatment by Fenton can improve its quality, including odor, color, and organic matter content remarkably. Fenton is capable of greatly reducing toxic and resistant organic compounds and increasing biodegradable organic compounds. This reaction is mainly based on the generation of OH radicals by catalytic decomposition of H_2O_2 in an acidic medium. Common Fenton, electro-Fenton, and photo-Fenton processes have recently been evaluated for leachate treatment (Neyens and Baeyens, 2003).

Due to the uniform nature of its decomposition process, Fenton is a simple process and no energy is needed to activate the process, thus reducing its energy consumption. The disadvantages of the Fenton process are the high cost of its operation due to the need for chemicals and the cost of sludge disposal (Kiwi et al., 2000).

Hydrogen peroxide (H_2O_2) and iron ions (Fe^{+2}) are the two major reaction agents in the Fenton process that produce hydroxyl radicals. Therefore, the concentration of H_2O_2 is an important factor in the oxidation of organic compounds and the progress of the oxidation process, and the ratio of H_2O_2 to organic matter that is being oxidized is an important parameter. The amount of H_2O_2 use is, on the other hand, an important economic factor in the Fenton reaction and is the main reason that the Fenton process is cheaper than other advanced oxidation processes (Wang et al., 2004).

Generally, Fenton oxidation consists of four steps: pH adjustment, oxidation, neutralization, and coagulation and precipitation. Since iron salt cannot be preserved during the decomposition process, the Fenton process generates a large amount of fine coagula that contain iron hydroxide as the side product of the precipitation and should be removed from the system (Wu et al., 2004).

The removal mechanisms are the use of the coagulation-flocculation process for organic compounds, which mainly contain humic acids, the attachment of cationic metal species to some parts of it, thereby neutralizing humic substances and reducing their solubility, and the adsorption of humic substances on non-crystallized metal hydroxide precipitates (Yu et al., 2003). The combination of the Fenton oxidation with coagulation and flocculation can have a synergistic effect on the benefits of the treatment while overcoming their limitations. A limitation of this type of combined treatment is that it prefers an acidic medium for the decomposition of organic matter whereas, in the coagulation process that uses $FeCl_3$, the coagulant performs better at pH 4 to 6 (Cui et al., 2020).

2. METHODOLOGY

2.1 Anaerobic process

Raw leachate was transferred from Saravan, Rasht to a laboratory to determine its characteristics, and the assay was performed by the bench-scale method (Table 1). In Pilot 1 as the main anaerobic reactor, 2.5 L of the raw leachate was first poured into a glass container. Then, 3 g of Guigoz milk powder was added to provide the macro and microelements required for microbial reinforcement and growth in the pilot reactors, and 250 g of activated sludge (from Pegah Factory of Guilan) was added to the reactor as the nutrient (Figure 1). Analyses to determine pH and heavy metals, including Cu, As, Ni, Mn, and Hg, in the reactor containing leachate, seed, and nutrient were carried out at time zero, before precipitation, and two hours after precipitation (Eaton, 2005). The amount of heavy metals was estimated by Inductive Couple Plasma spectrometry (ICP-Qes-Spectro arcos, Germany). Instrument conditions were: ICP-QES (Spectro arcos); pump rate, 30 rpm; ICP torch injector, 2.5 mm; RF power, 1,400 w; plasma gas flow rate, 14.5/min; auxiliary gas flow rate, 0.9/min; and nebulizer gas flow rate, 0.85/min.

Five glass reactors were made with a volume of 3 L, and the same amounts of leachate, activated sludge, and milk powder were added to them. Then, the lid was closed to create anaerobic and batch conditions. Each reactor was placed on a mixer with five different retention times of 5, 10, 15, 20, 25 days. After the retention time was over, the reactor mixer was switched off and after two hours of settlement, the pH and Cu, As, Ni, Mn, and Hg were analyzed.

The experiment was carried out in Pilot 2 of the anaerobic reactor as the control reactor with the same times specified in the previous reactor and the analyses described in the previous reactor without the addition of seed or nutrient (Kheradmand et al., 2009).

Table 1. Specifications of raw waste leachate of Saravan, Rasht

pH	8.2
Copper	0.313 mg/L
Arsenic	0.033 mg/L
Nickel	0.138 mg/L
Manganese	1.48 mg/L
Mercury	0.011 mg/L

Figure 1. The primary reactors with retention times of 5-25 days

2.2 Examination of the Fenton process in the main reactor

After the anaerobic phase was over and the optimal retention time was determined in the anaerobic reactor, the Fenton process was explored. The study used an H_2O_2 solution with a weight percent of 35% and a mass volume of 1.13 and iron sulfate ($FeSO_4 \cdot 7H_2O$).

First, the leachate was poured into the container and its pH was adjusted to the desired level by sodium hydroxide and sulfuric acid (98% w/w). In the next step, Fe^{2+} was adjusted to the desired concentration by adding iron sulfate and the optimal amount of Fe^{+2} was obtained. Then, a certain volume of H_2O_2 was added and after the reaction time was passed, the optimal amount of H_2O_2 was attained. Finally, the optimal molar ratio of H_2O_2/Fe^{+2} was obtained (Figure 2). Finally, the result was given 30 min for the formed sludge to precipitate. The heavy metals Cu, As, Ni, Mn, and Hg in the supernatant were, then, measured for treatment efficiency. The jar test device was first set at 200 rpm for 30 min for rapid mixing and then at 120 rpm for 60 min for slow mixing (Kargi and Pamukoglu, 2003).

Figure 2. The study of the Fenton process in the jar test at different ratios of H_2O_2/Fe^{+2}

2.3 Efficiency of silica nanoparticles

To determine the efficiency of nanosilica absorbent in the treatment of waste leachate, the efficiency of the removal of heavy metals Cu, As, Ni, Mn, and Hg was estimated at all steps for retention times of 15-75 min as per the standard guideline (Kashitarash et al., 2012). Nanosilica is extensively used in the industry. Due to its higher specific surface area, nanosilica has higher absorbance potential than the micrometer state at the nanoscale (Tzvetkova and Nickolov, 2012). Experimental nanosilica adsorbent properties were: non-crystalline, 99.5% purity, 20-30 nm, and specific surface area 180-600 m^2/gr.

3. RESULTS AND DISCUSSION

3.1 Removal of heavy metals by the anaerobic process

The efficiency of the anaerobic reactor in removing heavy metals was investigated. According to Figures 3 and 4, the optimal retention time for heavy metal removal was 20 days in the primary and control reactors. In the primary anaerobic reactor (Figure 3), the highest removal rate was 59 and 39% for Ni and Cu and in the control reactor (Figure 4), the lowest removal rate was 48, 12, and 12% for As, Mn, and Hg, respectively. In present study, approximately, the removal percentage of all metals under aerobic bioreactor was higher than the control bioreactor.

Kheradmand et al. (2009) emphasized biological methods for the removal of heavy metals from wastes due to their advantages as they are economical and environmentally friendly. They measured the removal rate for six metals of Cu, Fe, Mg, Mn, Ni, and Zn. The anaerobic reactors showed a higher capability in removing heavy metals as they generated adequate sulfide for sequencing heavy metals. The removal rates of Cu, Fe, Mg, Mn, Ni, and Cu per unit of input at the optimal load, i.e., 2.2 g/L, were 100, 88, 0, 100, 82, and 36% in the first anaerobic digester and 15, 0, 67, 37 and 25% in the second anaerobic digester, respectively (Fouladifard et al., 2008). Qiu et al. (2016) reported that the removal efficiency of Zn, Cd, Ni, and Cr was 89.8, 100, 52 and 31.1%, respectively. High heavy metal concentrations inhibit the anaerobic co-digestion process, resulting in reduction of removal of organic substances and biogas (Nguyen et al., 2019). In a study by Kalyuzhnyi et al. (2003), the removal efficiency of Cd, Pb, Cu, Zn, and Fe was perfect with three anaerobic methods used by concomitant sequencing in the form of sulfides that were insoluble in the sludge bed. According to Bilgili et al. (2007), metals started to precipitate after reaching the methanogenesis phase and the increase in pH up to the neutral level. Our results are consistent with Kheradmand et al. (2010) and Qiu et al. (2016). The different removal rates of heavy metals at the retention time of 20 days is likely to be related to the capability of anaerobic bacteria including Sulfate-reducing bacteria and cyanobacteria in biologically converting some metal ions into sulfides (Lefebvre et al., 2007).

3.2 Data derived from the Fenton process

Based on the results concerning the effect of the Fenton process on the removal of As, Cu, Hg, Mn, and Ni from the leachate of the Saravan landfill, the highest and lowest removal rate at the optimal ratio of H_2O_2/Fe^{+2} were 22.4 and 54.54% related to Cu and Hg, respectively (Table 2).

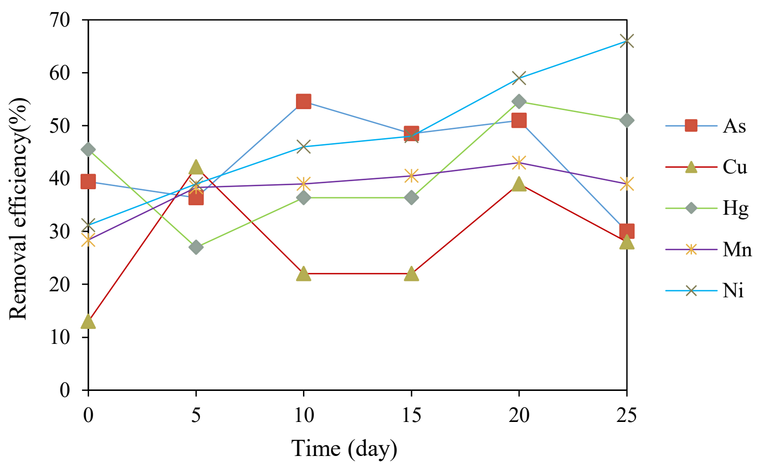

Figure 3. The removal efficiency of heavy metals As, Cu, Hg, Mn, and Ni in the primary reactor with the retention time of 5-25 days

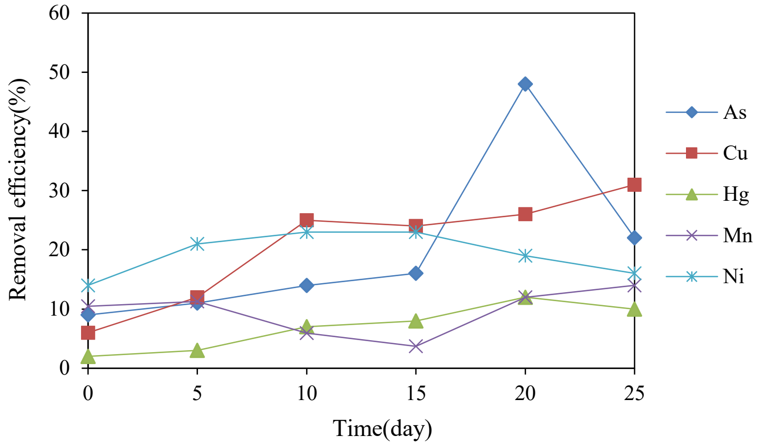

Figure 4. The removal efficiency of heavy metals As, Cu, Hg, Mn, and Ni in the control reactor with the retention time of 5-25 days

To study the effect of iron ion concentration on this process, Malakootian et al. (2011) set it at 100, 200, 400, 800, 1,600, and 3,200 mg/L. The highest Cr removal rate of 99.7%, COD of 68 %, and turbidity of 97.6 % were obtained from Fe concentrations of 1,600, 800, and 400 mg/L, respectively. An increase in Fe ion concentrations beyond these levels reduced the efficiency of Cr removal, COD, and turbidity, which may be attributed to the tendency of hydroxyl radicals to oxidative-reductive reaction with Fe^{+2} and H_2O_2. In our experiment, BOD and COD efficiency in the Fenton process was found 95.9 and 75% at Fe^{2+} rate of 1,800 mg/L and 95.3 and 83.3% at H_2O_2 rate of 4,500 mg/L, respectively. Zazouli et al. (2012) evaluated the removal of Fe, Cu, and Cr. In general, since Fe was added to all processes as a catalyzer, it was increased in both effluents and the generated sludge, which was a constraint of the Fenton-based process. The application of UV radiation reduced the Fe content of both sludge and effluent. As well, the Cu removal rate reached over 70% in the Fenton and photo-Fenton processes. The lowest removal rate of Cu was about 28% in the modified Fenton process. The removal rate of Cr was 100% in the photo-Fenton process. In a study reported by Malakootian et al. (2010), the maximum Ni removal rate was 98 % obtained under the optimal conditions, the contact time of 60 minutes, the pH of 4, the Fe^{+2} content of 1,600 mg/L, and the H_2O_2 content of 2,500 mg/L. Azhdarpoor et al. (2015) reported that when the Fenton reaction was applied in the biological sludge, the removal rate reached 75.3, 72.6, 34.5, and 65.4% for Zn, Cu, Pb, and Cd, respectively. According to Malakootian et al. (2011), the removal of heavy metals including Cr, organic matter, and turbidity by the Fenton process is affected by diverse factors such as oxidant concentration, catalyst, contaminant concentration, pH, and reaction time. These factors played a significant role in the generation of hydroxyl radical and the efficiency of the Fenton process so that higher H_2O_2 content caused the floatation of sludge and the disruption of biological purification after the Fenton process, higher Ferro-iron content increased TDS and EC of the effluent making it necessary to treat the generated sludge, and higher pH beyond the optimal level reduced the generation of hydroxyl radicals, the rapid decomposition of H_2O_2 into water and oxygen, and the precipitation of Ferro-iron with longer contact time resulting in higher treatment costs. Our results are in agreement with Azhdarpoor et al. (2015).

Table 2. The removal rate of heavy metals with the optimal H_2O_2/Fe^{+2} ratio

Metals	Mn	Ni	As	Cu	Hg
Removal rate (mg/L)	46	32	51	22.4	54.54

3.3 Data derived from nanosilica absorbent

According to the results concerning the effect of the optimal amount of nanosilica absorbent on the removal of As, Cu, Hg, Mn, and Ni from the leachate of the Saravan landfill, the highest removal efficiency at the retention time of 15 min was 38 and 25% for As and Cu, respectively and it was 58 and 31.25% for Hg and As at the pH of 3, respectively (Figure 5). When the retention time was increased to 30 min, Mn and Ni removal rates were increased slightly, but further increase in the retention time to 75 min resulted in the reduction of their removal efficiencies. At the nanosilica absorbent rate of 0.5 g/L, the retention time of 15 min, and the pH of 9, the highest and lowest removal rates were 97.36% and 10% related to Hg and Cu, respectively.

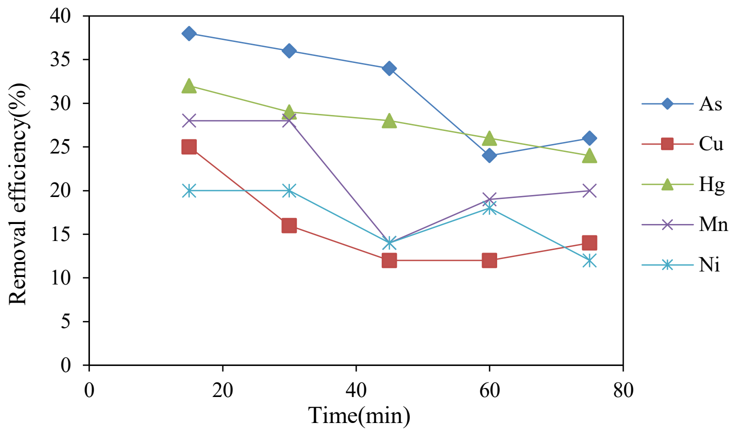

Figure 5. The removal efficiency of heavy metals As, Cu, Hg, Mn, and Ni at different retention times with 4 g/L nanosilica

In Onyeji and Aboje's (2011) study, 2 g of activated carbon entailed over 80% removal of Hg(II) and Pb(II). As well, the absorption of Hg(II), Pb(II), and Cu(II) by the activated carbon depended on the absorbent amount and initial metal concentrations. Onundi et al. (2011) reported that under laboratory conditions, nano-size composite resulted in the optimal absorption of metals at a pH of 5, an amount of 1 g/L, and a contact time of 60 min. Kiani et al. (2015) found that the application of all five coagulators reduced the concentration of residual heavy metals below the standard limits of treated effluents of Iran. The efficiency by which poly-ferric sulfate removed heavy metals and COD from the leachate with a pH of 11 reached 70-87 and 50%, respectively (Figure 6). Mojiri et al. (2015) studied three SBR reactors with 3 g/L of powdered ZELIAC, powdered activated carbon, and powdered zeolite with 90 min of settling time and 20% of leachate-to-wastewater mixing ratio. The reactor containing powdered ZELIAC exhibited an efficiency of 79.24% for Cr removal and outperformed the other reactors. Zeolites are naturally occurring silicate minerals whose capability of cation exchange is a decisive factor for the removal of heavy metals from industrial sewage (Hlihor and Gavrilescu, 2009).

Kocaoba et al. (2007) carried out several trials on the removal of heavy metals from aqueous solutions using clinoptilolite in Biga-Canakkale, Turkey. They determined the efficiency of zeolite absorbent in removing Cu(II), Cd(II), and Ni(II) from the aqueous solutions at different initial concentrations, zeolite rates, agitation speeds, and pHs. The best metals selected in this study were Cd(II)>Ni(II)>Cu(II). The rate of metal absorption to zeolite showed that the process was fast and the maximum absorption happened at the first contact time. This very slow initial absorption was subsequently stabilized and saturated in 20-30 min. Johnson et al. (2008) reported that chemically enhanced primary treatment with 40 mg/L of ferric chloride and 0.5 mg/L of polymer yielded over 200% efficiency in removing Cr, Cu, Zn, and Ni and it was 47.5% for Pb removal as compared to traditional primary treatment. Our results are consistent with Kiani et al. (2015).

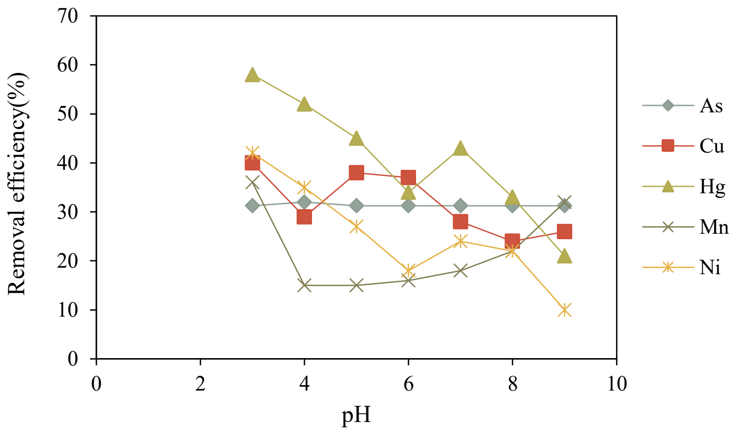

Figure 6. The removal efficiency of heavy metals As, Cu, Hg, Mn, and Ni at different pH values with 4 g/L nanosilica

Increasing coagulator dosage beyond the optimal level results in the re-stabilization of colloids (Ayeche, 2012). We found that the integration of the anaerobic process with the Fenton process and nanosilica absorbent was very effective in removing heavy metals from aged leachate (Figure 7). Feki et al. (2020) found that batch and semi-continuous anaerobic fermentations had a positive effect on the electro-Fenton (EF) pretreatment in enhancing the biogas potential and stability of the anaerobic system. They revealed that the EF process can be a more consistent solution for the improvement of waste-activated sludge anaerobic treatment.

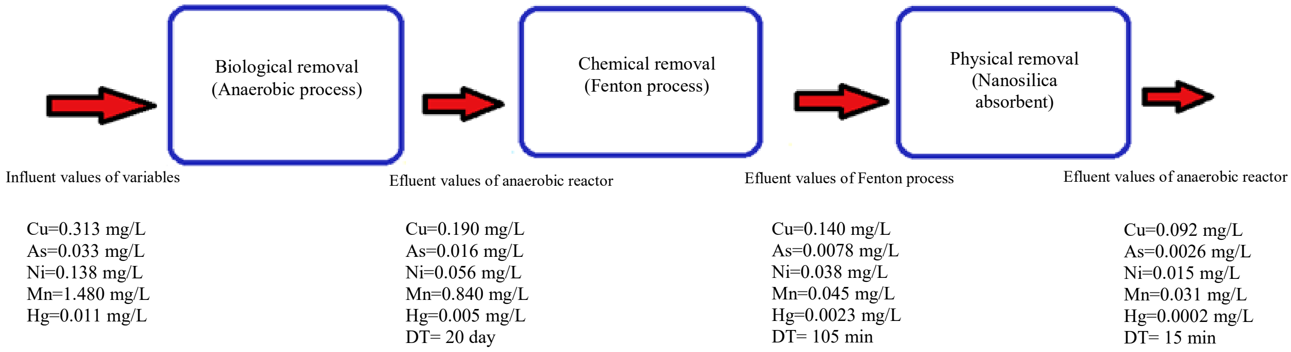

Figure 7. Steps of biological, chemical and physical removal of leachate in the primary reactor

4. CONCLUSION

The integration of the anaerobic process with the Fenton process and nanosilica absorbent was very effective in removing heavy metals from aged leachate. Since Fe was added to all processes as a catalyst, it was increased in both effluents and the generated sludge and this was a constraint of the Fenton-based process. Regarding the effect of the Fenton process on the removal of some heavy metals including As, Cu, Hg, Mn, and Ni from the experimental leachate, the utmost and minimum removal rate at the optimal ratio of H_2O_2/Fe^{+2} were 22.4 and 54.54% related to Cu and Hg, respectively. The optimal retention time for heavy metal removal was 20 days in the primary and control reactors. Since old leachates have a lot of non-biodegradable organic matter, anaerobic treatment should be used in the first stage to remove biodegradable organic matter, and in the next steps the Fenton and nanosilica adsorbent process removes non-biodegradable organic matter. Further studies are suggested to perform on the nanosorbents with higher adsorption capacity, such as carbon nanocomposites, on old leachate as well as on young leachate.

ACKNOWLEDGEMENTS

This paper was a part of faculty approved research project and supported financially by a grant (No: 96041002) from Guilan University of Medical Sciences, Rasht, Iran.

REFERENCES

Ayeche R. Treatment by coagulation-flocculation of dairy wastewater with the residual lime of national Algerian industrial gases company (NIGC-Annaba). Energy Procedia 2012;18:147-56.

Azhdarpoor A, Hoseini R, Dehghani M. Leaching Zn, Cd, Pb, and Cu from wastewater sludge using Fenton process. Journal of Health Sciences and Suroiveillance System 2015;3(4):153-9.

Bilgili MS, Demir A, Ince M, Ozkaya B. Metal concentrations of simulated aerobic and anaerobic pilot scale landfill reactors. Journal of Hazardous Materials 2007;145:186-94.

Cui H, Huang X, Yu Z, Chen P, Caoa X. Application progress of enhanced coagulation in water treatment. RSC Advances 2020;10(34):20231-44.

Eaton AD. Standard Methods for the Examination of Water and Wastewater. Washington D.C., USA: APHA-AWWA-WEF National Government Publication; 2005.

Feki E, Battimelli A, Sayadi S, Dhouib A, Khoufi S. High-rate anaerobic digestion of waste activated sludge by integration of electro-Fenton Process. Molecules 2020;25(3):626.

Fouladifard R, Azimi A, Bidhendi GN. Cadmium biosorption in a batch reactor using excess municipal sludge powder. Journal of Water and Wastewater 2008;67:2-8.

Ghasemi M, Hagalifard Z. Waste Leachate Treatment Methods and Approaches. Tehran, Iran: Khaniran; 2014.

Hlihor RM, Gavrilescu M. Removal of some environmentally relevant heavy metals using low-cost natural sorbents. Environmental Engineering and Management Journal 2009; 8(2):353-72.

Johnson PD, Girinathannair P, Ohlinger KN, Ritchie S, Teuber L, Kirby J. Enhanced removal of heavy metals in primary treatment using coagulation and flocculation. Water Environment Researchm 2008;80(5):472-9.

Kalyuzhnyi S, Gladchenko M, Epov A, Appanna V. Removal of chemical oxygen demand, nitrogen, and heavy metals using a sequenced anaerobic-aerobic treatment of landfill leachates at

10-30°C. Applied Biochemistry and Biotechnology 2003; 109:181-95.

Kargi F, Pamukoglu MY. Aerobic biological treatment of pre-treated landfill leachate by fed-batch operation. Enzyme and Microbial Technology 2003;33:588-95.

Karimpour-Fard M, Machado SL, Hasanzadehshooiili H. Energy recovery from aged waste in the Saravan dumpsite, Rasht, Iran. Journal of Environmental Engineering and Science 2020;15:61-70.

Kashitarash Z, Samadi MT, Naddafi K, Afkhami A, Rahmani A. Application of iron nanoparticles in landfill leachate treatment-case study: Hamadan landfill leachate. Iranian Journal of Environmental Health Sciences and Engineering 2012;9:361-5.

Kheradmand S, Jashni AK, Monadjemi P. Anaerobic treatment of landfill leachate: A case study of. Shiraz landfill leachate. Journal of Water and Wastewater 2009;4:90-82.

Kiani G, Mahvi A, Dehghani M. Leachate treatment of Isfahan composting plant by coagulation-flocculation process. Scientific Journal of Ilam University of Medical Sciences 2015;23(4):20-31.

Kiwi J, Lopez A, Nadtochenko V. Mechanism and kinetics of the OH-radical intervention during Fenton oxidation in the presence of a significant amount of radical scavenger (Cl^{-}_2). Environmental Science and Technology 2000;34:2162-8.

Kocaoba S, Orhan Y, Akyuz T. Kinetics and equilibrium studies of heavy metal ions removal by use of natural zeolite. Desalination 2007;214:1-10.

Lefebvre DD, Kelly D, Budd K. Biotransformation of Hg(II) by cyanobacteria. Applied and Environmental Microbiology 2007;73(1):243-9.

Malakootian M, Mansoorian HJ, Moosavi S, Daneshpazhoh M. Performance evaluation of Fenton process to remove chromium, COD and turbidity from electroplating industry waste. Journal of Water and Wastewater 2011;2:2-10.

Malakootian M, Haghighifard NJ, Ahmadian M, Loloei M. Influence of Fenton process on treatability of Kerman city solid waste leachate. Iranian Journal of Health and Environment 2010;3(2):123-34.

Mojiri A, Aziz HA, Tajuddin RM. Sulfide, phenols and chromium (VI) removal from landfill leachate and domestic wastewater by zellac, zeolite and activated carbon augmented sequencing batch reactor (SBR). Research Journal of Environmental Toxicology 2015;9(4):179-87.

Nguyen QM, Bui DC, Phuong T, Doan VH, Nguyen TN, Nguyen MV, et al. Investigation of heavy metal effects on the anaerobic co-digestion process of waste activated sludge and septic tank sludge. International Journal of Chemical Engineering 2019;5138060:1-9.

Neyens E, Baeyens J. A review of classic Fenton's peroxidation as an advanced oxidation technique. Journal Hazardous Materials 2003;98:33-50.

Onundi YB, Mamun AA, Al Khatib MF, Al Saadi MA, Suleyman AM. Heavy metals removal from synthetic wastewater by a novel nano-size composite adsorbent. International Journal of Environmental Science and Technology 2011;8(4):799-806.

Onyeji LI, Aboje AA. Removal of heavy metals from dye effluent using activated carbon produced from coconut shell. International Journal of Engineering Science and Technology 2011;3:8238-46.

Pirouz B, Razdar B, Bagherzadeh A, Kavianpour M. Improvement and treatment of Rasht city waste landfill within Saravan forest. Proceedings of the 4th Conference and Exhibition on Environmental Engineering; 2010 Nov 1; Tehran, Iran; 2010.

Qiu A, Cai Q, Zhao Y, Guo Y, Zhao L. Treatment process of landfill leachate using the toxicity assessment method. International Journal of Environmental Research and Public Health 2016;13(12):2-16.

Saadatmand A. Study of New Methods of Treatment of Landfill Leachate Waste [dissertation]. Tehran, Islamic Azad University, Science and Research Branch; 2012.

Sheng HL, Chih CC. Treatment of landfill leachate by combined electro-Fenton oxidation and sequencing batch reactor method. Water Research 2000;34(17):4243-9.

Taghipour A. Study the Efficiency of the Combined System of Coagulation and Flocculation/Ozonation in Treatment of Fresh Landfill Leachates in Tabriz city [dissertation]. Tabriz, Tabriz University of Medical Sciences; 2009.

Tzvetkova P, Nickolov R. Modified and unmodified silica gel used for heavy metal ions removal from aqueous solutions. Journal of the University of Chemical Technology and Metallurgy 2012;47:498-504.

Wang MF, El-Din MG, Smith DW. Oxidation of aged raw landfill leachate with ozone and ozone-H_2O_2: treatment efficiency and molecular size distribution analysis. Ozone Science and Engineering 2004;26:287-98.

Wu JJ, Wu CC, Ma HW, Chang CC. Treatment of landfill leachate by ozone-based advanced oxidation processes. Chemosphere 2004;54:997-1003.

Yu J, Sun DD, Tay JH. Characteristics of coagulation-flocculation of humic acid with effective performance of polymeric flocculant and inorganic coagulant. Water Science and Technology 2003;47(1):89-95.

Zazouli MA, Yousefi Z, Eslami A, Ardebilian MB. Evaluation of the different Fenton processes combined with coagulation-flocculation pretreatment in landfill leachate treatment. Journal of Toloo-e-Behdasht 2012;11(2):83-97.

Energy Use and Consumption Patterns of Maize Cultivation - A Case Study in Thailand

Sirikarn Thongmai[1], Thanakrit Neamhom[1,2,*], Withida Patthanaissaranukool[1,2], and Supawadee Polprasert[1,2]

[1]Department of Environmental Health Sciences, Faculty of Public Health, Mahidol University, Rajvithi Road, Bangkok 10400, Thailand
[2]Center of Excellence on Environmental Health and Toxicology (EHT), Bangkok 10400, Thailand

ARTICLE INFO

Received: 15 May 2021
Received in revised: 21 Jun 2021
Accepted: 28 Jun 2021
Published online: 4 Aug 2021
DOI: 10.32526/ennrj/19/202100086

Keywords:
Energy analysis/ Net energy value/ Energy transfer efficiency/ Maize cultivation/ Thailand

*** Corresponding author:**
E-mail: Nt.thanakrit@gmail.com

ABSTRACT

This study explored energy inputs and consumption patterns to determine energy and economical indices for maize cultivation in Thailand. To assess the energy performance of four used cropping systems, namely, highland cultivation in wet season (HLWS), highland cultivation in dry season (HLDS), plains cultivation in wet season (PLWS), and plains cultivation in dry season (PLDS), data from energy consumed and produced show Net Energy Value (NEV) gains of +77.0, +106.5, +191.6, and +228.5 GJ/ha, respectively. Positive signs indicate that the required energy was less than energy produced which reveals sustainability. Use of fertilizer accounted for the major input energy in all systems, followed by fossil fuels, human labor and seeds. A cost performance analysis demonstrated PLDS production exhibited the highest profit earnings (1,365.2 USD/ha). To establish an alternative way to reduce the amount of energy consumed together with increased profit returns to farmers, the renewable energy from waste manure was used to replace dependence on chemical fertilizers. Scenarios using manure from cows, chickens, and farmyards were considered. Results showed that the use of farmyard manure created greater amounts of energy efficiency and economical return rates. Moreover, the benefits increased with increased amounts of organic material applied.

1. INTRODUCTION

In the 21st century, critical issues concerning energy have drawn the attention of the United Nations Environment Programme (UNEP, 2012). High energy need, depletion of non-renewable energy resources and unlimited negative level of local environmental topics were cited frequently in many previous studies (Demirbas, 2009; Singh et al., 2019). With currently increasing rapid development and world population, staple and non-staple foods are required to serve both human and animal needs and have created competition for land and water, and increased greenhouse gas (GHGs) emissions as well as energy consumption (Qi et al., 2018; Silalertruksa and Gheewala, 2018; Jiang et al., 2020). To meet the global requirement of food in 2050, food production needs to increase 60% to meet all population demands (FAO, 2011; van Dijk and Meijerink, 2014).

The agriculture sector is one of the main producers and consumers of energy where the operations need both direct and indirect energy including human labor, fossil fuel, electricity, fertilizers and herbicides, etc. (Elsoragaby et al., 2019a; Kosemani and Bamgboye, 2020). With the progression of agriculture, energy has become a key input for activities during the age of subsistence agriculture (Król-Badziak et al., 2021). The demand of energy in the cultivation sector has increased considerably with the need for high-yielding varieties and introduction of mechanized production practices (Canakci and Akinci, 2006). Their expansion has further resulted in significant increase in food production and energy security together with the risk of environmental contamination and economic development (Nutongkaew et al., 2019; Zhong et al., 2020). To address these issues, the link between resource consumption and agricultural activity was

Citation: Thongmai S, Neamhom T, Patthanaissaranukool W, Polprasert S. Energy use and consumption patterns of maize cultivation – A case study in Thailand. Environ. Nat. Resour. J. 2021;19(6):435-448. (https://doi.org/10.32526/ennrj/19/202100086)

analyzed. Several studies have concerned environmental problems in agricultural areas during the last decade such as loss of biodiversity and pollution in the soil and aquatic media by nitrogen and phosphorus fertilizers (Nemecek et al., 2011; Yousefi et al., 2014). However, developing energy efficient agricultural production systems with lower energy input compared with the output has been recommended from the Thai government by adopting the 4th Thai National Economic and Social Development Plan together with creating equilibrium among production, environmental, and economic dimensions to achieve the sustainable development goals (Dalgaard et al., 2001; Esengun et al., 2007; Manzone and Calvo, 2016; Singh et al., 2019).

Two evaluation methods for energy use in agricultural production system are economic analysis of energy and input-output analysis of energy use (Kusek et al., 2016; Lal et al., 2019; Elsoragaby et al., 2019b). Lately, energy input-output analysis has been widely used to investigate efficiency and environmental performance which can be applied to energy management in production systems. It can be used as the first step to identify how benefits can be obtained and further show methods to minimize energy input and increase productivity (Mohammadi et al., 2008; Mohammadi et al., 2010). Energy analysis has become an important issue and a reliable approach that can provide reasonable opportunities for planners and policy makers to determine the interactions between energy use and efficiency (Ozkan et al., 2004; Hatirli et al., 2006; Yousefi et al., 2014).

Thailand has 51.3 million hectares of land of which 41% is under cultivation of various crops (OAE, 2020). Maize (*Zea mays* L.) is one of the most important crops in tropical climatic zone plantations including Thailand (Gong et al., 2015). In 2019/2020, their total production of 4.54 million tons in a cultivation area of 1.13 million hectares proved important for both food and feed (OAE, 2021). Maize is valued as the fifth most important economic crops after rice, cassava, sugarcane, and rubber in Thailand. Its demand increased by 3.6% from previous years due to the expanding livestock industry corresponding to the increased demand for maize in animal feed. It occupies 33% of Thai upland rainfed farmlands after the rainy season with a portion of in total and debuts in paddy rice fields in the dry season in recent years from the promotion of many governmental projects (Supasri et al., 2020). To date, differences in production areas may pose varying management performances for both resource use and energy efficiency. The diversity renders difficulty in decision making and appears attractive to researchers. Therefore, several studies conducted in Thailand have concentrated on energy efficiency in field crop production such as sugarcane, tapioca, para rubber, paddy rice, etc., to improve sustainability and find strategies to minimize environmental problems (Gajaseni, 1995; Demircan et al., 2006; Neamhom et al., 2016; Silalertruksa and Gheewala, 2018; Jaroenkietkajorn and Gheewala, 2020; Prasara-A and Gheewala, 2021).

Because of the few energy analysis studies concerning maize farming in Thailand, this study aimed to determine energy input and consumption patterns of different cultivation systems of maize in Thailand. The assessment of energy consumption for maize cultivation is required to understand its existing operations and identify alternative approaches to reduce energy requirements. It will help to increase production, productivity, and profitable returns contributing to the Thai economy, and make maize production systems sustainable.

2. METHODOLOGY

2.1 Scope of study and system boundary

The energy requirements and performance of energy indicators were evaluated using energy and resource materials consumed and produced in the cultivation of maize for the animal feed industry. Figure 1 presents a schematic flow diagram of overall maize cultivation practices in Thailand divided into eight basic steps. The activity occurs by using resources and materials applied in the field including chemical fertilizers, herbicides and pesticides and fossil fuel energy. In general, maize is grown mostly in rainfed upland areas divided in two seasonal crops which are crop planted from May to September and planted from August to December (MCC, 1999; Ekasingh et al., 2004). Currently, the practices of farmers contributing to increased production of maize and reducing paddy rice cultivated during the dry season (March to July) have become common due to the lack of water and their local market price. Four maize cultivation systems were classified based on the location and growing season of the crop. These four systemsare designated as: (1) highlands in wet season (HLWS); (2) highlands in dry season (HLDS); (3) plains in wet season (PLWS) and, (4) plains in dry season (PLDS). This study used the functional unit of energy or mass per unit area to express the quantity of energy and materials consumed or produced throughout these systems. The quantity per unit area (hectare; ha) is used to indicate the importance of land where photosynthesis takes place to produce maize seed as a main product and three other co-products. These include maize straw, maize husk, and maize cob. Notably, machinery energy was not accounted for in this study as their quantity was much less than those of solar energy radiation throughout the working lifetime of the machines.

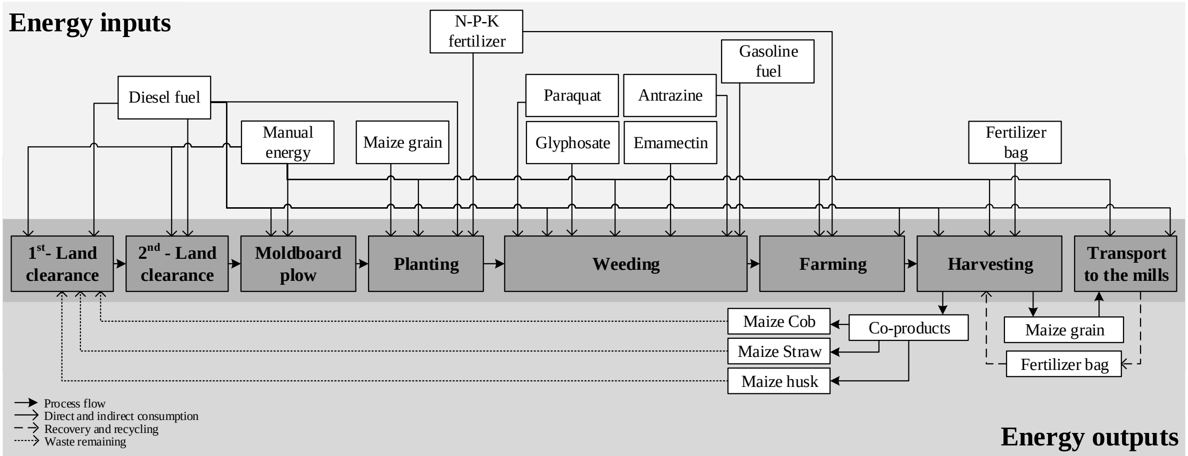

Figure 1. System boundary and pattern of energy flow in maize cultivation in Thailand

2.2 Field survey and data collection

In this study, the value of energy occurring in maize cultivation was determined using both primary and secondary data from a field survey and literature reviews, respectively. For the field survey, a face-to-face questionnaire was used to gather relevant information from 110 Thai maize farmers in HLWS, HLPS, PLWS, and PLDS systems. Sample size was calculated using a simplified formula to determine 80% confidence level and 0.2 precision (Yamane, 1967). Data were collected for one hectare maize cultivation regarding productivity, resources used, type and quantities of fossil fuel energy and fossil fuel-based materials, i.e., diesel and gasoline for machinery operation, chemical fertilizer, herbicides and pesticides for crop maintenance. Also, related human labor requirements and payroll information were obtained using the questionnaires. The energy equivalents of various energy inputs and local market prices of energy and products used in this study were sought from the literature and reliable webpages. Only energy equivalents in the maize yield collected from field trips (both product and co-products) were analyzed following the standard method for food and nutrition (FAO, 2003). Cultivation, prior to harvest, takes approximately three months beginning in October until February for the wet season and March until July for the dry season yearly. However, data variation was analyzed and presented with average values and standard deviation.

2.3 Computation of energy indicators

Data values of energy and material input and output were measured to determine the demand of energy in the production of maize and interpreted in terms of energy equivalences. In this study, the environmental input of solar radiation was considered as 168 W/m^2 over 12 h daily. Table 1 provides the energy coefficients for various materials and energy input sources.

2.3.1 Energy input-output analysis

Energy input (EI) and energy output (EO) were calculated using Equation 1 and Equation 2, respectively.

$$EI = \frac{\sum(E_s \times \epsilon_s)}{A} \qquad (1)$$

$$EO = \frac{\sum(P_{mc} \times \varepsilon_{om}) + \sum(P_{bc} \times \varepsilon_{ob})}{A} \qquad (2)$$

Where; EI is the total energy input for maize production (MJ/ha); E_s is the total amount of energy input and output components used for maize production (their functional units are presented in Table 1); ε_s is the energy equivalent coefficient for input energy forms; P_{mc} is the total production quantity of maize seed yield (kg); P_{bc} is the total production of by-products or co-products (kg); ε_{om} and ε_{ob} are the net calorific value (NCV) of maize seed yield and co-products (MJ/kg), respectively; and A is the total harvested area under cropping systems (ha).

Table 1. Energy equivalent coefficient of inputs and outputs for agricultural components

Energy inputs/productivities	Energy equivalent (MJ)	References
Organic carbon		
Diesel fuel (L)	39.6	Kosemani and Bamgboye (2020)
Gasoline fuel (L)	32.4	Kosemani and Bamgboye (2020)
Energy inputs/ Fossil-based materials		
Manual energy (h)	1.96	Šarauskis et al. (2014)
Pesticides		
i. Glyphosate (L)	454.2	Ferreira et al. (2018)
ii. Paraquat (L)	459.6	Romanelli and Milan (2005)
iii. Atrazine (L)	188.4	Ferreira et al. (2018)
iv. Emamectin (kg)	69.6	Šarauskis et al. (2014)
Chemical fertilizers (kg)		
i. Nitrogen (N)	78.1	Kosemani and Bamgboye (2020)
ii. Phosphorus (P_2O_5)	17.4	Kosemani and Bamgboye (2020)
iii. Potassium (K_2O)	13.7	Kosemani and Bamgboye (2020)
Productivities		
Maize grain (kg)	17.3	This study
Maize straw (kg)	16.3	This study
Maize cob (kg)	16.2	This study
Maize husk (kg)	16.5	This study
Organic materials		
Cow manure (kg)[a]	4.4	European Commission (2021)
Chicken manure (kg)[a]	1.7	European Commission (2021)
Farm Yard manure (kg)	0.3	Soni et al. (2018)

[a]Calculated from the net calorific value reported in (European Commission, 2021)

2.3.2 Net energy value (NEV)

NEV (MJ/ha) is the difference between the energy output and fossil fuel input required in the production processes which is calculated using Equation 3 (Dai et al., 2006; Khatiwada and Silveira, 2009; Kusek et al., 2016; Neamhom et al., 2016; Nguyen et al., 2008). When the NEV value is positive (output more than input), the products produced are said to be acceptable in terms of production efficiency.

$$NEV = EO - EI \quad (3)$$

2.3.3 Energy transfer efficiency (ETE)

ETE indicates how efficiently a crop production system is in terms of its energy output and input forms. Modified from energy use efficiency (EUE), ETE is calculated beginning with solar radiation absorbed by the earth and continues until the energy content is stored in the end-user product (Neamhom et al., 2016). This ratio has been used to express the ineffectiveness of crop production systems (Kaur et al., 2021; Soni et al., 2018). It is calculated, using Equation 4.

$$ETE\ (\%) = \frac{EO}{EI} \times 100 \quad (4)$$

2.4 Net return (NR)

NR is the total profit gain to farmer in a particular cropping system. Residual income remains after all production factors mentioned are paid off to calculate this value (Soni et al., 2018). It considers the farm labor cost, management cost, other resources used for operation and production of the crops which is calculated using Equation 5. Where gross income is calculated by multiplying the total crop produced by its local market price, and total input cost represents all the cost fixed to produce the crop.

$$NR = \text{Gross income} - \text{Total input cost} \quad (5)$$

3. RESULTS AND DISCUSSION

3.1 Overall maize cultivation systems

Data information concerning energy and materials consumed in the field were collected from four different maize cultivation systems in Thailand. Farmers always plant maize in two seasons annually. The first crop in is planted in March and planting the second crop starts in October. To produce maize seed products, the tillage for land clearance, aimed to plow crop residues under the soil, is first operated using tractors with 3, 4, or 7-disk plows. Following the plowing using a moldboard, the soil is tilled using a 7-disk plow tractor. The planting process then employs various methods, e.g., manual and tractor-mounted seeder, which use a seed ratio of 17.6 to 23.3 kg/ha. During the cultivation process, farmers use four types of synthetic herbicides and pesticide, Emamectin, Glyphosate, Paraquat, and Atrazine, to control insects and maize diseases. Fertilizers are also applied on land using different formulae, e.g., 15-15-15, 16-20-0, and 46-0-0. Three months after planting, maize is fully mature for harvesting. Maize is harvested manually or using a seed milling machine, depending on land terrain. Not only is the maize seed produced, other co-products are also generated, i.e., maize straw, maize husk, and maize cob. Figure 2 shows the production rate of product and co-products in maize cultivation systems in Thailand. After harvesting, the maize seed yield is transported by tractor or truck to a mill located within a 10-km radius. Meanwhile, the co-products remain on the farm for the next crop planting.

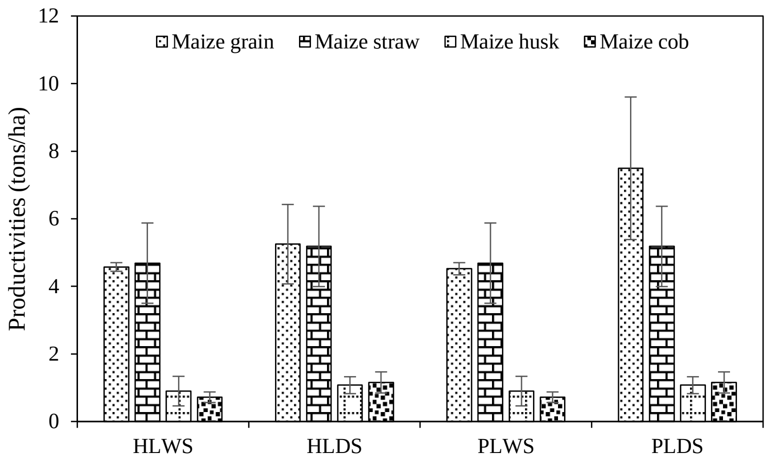

Figure 2. Yield of product and co-products in maize productions

The average main productivity of maize cultivation ranges from 4.5 to 7.5 tons per hectare and is highest in the PLDS system (7.5±2.1 tons/ha). To achieve these yields, four types and quantities of resources are consumed and applied to the maize field. First, maize farmers apply chemical fertilizers around three times per crop, first at the time of maize seed planting and then approximately 30 and 60 days later. As presented in Figure 3, the quantities of chemicals are classified ranging from 128.1 to 245.7 kg/ha for nitrogen, 31.3 to 121.9 kg/ha for phosphorus, and 31.3 to 107.5 kg/ha for potassium. Importantly, the cultivations in dry season during March consumed more overall nutrients (461.0 kg/ha for PLDS and 425.1 kg/ha for HLDS) compared with 342.7 kg/ha for HLWS and 201.9 kg/ha for PLWS. Second, diesel fuel is consumed at 66.5, 108.6, 133.8, and 204.3 L/ha for HLWS, HLDS, PLWS, and PLDS, respectively. Details of diesel fuel consumed for production processes are shown in Figure 4. Notably, around 30% of total diesel fuel consumption was applied to operate water pumping machines for plains cultivation (both in wet and dry seasons). Third, gasoline fuel for lawn mower machine operation was consumed at a rate of 40 L/ha in HLWS and PLWS while 6.3 and was for 14.1 L/ha for HLDS and PLDS, respectively. Lastly, concerning herbicide and pesticide consumption, farmers spray pre-emergence herbicide after planting and perform mechanical weeding at 7 and 45 days later.

3.2 Energy inputs

As tabulated in Table 2, summarized data were calculated from existing operations. The high land cultivation systems, in wet and dry season, required an average energy input of 32.6 GJ/ha and 32.9 GJ/ha, respectively. However, plains cultivations showed a variation of 37.2 GJ/ha in dry season and 22.1 GJ/ha during the wet season, a difference of 32%. The results showed that fertilizer had the greatest input in all systems, comprising approximately 48.5, 66.3, 52.9, and 68.9% of totals for HLWS, HLDS, PLWS, and PLDS, respectively. Nitrogen was the largest component in all fertilizer input followed by phosphorus and potash. When compared with other studies (Banaeian and Zangeneh, 2011; Kosemani and Bamgboye, 2020; Šarauskis et al., 2014), these values show similar movements due to the mindset of farmers who believe that the productivity yield depended on the direct consumption of fertilizers (Soni et al., 2018). Diesel fuel was the second ranked contributor due to its requirement in all steps of cultivation. For highlands, higher fuel consumption could be attributed to the operation of machinery for land preparation and harvesting. However, in plains, fuel was consumed significantly to pump water, around 32% and 35% of the total for WS and DS, respectively. The findings of this study were in line with those of other studies in maize cultivation reporting fertilizers and diesel fuel were the two main contributors in terms of energy input (Kaur et al., 2021; Manzone and Calvo, 2016; Yousefi et al., 2014). Energy from human work, expressed for each operation, is summarized in Table 2. The operations with the highest manpower consumption were in planting and fertilizer spreading during planting, weeding, and harvesting, respectively.

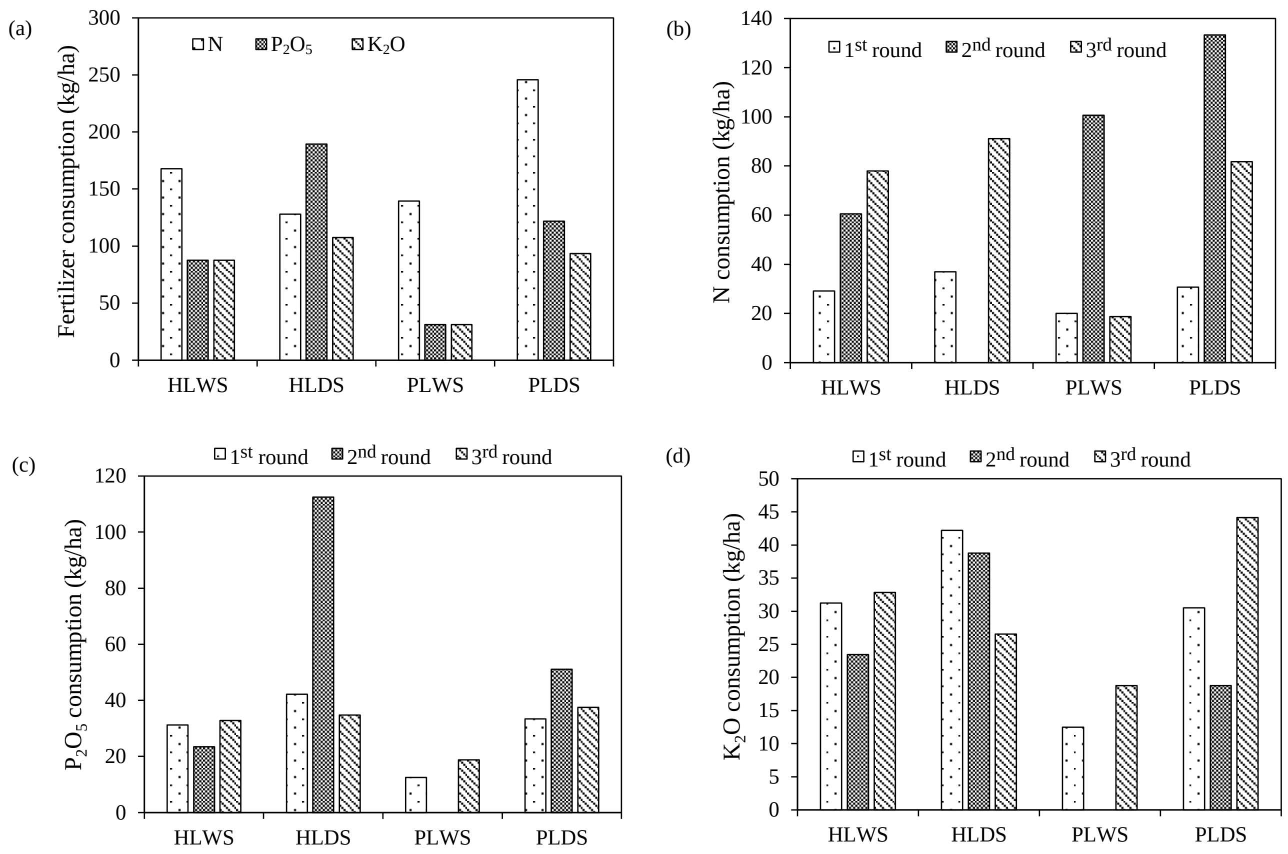

Figure 3. Quantity of fertilizer consumption in maize cultivation systems; (a) Total; (b) N fertilizer; (c) P_2O_5 fertilizer; (d) K_2O fertilizer

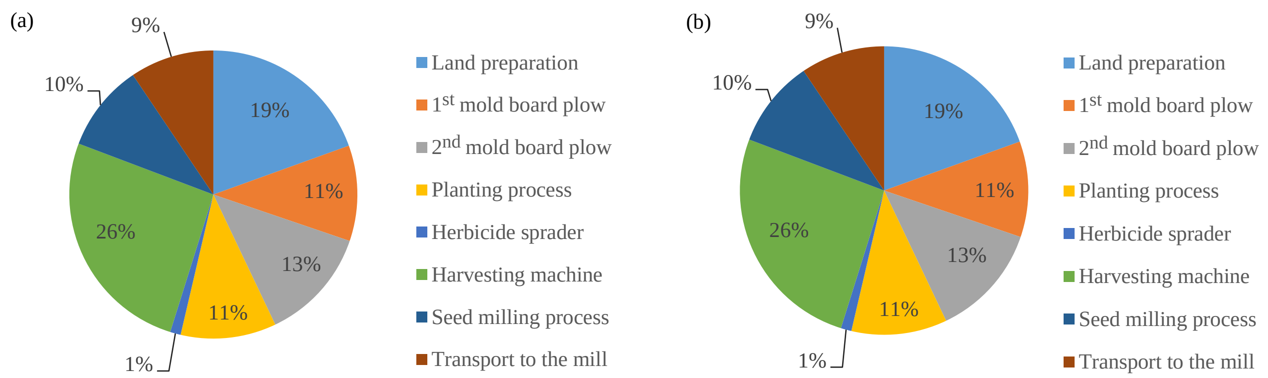

Figure 4. Diesel fuel consumption (L/ha) in maize cultivation systems; (a) HLWS; (b) HLDS; (c) PLWS; (d) PLDS

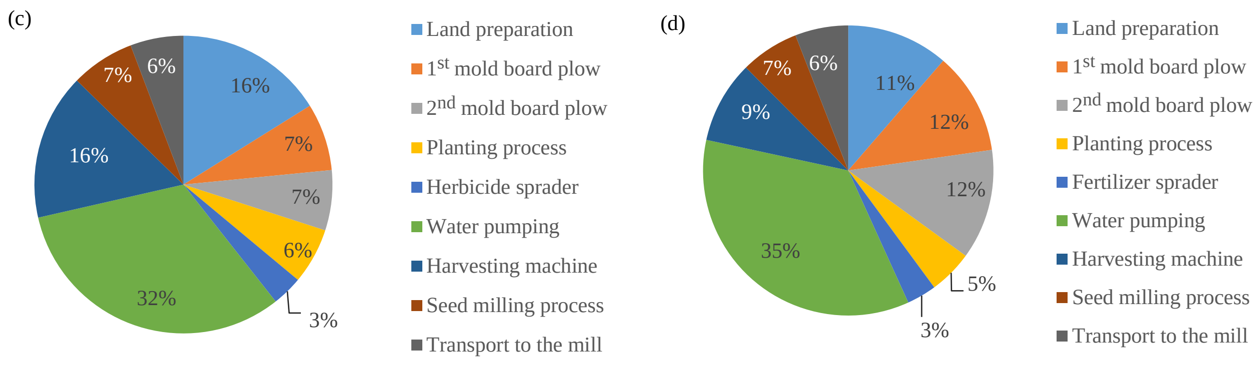

Figure 4. Diesel fuel consumption (L/ha) in maize cultivation systems; (a) HLWS; (b) HLDS; (c) PLWS; (d) PLDS (cont.)

Table 2. Energy and energy indicators analyses for four maize production systems

Resources/Productivities	Unit	Energy (MJ/ha)			
		HLWS	HLDS	PLWS	PLDS
1st Land clearance (1)					
Diesel (for plowing machine)	L	922.8±53.1	838.0±58.4	853.9±306.1	918.3±522.8
Manual energy	h	24.5±6.3	19.4±13.4	45.9±48.6	58.0±29.5
2nd Land clearance (2)					
Diesel (for tractor)	L	466.7±178.7	431.3±111.9	387.8±62.3	921.0±269.8
Manual energy	h	24.5±6.3	16.1±11.5	45.9±8.6	55.4±21.7
Moldboard plow (3)					
Diesel (for tractor)	L	618.8±525.0	546.2±153.4	346.5±0.0	993.7±347.0
Manual energy	h	17.2±3.5	18.6±12.5	45.9±8.6	54.9±27.9
Planting (4)					
Maize seed	kg	269.1±53.1	326.1±58.4	318.0±45.1	356.4±73.9
Diesel (for tractor)	L	-	-	321.8±35.0	396.6±126.4
Diesel (for fertilizer spreader)	L	-	-	-	89.1±0.0
Manual energy (for planting)	h	499.8±0.0	18.6±12.2	45.9±8.6	427.7±405.3
Nitrogen fertilizer	kg	2,277.9±1,491.2	2,889.3±1,081.3	1,562.0±390.5	2,395.9±1,054.0
Phosphorus fertilizer	kg	543.8±108.8	734.1±276.4	217.5±0.0	580.3±287.1
Potassium fertilizer	kg	428.1±121.1	578.0±135.4	171.3±0.0	417.9±206.7
Manual energy (for fertilizer spreader)	h	18.0±2.8	18.6±12.2	57.9±51.7	427.7±405.3
Weeding (5)					
Diesel (for herbicide spreader)	L	-	51.2±10.0	175.7±0.0	-
Gasoline (for lawn mower)	L	1,296.0±0.0	202.5±0.0	1,296.0±0.0	456.4±140.1
Emamectin	kg	391.5±130.5	173.8±57.2	229.6±64.6	443.2±123.5
Paraquat	L	4,883.3±3,745.3	2,528.8±691.2	1,532.0±663.4	2,238.1±503.9
Glyphosate	L	5,109.8±2,007.3	2,838.8±0.0	-	1,520.2±442.4
Antrazine	L	-	-	459.2±23.2	52.6±27.9
Manual energy	h	179.3±27.4	114.1±62.2	209.4±157.7	364.7±174.8
Farming (6)					
Diesel (for fertilizer spreader)	L	-	-	-	178.2±0.0
Diesel (for water pumping)	L	-	-	1,697.9±0.0	2,846.3±808.5
Nitrogen fertilizer	kg	10,820.1±7,119.3	15,903.4±6,879.3	9,323.2±4,763.2	16,815.1±7,457.3
Phosphorus fertilizer	kg	978.8±0.0	1,280.1±1,039.6	217.5±0.0	1,540.8±513.7
Potassium fertilizer	kg	770.6±0.0	385.3±172.8	171.3±0.0	861.6±476.4
Manual energy	h	187.8±62.7	40.5±25.5	237.9±2.3	183.7±82.7

Table 2. Energy and energy indicators analyses for four maize production systems (cont.)

Resources/Productivities	Unit	Energy (MJ/ha)			
		HLWS	HLDS	PLWS	PLDS
Harvesting (7)					
Diesel (for seed milling tractor)	L	366.3±0.0	422.1±96.3	366.3±0.0	527.5±131.8
Diesel (for small tractor)	L	-	1,113.8±0.0	841.5±373.7	742.5±0.0
Manual energy	h	1,176.0±0.0	21.0±12.8	294.0±0.0	294.0±0.0
Transport to the mills (8)					
Diesel (for truck truck)	L	307.2±8.6	481.6±212.9	305.3±14.3	479.0±137.7
Manual energy	h	24.5±6.3	21.4±14.0	57.9±51.7	56.0±27.2
Productivities (9)					
Maize grain	ton	79,065.7±2,205.8	90,738.1±20,329.6	78,165.2±3,119.5	129,572.5±36,470.3
Maize straw	ton	76,593.8±19,403.8	84,661.6±19,403.8	76,593.8±19,403.8	84,661.6±19,403.8
Maize husk	ton	14,886.0±7,236.3	17,780.5±4,135.0	14,886.0±7,236.3	17,780.5±4,135.0
Maize cob	ton	11,658.1±2,534.4	18,754.4±5,068.8	11,658.1±2,534.4	18,754.4±5,068.8
Total energy input (-) [(1)+(2)+(3)+(4)+(5)+(6)+(7)+(8)]		32,584.2	32,849.5	22,047.4	37,177.1
Total energy output (+) [(9)]		182,203.6	211,934.6	181,303.1	250,769.0
Net Energy Value (NEV)[a]	MJ/ha	77,043.4	106,509.1	86,679.7	141,015.9
	GJ/ha	77.0	106.5	86.7	141.0
Energy Transfer Efficiency (ETE)[b]		1.73	2.01	1.92	2.29

[a]Positive sign (+) means gain the energy from production process, Negative sign (-) means loss of energy.
[b]Calculated from the input starting from solar radiation (168 W/m^2, 12 h/day) through output as product and co-products.

3.3 Energy outputs of system

Total energy output from maize cultivation systems in Thailand are reported in Table 2. According to the product and co-products presented in Figure 2, energy output was computed from maize grain as a main product and co-products including maize straw, maize husk, and maize cob. In wet season, the reported values were 182.2 and 181.3 GJ/ha for HLWS and PLWS, respectively, whereas the values for HLDS and PLDS were higher. A greater amount of grain and straw products during dry season led to output energy results in more than 212.0 GJ/ha and peaked at 250.8 GJ/ha in PLDS. It could be said that production of maize and co-products cultivated during dry season (both in highlands and plains) had higher energy output. This outcome was significantly ($p<0.05$) greater to others. One reason related to this result was a significantly higher energy use resulting in greater grain yield in dry season. Moreover, different levels of climatic factors, geographical locations, and required water were also contributed. The results reported in studies of paddy rice, wheat, and other economic crops were similar to the results obtained in this study (Neamhom et al., 2016; Patthanaissaranukool and Polprasert, 2016; Soni et al., 2018).

3.4 Energy indicators

From existing maize cultivation, as shown in Figure 5, the four defined systems indicated positive values of 77.0, 106.5, 86.7, and 141.0 GJ/ha for HLWS, HLDS, PLWS, and PLDS, respectively. The positive sign showed an energy output greater than that of fossil fuel energy required in the production process. Lower values in wet season may have resulted from the loss of energy especially nutrients and crop residues (Khonpikul et al., 2017). Rainfall, pests, and the type of terrain make it difficult to grow, harvest, and collect crop residue. The results of the net energy value assessment were consistent with the findings of other studies as presented in Table 3. Grassini and Cassman (2012) reported higher NEV performance (159.0 GJ/ha) in US maize systems because of greater fertilizer input, higher yield, and more appropriate irrigated systems. Similar to the study in Germany by Felten et al. (2013) rounded net energy production amounted to 91.0 GJ/ha due to their high energy yields. Therefore, in most cases, beneficial co-products of straw, husk, and cob were absent from the computation resulting in a lower NEV.

By applying Equation 4 using the different net inputs of fossil fuel and fossil-based resources energy and sun energy radiated to the earth's mantle (168W/m^2, 12 h/d) (Masters, 1998) and the energy output of maize grain and co-products produced, ETE was found to be 1.73, 2.01, 1.92, and 2.29 for HLWS, HLDS, PLWS, and PLDS, respectively. As shown in Table 3, these values were relatively low compared with other related studied. This index for maize cultivation systems in different regions of Thailand was higher due to the high output energy obtained. The low energy efficiency of maize productions in Thailand was due to high energy consumption from activity and low product output.

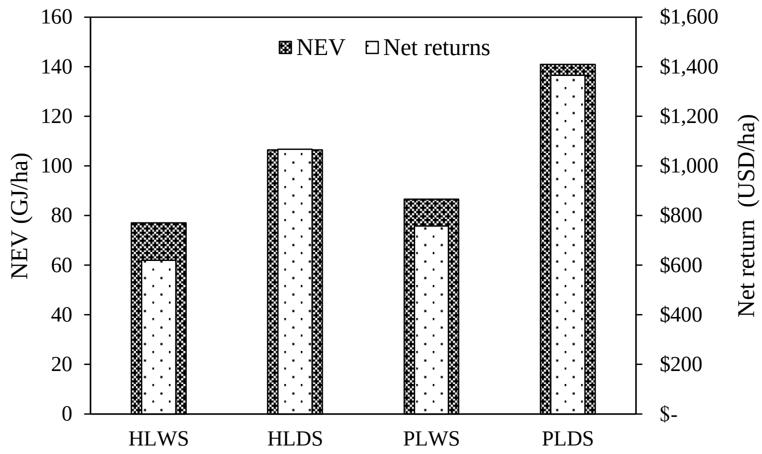

Figure 5. Net energy and cost performance in four different maize cultivation systems

Table 3. Comparison of Net Energy Value and ETE in maize cultivations

References	Country	NEV[a] (GJ/ha)	ETE (%)	Remarks
Lorzadeh et al. (2011)	Iran	+18.8	1.48	Not include co-products
Felten et al. (2013)	Germany	+91.0	5.5	High product and co-products
Akdemir et al. (2012)	Turkey	-	0.76	Not include co-products
Grassini and Cassman (2012)	USA	+159.0	6.6	-
Memon et al. (2015)	Pakistan	+52.0	5.2	Moldboard plow practice
		+47.0	5.1	Cultivator practice
		+31.8	4.1	Zero tillage practice
Chilur and Yadachi (2017)	India	+68.1	5.1	-
This study	Thailand	+77.0	1.73	HLWS
		+106.5	2.01	HLDS
		+86.7	1.92	PLWS
		+141.0	2.29	PLDS

[a]Positive sign (+) indicates energy gain; negative sign (-) indicates energy loss from production processes.

3.5 Economic return

From an economic point of view, the net return to the farmers was obtained from the difference between gross income and total input cost. At the time of this study, the current local market prices for maize grain and maize cob were found to be 0.3 USD/kg grain and 0.01 USD/kg cob. As summarized in Table 4, all cultivation systems were profitable operations in the studied region. PLDS had the highest cost of production (924.3±393.1 USD/ha), followed in rank by HLWS (778.0±208.6 USD/ha), PLWS (623.0±206.2 USD/ha), and HLDS (541.2±168.9 USD·/ha). Added chemical fertilizers, maize seed, and labor used during farming and weeding activities contributed to higher production costs. The highest gross incomes from selling the products of maize grain and maize cob were observed from the PLDS of 2,289.4±644.2 USD/ha. In wet season planting, the total selling price was lowest compared with 1,397.2±41.0 USD/ha and 1,381.4±57.0 USD/ha for HLWS and PLWS, respectively. In terms of NR, planting in dry season offered higher returns than wet season and reached the highest returns to farmers in PLDS (1,365.2 USD/ha). According to the beneficial by-products utilization occurring in the production processes, this value was relatively low as compared to 2,107.5 USD/ha/year of the sugarcane industry (Neamhom et al., 2016), 3,574.4 USD/ha/year of the palm oil production industry (Patthanaissaranukool et al., 2013), and 3,101.4 USD/ha/season of paddy rice cultivation (Polprasert and Chaiyachet, 2007).

Table 4. Cost analysis for maize cultivation systems in Thailand

Cultivation systems	Total input cost (USD/ha)	Total selling price (USD/ha)	NR[a] (USD/ha)
HLWS	778.0±208.6	1,397.2±41.0	619.2
HLDS	541.2±168.9	1,608.5±361.2	1,067.3
PLWS	623.0±206.2	1,381.4±57.0	758.4
PLDS	924.3±393.1	2,289.4±644.2	1,365.2

[a]Positive sign indicates the cost saving, Negative value indicates that the resources cost is higher than the return values.

3.6 Simulations to reduce energy consumption

According to the criteria for energy saving in crop production and heavy consumption of agro-chemical fertilizer on maize field, sharing more than 48% of total energy inputs, 15 scenarios were established as described in the following to find the sustainable ways to produce maize grain used in the animal feed industry. In this work, they are replaced with bio-nutrients and organic residues from livestock farming. Selected materials and their nutrient components used are presented in Table 5. The scenarios were ranked from 20 to 100% replacement with organic residue materials. NEV and NR were calculated to measure how much the organic materials could help reduce energy input consumption and the returns to farmers, respectively. In terms of NEV, a positive sign indicated that the substitute could not help reduce energy input while a negative sign meant it helps reduce energy consumption. In the opposite way, a negative value of NR revealed that the gross input was higher than the incomes resulting in less return to the farmer. Figure 6 shows the net energy outcome from reduced chemical fertilizer consumption. Compared to existing operation, cow manure substitute created the higher energy requirement when the replacement ratios were more than 20%, whereas chicken and farmyard manures had a lower energy consumption movement. The resulting values of NEV and NR in the results of organic residue replacement activity for each scenario as compared with those of existing operations are summarized in Table 6. Although the use of chicken and farmyard manures exhibited lower energy requirement, only replacing of chemical fertilizer by farmyard manure could achieve the maximum returns for both energy gain and profit. Therefore, the economic benefits for implementing those approaches seem attractive for maize plantation owners and local governments to follow and encourage.

Table 5. Selected materials and nutrient components of substituted residues

Organic residues	Nitrogen (N, %)	Phosphorus (P_2O_5, %)	Potassium (K_2O, %)	References
Cow manure	1.10	1.84	0.52	Ministry of Agricultural and Cooperative (2016)
Chicken manure	2.42	6.29	2.11	Ministry of Agricultural and Cooperative (2016)
Farmyard manure	0.50	0.20	0.50	Tamil Nadu Agricultural University (2016)

Table 6. Energy reduction and cost-saving potential from chemical fertilizer replacements

Maize cultivation/scenarios	NEV[a] (GJ/ha)				NR[b] (USD/ha)			
	HLWS	HLDS	PLWS	PLDS	HLWS	HLDS	PLWS	PLDS
Existing condition	+15.8	+14.8	+11.9	+22.6	-106.1	-193.4	-61.5	-141.7
S-1: 20% Cow manure	+8.2	+16.5	+7.1	+12.1	-38.8	-81.1	-37.6	-59.6
S-2: 40% Cow manure	+16.4	+32.9	+14.1	+24.2	-77.6	-162.2	-75.2	-119.3
S-3: 60% Cow manure	+24.6	+49.4	+21.2	+36.4	-116.5	-243.3	-112.8	-178.9
S-4: 80% Cow manure	+32.8	+65.9	+28.3	+48.5	-155.3	-324.4	-150.4	-238.5
S-5: 100% Cow manure	+40.9	+82.3	+35.3	+60.6	-194.1	-405.5	-188.0	-298.2

Table 6. Energy reduction and cost-saving potential from chemical fertilizer replacements (cont.)

Maize cultivation/scenarios	NEV[a] (GJ/ha)				NR[b] (USD/ha)			
	HLWS	HLDS	PLWS	PLDS	HLWS	HLDS	PLWS	PLDS
S-6: 20% Chicken manure	-0.8	-1.5	-0.4	-1.1	-5.0	-13.6	-9.5	-10.1
S-7: 40% Chicken manure	-1.6	-3.0	-0.8	-2.1	-10.0	-27.2	-19.0	-20.1
S-8: 60% Chicken manure	-2.4	-4.4	-1.2	-3.2	-15.0	-40.8	-28.5	-30.2
S-9: 80% Chicken manure	-3.2	-5.9	-1.7	-4.3	-20.0	-54.4	-38.0	-40.3
S-10: 100% Chicken manure	-4.0	-7.4	-2.1	-5.3	-24.9	-68.0	-47.5	-50.3
S-11: 20% Farmyard manure	-1.2	-2.2	-0.7	-1.6	+14.7	+25.7	+6.9	+18.8
S-12: 40% Farmyard manure	-2.3	-4.3	-1.4	-3.1	+29.4	+51.4	+13.8	+37.6
S-13: 60% Farmyard manure	-3.5	-6.5	-2.1	-4.7	+44.2	+77.1	+20.7	+56.4
S-14: 80% Farmyard manure	-4.6	-8.7	-2.8	-6.3	+58.9	+102.8	+27.5	+75.2
S-15: 100% Farmyard manure	-5.8	-10.8	-3.5	-7.9	+73.6	+128.5	+34.4	+94.0

[a]Positive sign (+) means still consumed energy, Negative sign (-) means help reduce energy consumption.
[b]Positive sign indicates the cost saving, Negative value indicates that the resources cost is higher than the return values.

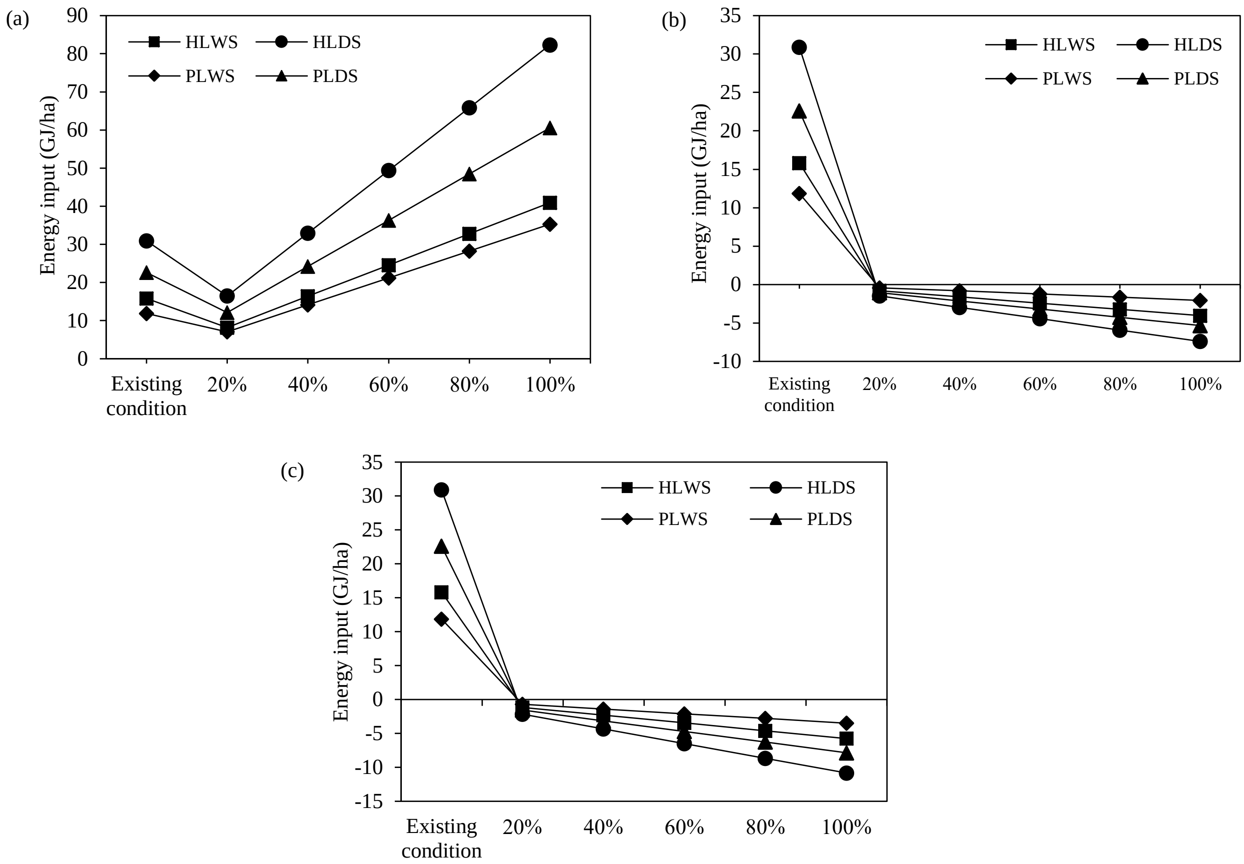

Figure 6. Methods to reduce energy consumption from organic material substitution; (a) cow manure; (b) chicken manure; (c) farmyard manure

4. CONCLUSION

The cultivations of maize fed to animal feed industry in Thailand depends on seasonal and geographical factors classified in four systems, HLWS, HLDS, PLWS, and PLDS. Regarding agricultural activity, consumption of chemical fertilizers created the highest energy input value followed by the consumption of fossil fuels for all methods. Following the concept of energy input-output analysis, the net energy value was found to be +77.0, +106.5, +191.6, and +228.5 GJ/ha, whereas ETE was computed to be 1.73, 2.01, 1.92, and 2.29%, respectively. The positive value of NEV presented a significantly energy gain from production processes. In terms of ETE, the values were quite lower than those found in previous studies because of the lack of further uses of co-products from the production processes, i.e., maize husk, straw, and cob. To determine a sustainable method to produce grain products together with lowering energy consumption, different scenarios were established. These included replacing chemical fertilizers with cow, chicken, and farmyard manures. Results showed that chicken manure and farmyard manure substitutions could achieve this goal. Although these results from chicken and farmyard manure appeared best and may achieve a lesser rate of energy input, only the use of farmyard manure provided profit returns to farmers.

Results from cost performance analysis showed that all systems produced profit returns of about 619.2 1,067.3 758.4 and 1,365.2 USD/ha for HLWS, HLDS, PLWS, and PLDS, respectively. The highest profit return was found in the PLDS system due to its huge amount of product, about 1.7 times compared with the lowest system.

ACKNOWLEDGEMENTS

This study was approved by the Ethics Committee for Research Involving Human Subjects (COA. No. MUPH 2020-163). This work was partially supported by funding from the Department of Environmental Health Sciences, Faculty of Public Health, Mahidol University. The authors would like to thank all maize farmers for the data provided to this study. Also, the authors would like to thank Mr. Thomas McManamon of Mahidol University Faculty of Public Health International Center for editing the English used in this paper.

REFERENCES

Akdemir S, Akcaoz H, Kizilay H. An analysis of energy use and input costs for maize production in Turkey. Journal of Food, Agriculture and Environment 2012;10(2):473-9.

Banaeian N, Zangeneh M. Study on energy efficiency in corn production of Iran. Energy 2011;36(8):5394-402.

Canakci M, Akinci I. Energy use pattern analyses of greenhouse vegetable production. Energy 2006;31(8-9):1243-56.

Chilur R, Yadachi S. Energy Audit of Maize Production System of Selected Villages of North Karnataka, India. International Journal of Current Microbiology and Applied Sciences 2017;6(8):3564-71.

Dai D, Hu Z, Pu G, Li H, Wang C. Energy efficiency and potentials of cassava fuel ethanol in Guangxi region of China. Energy Conversion and Management 2006;47(13-14):1686-99.

Dalgaard T, Halberg N, Porter JR. A model for fossil energy use in Danish agriculture used to compare organic and conventional farming. Agriculture, Ecosystems and Environment 2001; 87(1):51-65.

Demirbas A. Political, economic and environmental impacts of biofuels: A review. Applied Energy 2009;86(Supplement 1):108-17.

Demircan V, Ekinci K, Keener HM, Akbolat D, Ekinci C. Energy and economic analysis of sweet cherry production in Turkey: A case study from Isparta province. Energy Conversion and Management 2006;47(13-14):1761-9.

Ekasingh B, Gypmantasiri P, Thong-ngam K, Grudloyma P. Maize in Thailand: Production Systems, Constraints, and Research Priorities. Mexico: CIMMYT; 2004.

Elsoragaby S, Yahya A, Mahadi MR, Nawi NM, Mairghany M. Analysis of energy use and greenhouse gas emissions (GHG) of transplanting and broadcast seeding wetland rice cultivation. Energy 2019a;189:116160.

Elsoragaby S, Yahya A, Mahadi MR, Nawi NM, Mairghany M. Energy utilization in major crop cultivation. Energy 2019b; 173:1285-303.

Esengun K, Erdal G, Gündüz O, Erdal H. An economic analysis and energy use in stake-tomato production in Tokat province of Turkey. Renewable Energy 2007;32(11):1873-81.

European Commission. Database for the physico-chemical composition of (treated) lignocellulosic biomass, micro- and macroalgae, various feedstocks for biogas production and biochar [Internet]. 2021 [cited 2021 Jan 19]. Available from: https://phyllis.nl/.

Food and Agricuture Organization of the United Nation (FAO). “Energy-smart” food for people and climate: issue paper [Internet]. 2011 [cited 2021 Mar 6]. Available from: http://www.fao.org/sustainable-food-value-chains/library/details/en/c/266092/.

Food and Agricuture Organization of the United Nation (FAO). Food Energy-Methods of Analysis and Conversion Factors. Rome: FAO; 2003.

Felten D, Fröba N, Fries J, Emmerling C. Energy balances and greenhouse gas-mitigation potentials of bioenergy cropping systems (Miscanthus, rapeseed, and maize) based on farming conditions in Western Germany. Renewable Energy 2013; 55:160-74.

Ferreira TA, Ferreira SC, Barbosa JA, Volpato CES, Ferreira RC, da Silva MJ, Barbosa LM. Energy balance of irrigated maize silage. Ciencia Rural 2018;48(5):4-10.

Gong F, Wu X, Zhang H, Chen Y, Wang W. Making better maize plants for sustainable grain production in a changing climate. Frontiers in Plant Science 2015;6:1-6.

Grassini P, Cassman KG. High-yield maize with large net energy yield and small global warming intensity. Proceedings of the National Academy of Sciences of the United States of America 2012;109(10):4021.

Hatirli SA, Ozkan B, Fert C. Energy inputs and crop yield relationship in greenhouse tomato production. Renewable Energy 2006;31(4):427-38.

Jaroenkietkajorn U, Gheewala SH. Interlinkage between water-energy-food for oil palm cultivation in Thailand. Sustainable Production and Consumption 2020;22:205-17.

Jiang Z, Lin J, Liu Y, Mo C, Yang J. Double paddy rice conversion to maize-paddy rice reduces carbon footprint and enhances net carbon sink. Journal of Cleaner Production 2020;258:120643.

Gajaseni J. Energy analysis of wetland rice systems in Thailand. Agriculture, Ecosystems and Environment 1995;52(2-3):173-8.

Kaur N, Vashist KK, Brar AS. Energy and productivity analysis of maize based crop sequences compared to rice-wheat system under different moisture regimes. Energy 2021;216:119286.

Khatiwada D, Silveira S. Net energy balance of molasses based ethanol: The case of Nepal. Renewable and Sustainable Energy Reviews 2009;13(9):2515-24.

Khonpikul S, Jakrawatana N, Gheewala SH, Mungkalasiri J, Janrungautai J. Material flow analysis of maize supply chain in Thailand. Journal of Sustainable Energy and Environment 2017;8:87-9.

Kosemani BS, Bamgboye AI. Energy input-output analysis of rice production in Nigeria. Energy 2020:207:118258.

Król-Badziak A, Pishgar-Komleh SH, Rozakis S, Księżak J. Environmental and socio-economic performance of different tillage systems in maize grain production: Application of life cycle assessment and multi-criteria decision making. Journal of Cleaner Production 2021;278:123792.

Kusek G, Ozturk HH, Akdemir S. An assessment of energy use of different cultivation methods for sustainable rapeseed production. Journal of Cleaner Production 2016;112: 2772-83.

Lal B, Gautam P, Nayak AK, Panda BB, Bihari P, Tripathi R, et al. Energy and carbon budgeting of tillage for environmentally clean and resilient soil health of rice-maize cropping system. Journal of Cleaner Production 2019;226:815-30.

Lorzadeh SH, Mahdavidamghani A, Enayatgholizadeh MR, Yousefi M. Energy input-output analysis for maize production systems in Shooshtar, Iran. Advances in Environmental Biology 2011;5(11):3641-4.

Manzone M, Calvo A. Energy and CO_2 analysis of poplar and maize crops for biomass production in north Italy. Renewable Energy 2016;86:675-81.

Masters GM. Introduction to Environmental Engineering and Science. 2nd ed. New Jersey, USA: Prentice-Hall; 1998.

Multiple Cropping Center (MCC). Maize Research in Thailand Past Impacts and Future Prospects. Chiang Mai, Thailand: MCC; 1999.

Memon SQ, Amjad N, Dayo RH, Jarwar G. Energy requirement and energy efficiency for production of maize crop. European Academic Research 2015;2(2):14609-14.

Ministry of Agricultural and Cooperative. Soil management and nutrients in rice farming [Internet]. 2016 [cited 2021 Jan 22]. Available from: http://www.ricethailand.go.th/rkb3/title-index.php-file=content.php&id=005.htm.

Mohammadi A, Rafiee S, Mohtasebi SS, Rafiee H. Energy inputs-yield relationship and cost analysis of kiwifruit production in Iran. Renewable Energy 2010;35(5):1071-5.

Mohammadi A, Tabatabaeefar A, Shahin S, Rafiee S, Keyhani A. Energy use and economical analysis of potato production in Iran a case study: Ardabil province. Energy Conversion and Management 2008;49(12):3566-70.

Neamhom T, Polprasert C, Englande AJ. Ways that sugarcane industry can help reduce carbon emissions in Thailand. Journal of Cleaner Production 2016;131:561-71.

Nemecek T, Dubois D, Huguenin-Elie O, Gaillard G. Life cycle assessment of Swiss farming systems: I. Integrated and organic farming. Agricultural Systems 2011;104(3):217-32.

Nguyen TLT, Gheewala SH, Garivait S. Full chain energy analysis of fuel ethanol from cane molasses in Thailand. Applied Energy 2008;85(8):722-34.

Nutongkaew P, Waewsak J, Riansut W, Kongruang C, Gagnon Y. The potential of palm oil production as a pathway to energy security in Thailand. Sustainable Energy Technologies and Assessments 2019;35:189-203.

Office of Agricultural Economics (OAE). Land utilization by provience in 2019 [Internet]. 2020 [cited 2021 Mar 6]. Available from: http://www.oae.go.th/assets/portals/1/files/socio/LandUtilization2562.pdf.

Office of Agricultural Economics (OAE). Maize: plantation area, cultivation area, yields, and product by province for 2019/2020 [Internet]. 2021 [cited 2021 Mar 4]. Available from: http://www.oae.go.th.

Ozkan B, Akcaoz H, Karadeniz F. Energy requirement and economic analysis of citrus production in Turkey. Energy Conversion and Management 2004;45(11-12):1821-30.

Patthanaissaranukool W, Polprasert C. Reducing carbon emissions from soybean cultivation to oil production in Thailand. Journal of Cleaner Production 2016;131:170-8.

Patthanaissaranukool W, Polprasert C, Englande AJ. Potential reduction of carbon emissions from Crude Palm Oil production based on energy and carbon balances. Applied Energy 2013;102:710-7.

Polprasert C, Chaiyachet Y. Biological potential: A concept for sustainable development based on a carbon balance model. Proceedings of the 1st GMSARN International Conference on Sustainable Development: Challenges and Opportunities for GMS; 2007 Dec 12-14; The Ambassador City Jomtien Hotel, Pattaya: Thailand; 2007.

Prasara-A J, Gheewala SH. An assessment of social sustainability of sugarcane and cassava cultivation in Thailand. Sustainable Production and Consumption 2021;27:372-82.

Qi JY, Yang ST, Xue JF, Liu CX, Du TQ, Hao JP, et al. Response of carbon footprint of spring maize production to cultivation patterns in the Loess Plateau, China. Journal of Cleaner Production 2018;187:525-36.

Romanelli TL, Milan M. Energy balance methodology and modeling of supplementary forage production for cattle in Brazil. Scientia Agricola 2005;62(1):1-7.

Šarauskis E, Buragiene S, Masilionyte L, Romaneckas K, Avižienyte D, Sakalauskas A. Energy balance, costs and CO_2 analysis of tillage technologies in maize cultivation. Energy 2014;69:227-35.

Silalertruksa T, Gheewala SH. Land-water-energy nexus of sugarcane production in Thailand. Journal of Cleaner Production 2018;182:521-8.

Singh P, Singh G, Sodhi GPS. Energy auditing and optimization approach for improving energy efficiency of rice cultivation in south-western Punjab, India. Energy 2019;174:269-79.

Soni P, Sinha R, Perret SR. Energy use and efficiency in selected rice-based cropping systems of the Middle-Indo Gangetic Plains in India. Energy Reports 2018;4:554-64.

Supasri T, Itsubo N, Gheewala SH, Sampattagul S. Life cycle assessment of maize cultivation and biomass utilization in northern Thailand. Scientific Reports 2020;10(1): 1-13.

Tamil Nadu Agricultural University. Organic farming: Organic inputs and techniques [Internet]. 2016 [cited 2021 Jan 22]. Available from: https://agritech.tnau.ac.in/org_farm/orgfarm_manure.html.

United Nations Environment Programme (UNEP). 21 Issues for the 21st Century - Results of the UNEP Foresight Process on Emerging Environmental Issues. Environmental Development (Vol. 2) [Internet]. 2012 [cited 2016 Jun 20]. Available from: http://www.unep.org/pdf/Foresight_Report-21_Issues_for_the_21st_Century.pdf.

van Dijk M, Meijerink GW. A review of global food security scenario and assessment studies: Results, gaps and research priorities. Global Food Security 2014;3(3-4):227-38.

Yamane T. Statistics: An Introductory Analysis. 2nd ed. New York, USA: Harper and Row; 1967.

Yousefi M, Damghani AM, Khoramivafa M. Energy consumption, greenhouse gas emissions and assessment of sustainability index in corn agroecosystems of Iran. Science of the Total Environment 2014;493:330-5.

Zhong F, Jiang D, Zhao Q, Guo A, Ullah A, Yang X, et al. Eco-efficiency of oasis seed maize production in an arid region, Northwest China. Journal of Cleaner Production 2020; 268:122220.

Adaptability of Siamese Rosewood and Teak Seedlings to Varying Light Conditions

Nisa Leksungnoen[1], Suwimon Uthairatsamee[1*], and Tushar Andriyas[2]

[1]*Department of Forest Biology, Faculty of Forestry, Kasetsart University, Bangkok 10900, Thailand*
[2]*Post-Doctoral Fellow, Department of Environmental Science, Chulalongkorn University, Bangkok 10330, Thailand*

ARTICLE INFO

Received: 2 Feb 2021
Received in revised: 22 Jun 2021
Accepted: 29 Jun 2021
Published online: 11 Aug 2021
DOI: 10.32526/ennrj/19/202100003

Keywords:
Siamese Rosewood/ Teak/ Shade and sunlight/ Relative growth rate/ Chlorophyll efficiency

*** Corresponding author:**
E-mail: fforsmu@ku.ac.th

ABSTRACT

Rosewood and Teak are valuable timber species, which have been heavily logged from both natural forests and plantations. Climate change has also contributed to a reduction in their numbers. We studied their light adaptability at the seedling stage to quantify the growth and physiological characteristics under 10% and 100% of full sunlight. Rosewood performed better, as indicated by the relative growth rate, chlorophyll content, and chlorophyll efficiency, under both shade and sunlight. We also simulated a sudden change in light intensity (gap opening up in the canopy) by exposing seedlings, previously under shade, to full sunlight. Rosewood seedlings responded faster (higher relative growth rate) to changing light conditions relative to Teak. We conclude that Rosewood seedlings can be planted either under shade, or in full sunlight, or in a location experiencing sudden change from shade to sunlight, while Teak seedlings should be planted under at least 10% sunlight, but not in full sunlight, as it can lead to chlorophyll and tissue damage.

1. INTRODUCTION

Siamese Rosewood (hereafter; Rosewood) (*Dalbergia cochinchinensis* Pierre ex Laness.), which is a dominant species in dry evergreen forests, and Teak (*Tectona grandis* L.f.), are commonly found in mixed deciduous forests of Thailand (Santisuk et al., 2018). Given the red and golden finishing of furniture derived from Rosewood and Teak, respectively, they are highly sought after hardwoods in the global market, resulting in excessive illegal logging (Aerts et al., 2009), especially of Rosewood. Appendix II of the Convention on International Trade of Endangered Species (CITES) states that Rosewood has been threatened with extinction and requires rigorous monitoring and regulation (Siriwat and Nijman, 2018).

Planting native species can help to diversify impoverished forests, attract seed-dispersing animals and assist natural regeneration (Elliott et al., 2003; Wydhayagarn et al., 2009). Using valuable timber species for restoration can serve both conservation and economic purposes. Being a leguminous tree, Rosewood is likely to form a symbiotic association with nitrogen fixing bacteria (Seemakram et al., 2021). It can also improve the soil chemical properties in degraded sites, as its fast decomposing litter is rich in nitrogen, phosphorus, and organic carbon (Maikhuri et al., 2000; Mishra et al., 2003; Banerjee et al., 2004; Piotto et al., 2004). Teak is considered for the restoration of hydrological services (FAO, 2006) and to improve soil hydraulic properties (Mapa, 1995; Udayana et al., 2019). Moreover, Teak can be used as a shading tree in coffee plantations due to its large leaf area and high litter yield for soil humus (Khusnul et al., 2021).

Restoration of natural forests or plantations requires specific knowledge about the environmental factors affecting the growth, especially light conditions (Popma and Bongers, 1988). Leaf photosynthesis requires sufficient quantity and quality of light, with the under-story receiving less than optimal light (Rahman et al., 2021). Under natural propagation, seedlings grow under canopy until the older trees are cut down or die of natural causes (Snook et al., 2021), allowing light to penetrate through. A spurt in growth would guarantee that a tree dominates the gap and possibly ensure reproduction. Abrupt changes in light conditions can alter seedling performance in terms of successional status and wood

Citation: Leksungnoen N, Uthairatsamee S, Andriyas T. Adaptability of Siamese Rosewood and Teak seedlings to varying light conditions. Environ. Nat. Resour. J. 2021;19(6):449-458. (https://doi.org/10.32526/ennrj/19/202100003)

traits, like wood density (Turnbull et al., 1993; Yamashita et al., 2000).

At low intensities, increase in light intensity causes an increase in the rate of photosynthesis, but the rate later reduces as an asymptotic maximum is reached (Singh and Singh, 2003; Fan et al., 2013). Most canopies are unable to reach the photosynthetic light saturation levels due to varying orientations and leaf shading (Zotz and Winter, 1993). It has been reported that Rosewood has the greatest growth under high light intensity (75-100%) (Phonguodume et al., 2012). While Teak requires a light intensity between 50-75% for optimum growth and development (Kadambi, 1972; Nwoboshi, 1972) and recently, Moonchun et al. (2017) reported an optimum growth of Teak seedlings between 40-80% of full sunlight. However, none of studies reported observations about a sudden light change from shade to full sunlight due to a gap opening or while transferring plants, growing in shade of a nursery, for transplantation to full sunlight conditions in the field.

Kenzo et al. (2008) reported leaf ecophysiological response and height of trees affected by different canopy size openings in a degraded tropical secondary forest. It is important to determine species-specific light conditions to ensure a successful establishment of seedlings in degraded forests or plantations. We used various measurements including relative growth rate, stomatal conductance, chlorophyll content, and chlorophyll efficiency to determine the adaptability of Rosewood and Teak seedlings to 10% (under-story) and 100% intensity relative to full sunlight. Additionally, we also simulated a canopy opening scenario under which the seedlings experienced a sudden change from shade to full sunlight.

2. METHODOLOGY

2.1 Seedling preparation

Rosewood and Teak seedlings were purchased in December 2014. Although their exact age was not documented by the nursery, the seedlings were all planted during the same year. The diameter at breast height (DBH) was measured between 0.40-0.55 cm, while their height was between 32-36 cm. Seedlings were transplanted into black plastic pots filled with garden soil and coconut fibre and fertilized with 200 g of slow releasing fertilizer (14-14-14 Osmocote Suffolk, UK). The pots were placed at the Faculty of Forestry, Kasetsart University, Bangkok, for a month before the experiment began, to acclimatize them to the conditions. The temperature during the year (February 2015 to January 2016) was between 27.5-32.5°C, while the relative humidity fluctuated between 52 and 68%. The vapor pressure deficit ranged between 1.8 and 3.2 kPa (Figure 1(a)) with the average daylight intensity measured between 20,000 to 120,000 Lux (Figure 1(b)).

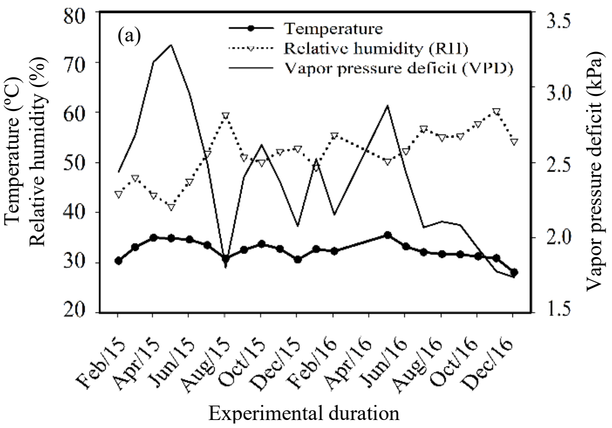

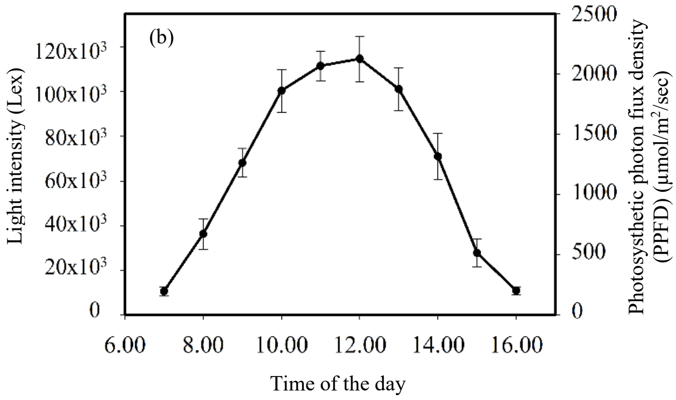

Figure 1. Weather data during the experiment; (a) temperature (solid line with closed circle), relative humidity (dotted line with triangle), and vapor pressure deficit (solid line) (b) average hourly light intensity at full sunlight (100%) over a day and photosynthetic photon flux density (PPFD).

2.2 Experimental treatments

2.2.1 Seedling response under full sunlight and shade conditions

The experiment was conducted for one year from February 2015 to February 2016, with the seedlings divided into two treatment groups and seven random pots acting as replicates for each treatment. Full sunlight (100% sunlight; sun) and shade conditions (10% of full sunlight; shade) were the treatments. Seedlings were randomly placed in a nursery of dimensions 1.5 m×2 m×3 m under each treatment, creating a split plot design (no replications of light intensity levels were done due to limited space).

The shaded area was covered with a black cloth preventing the penetration of ~90% sunlight. The ambient light conditions were measured through three light sensors (HOBO UA002-64, Onset Computer Corporation, Bourne, MA, USA) at a height of 1.50 m, every minute for three days prior to beginning the experiment. The light intensity in shade was 10.16±0.45% relative to that under full sunlight. All the seedlings were irrigated with a sprinkler system programmed to water every other day between 6 am to 7 am, to ensure sufficient soil and air moisture.

2.2.2 Relative growth rate measurements

Relative growth rate (RGR) was determined using the measurements of diameter, height, and leaf number. Diameter at root collar (DRC) was measured at the edge height of a plastic pot with a Vernier calliper. Height was measured from the edge of a pot to the top of a seedling, while mature leaves were counted for each seedling. The RGR was then calculated per month using the equation;

$$\text{RGR } (\%) = \frac{\ln(\text{G2}) - \ln(\text{G1})}{\text{time duration}} \times 100, \quad (1)$$

Where; G2 is either the diameter, height, or leaf number measured at the end of experiment (February 2016); and G1 is either the diameter, height, or leaf number measured at the beginning of experiment (February 2015).

2.2.3 Physiological measurements

All the physiological measurements were taken one time every month for 12 months from February 2015 to February 2016. Plant replications were accomplished by using seven plots for each treatment (shade and sunlight).

Stomatal conductance (G_s), chlorophyll content (CC), and chlorophyll efficiency (Fv/Fm) were also measured. G_s was measured around midday from 11 am to 2 pm (when the light intensity and air temperature was the highest during the day; Figure 1(b) with a Porometer (Decagon Device Inc., WA, USA). A mature expanded leaf from each plant was used to measure the listed parameters (7 replicates/ month). CC and Fv/Fm was measured from predawn to early morning (5.30-7.00 am), to avoid excessive radiation stress during the day. Five different locations were chosen on two mature expanded leaves, to measure CC with an SPAD meter (Model SPAD-502, Konica Minolta, Inc., Japan). Two mature expanded leaves were chosen to measure Fv/Fm using a chlorophyll fluorometer (Model OS-30p+, Opti-Sciences, Inc., Hudson, NH, USA). Two sliding clips were attached to each chosen leaf and left for 15 min for the leaf to adapt to the ambient dark lighting condition before the measurement.

2.2.4 Leaf-to-air vapor pressure deficit measurement

Leaf-to-air vapor pressure deficit (LAVPD) is the difference between vapor pressure of leaf and air and indicates the strength of driving force needed for transpiration. LAVPD is calculated using the equation;

$$\text{LAVPD} = e_{leaf} - e_{air} \text{ (kPa)}, \quad (2)$$

Where; e_{leaf} and e_{air} are the leaf and air vapor pressures, respectively.

$$\text{Vapor pressure (e)} = 0.61121 \exp\left[\frac{17.502\text{T}}{240.97+\text{T}}\right] \times \text{RH}, \quad (3)$$

Where; T is the temperature in Celsius and RH is relative humidity in %.

For e_{leaf}, T is the leaf temperature, which was measured at the same time when Gs was measured every month. RH of leaf is assumed to be close to 100%.

While e_{air}, T is air temperature which was measured at the weather station located 2 km away from study site on the same day when G_s was measured. RH was also measured from the same weather station.

2.2.5 Shade seedlings exposed to full sunlight

The response of Rosewood and Teak seedlings, growing in the understory for a year, was measured when they were suddenly exposed to full sunlight, simulating a gap opening up in the canopy. We used the seedlings (previously under shade for 1 year) for this experiment and exposed them for 9 months (March 2016 to December 2016) to 100% sunlight by removing the shade cloth. Seedlings were acclimatized for 3 months prior to the measurement during May 2016 to December 2016 (6 months). The same procedural steps used in the experiment sun vs. shade were followed to estimate the seedling growth.

2.3 Statistical analysis

The mean difference in relative growth and physiological parameters was analyzed through analysis of variance (ANOVA) with a pairwise test using least square difference (LSD). For the sun vs. shade experiment, a two-way split plot factorial design with two main factors was analyzed. The factors were the species (Rosewood and Teak) and light treatments (sun and shade conditions) with seven replicates (plants). Scatter plots with trend lines between LAVPD and G_s were created to determine the seedling behaviour over a range of driving force causing transpiration. For the shade to light experiment, a t-test was used test the significance of the mean differences between the species

3. RESULTS

3.1 Seedling response under full sun and shade

RGR was compared between sun and shade conditions for the two species. The relative diameter had no interaction difference between species and light conditions (Table 1). Only the light conditions had a statistically significant difference on the growth rate of diameter, with the plants under sun having a larger diameter compared to those under shade ($p<0.001$) (Figure 2(a) and Table 1). Relative height had no significant interaction difference between the species and light conditions. Rosewood grew taller than Teak ($p<0.05$) and seedlings kept under shade tended to have a relatively shorter height ($p<0.001$) (Figure 2(b) and Table 1). The relative leaf number followed a trend similar to relative height (Figure 2(c) and Table 1).

Physiological measurements, including G_s, CC, and Fv/Fm, are closely related to tree growth and development. Light is an important factor influencing the opening and closing of stomata. An open stomata increases the chances of CO_2 uptake, resulting in photoassimilation. Simultaneously, open stomata would help dissipate heat through transpiration. In this study, G_s was higher for Teak, both under sun and shade (Figure 2(d), Table 2). Both species are likely to be light-demanding, resulting in higher number of open stomata at higher light intensities. Chlorophyll is a key organelle for photosynthesis, with higher levels tending to increase food production. CC for both the species was higher for seedlings under shade compared to full sunlight (Figure 2(e), Table 2). For photosynthesis, both the quantity and quality of chlorophyll is important. Fv/Fm can also be used to indicate plant stress under different light conditions. Both species had no statistical difference in Fv/Fm, but this differed under each light treatment (Figure 2(f), Table 2). Seedlings under shade had a higher Fv/Fm than those in full sunlight.

Table 1. Analysis of variance (ANOVA) for RGR in rosewood and teak seedlings with the respective p-values.

Sources	DF	Sum square	Mean square	F-value	p-value
Diameter					
Species	1	0.0001613	0.0001613	2.256	0.146
Light	1	0.0030437	0.0030437	42.581	<0.0001***
Species × Light	1	0.0000004	0.0000004	0.006	0.939
Residuals	24	0.0017155	0.0000715	-	-
Height					
Species	1	0.000971	0.000971	5.573	0.027*
Light	1	0.001947	0.001947	11.176	0.003**
Species × Light	1	0.000441	0.000441	2.534	0.124
Residuals	24	0.004180	0.000174	-	-
Leaf number					
Species	1	0.001969	0.001969	4.366	0.047*
Light	1	0.006841	0.006841	15.171	0.0001***
Species × Light	1	0.000000	0.000000	0.0000	0.989
Residuals	24	0.010822	0.0000451	-	-

* indicate significant differences at 95% while, ** indicate significant differences at 99%, and *** significant differences at 99.99% indicate confidence level.

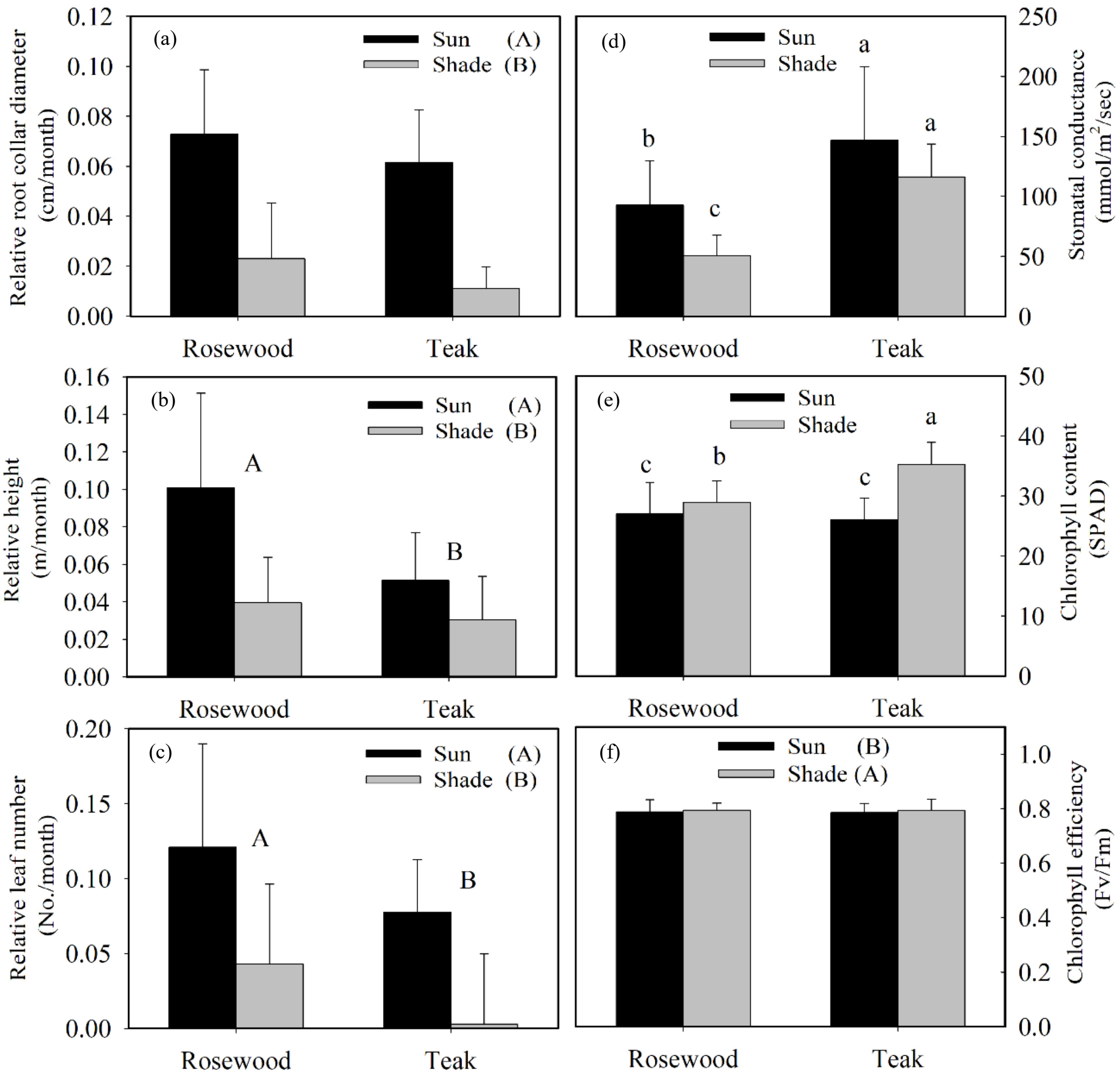

Figure 2. Relative growth (a-c) and physiological characteristics (d-f) of Rosewood and Teak seedlings. On the left panel; (a) relative diameter, (b) height, and (c) leaf number and on the right panel; (d) G_s, (e) CC, and (f) Fv/Fm for seedlings under sun (100%) and shade (10%) for 1 year (February 2015 to February 2016). The letters indicate a significant statistical difference (see Tables 1 and 2). The UPPERCASE letters indicate that only the main factor is statistically different while a lowercase lettering indicates that the interaction between the main factors is significantly different.

Table 2. Analysis of variance (ANOVA) for the relative physiological characteristics in rosewood and teak seedlings.

Sources	DF	Sum Square	Mean Square	F-value	p-value
G_s					
Species	1	3.0101	3.0101	129.150	<0.0001***
Light	1	0.5886	0.5886	25.252	<0.0001***
Species x Light	1	0.1924	0.1924	8.254	0.005**
Residuals	103	2.4006	0.0233	-	-
CC					
Species	1	616.9	616.9	39.78	<0.0001***
Light	1	1573.1	1573.1	101.44	<0.0001***
Species x Light	1	600.1	600.1	38.70	<0.0001***
Residuals	192	2977.6	15.5	-	-

* indicate significant differences at 95% while, ** indicate significant differences at 99%, and *** significant differences at 99.99% indicate confidence level.

Table 2. Analysis of variance (ANOVA) for the relative physiological characteristics in rosewood and teak seedlings (cont.).

Sources	DF	Sum Square	Mean Square	F-value	p-value
Chlorophyll efficiency (Fv/Fm)					
Species	1	0.00015	0.00015	0.299	0.584
Light	1	0.00222	0.00222	4.579	0.032*
Species x Light	1	0.00001	0.00001	0.014	0.905
Residuals	529	0.25691	0.00048	-	-

* indicate significant differences at 95% while, ** indicate significant differences at 99%, and *** significant differences at 99.99% indicate confidence level.

The response of G_s to atmospheric demand, as indicated by LAVPD, is presented in Figure 3. G_s as a function of LAVPD was different between the species and light conditions with Rosewood having a linear and Teak having a curvilinear response. This indicates that G_s of Teak could be more sensitive to air dryness, with a higher reduction in G_s when elevated LAVPD. Under shade, LAVPD was low (1-3 kPa) while in sunlight, LAVPD was high, as indicated by values ranging between 1 to 12 kPa. G_s of Rosewood under sunlight had a weak linear relationship (negative slope) with LAVPD, while the response in shade increased linearly (positive slope). In other words, seedlings under shade readily opened more stomata when air was slightly drier while the seedlings under full sunlight tended to close their stomata when the air was drier. However, the variation in G_s of Teak under both the light conditions followed a power law. For seedlings in shade, G_s responded weakly to LAVPD below 2 kPa and decreased rapidly thereafter (Figure 3(b)). Comparatively, after an initial rapid decrease in G_s for LAVPD values between 2-4 kPa, the relationship was weak thereafter. We conclude that Teak seedlings are relatively more sensitive to LAVPD, as evident by a rapid response to small changes in air vapor pressure.

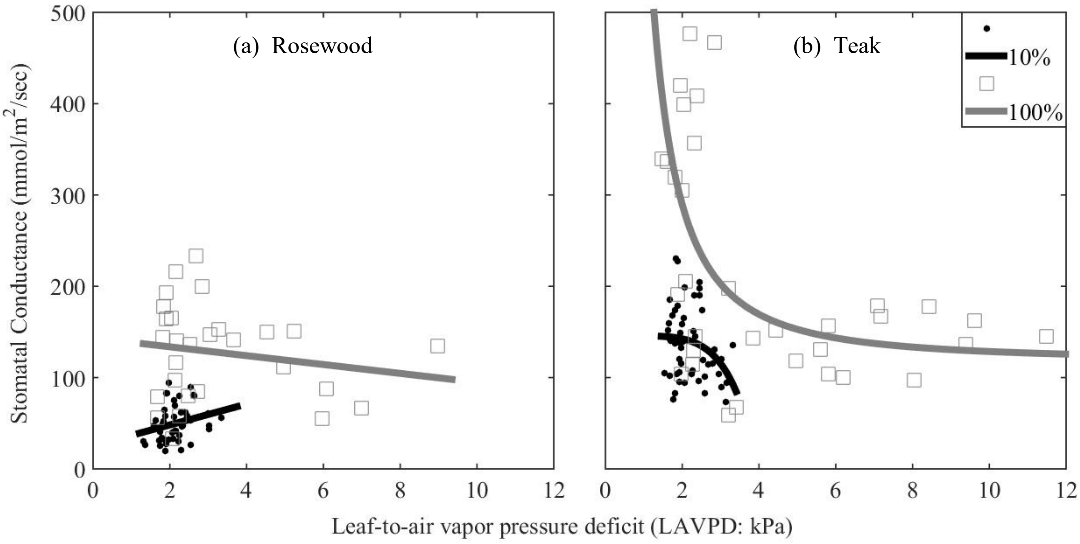

Figure 3. G_s response to LAVPD of seedlings exposed to full sunlight (open-squares with grey solid line) and those under shade (black dots with black solid line) of (a) Rosewood and (b) Teak. The trend lines indicate the differences in behaviour of both the species, with Rosewood having a linear response compared to a non-linear response in Teak.

3.2 Seedlings suddenly exposed to full sunlight after 1 year

With regards to seedling establishment (forest or plantation), a sudden change in light conditions from shade to full sunlight can affect the growth, depending on the seedling adaptability. We simulated such a scenario by exposing the seedlings, previously under shade (1 year), to full sunlight (9 months). The interspecies relative growth and physiological characteristics were compared (Figure 4). Rosewood had a higher overall RGR compared to Teak (Figure 4(a)). Among the physiological characteristics, G_s was significantly higher for Teak. However, CC and Fv/Fm were significantly higher for Rosewood (Figure 4(b)).

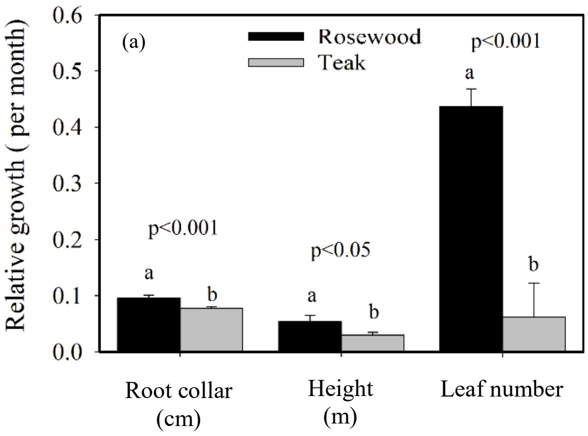

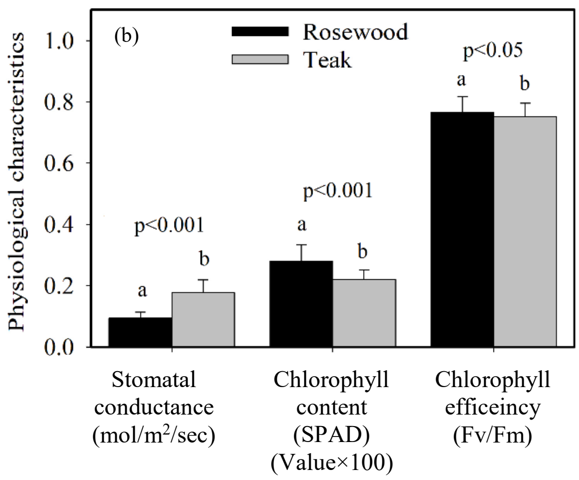

Figure 4. Relative growth (a) and physiological characteristics (b) of Rosewood and Teak seedlings, previously under 10% of full sunlight for 1 year (February 2015 to February 2016) exposed to full sunlight for 9 months (March 2016 to December 2016). The lowercase letters (a, b) indicate statistically significant differences between the species, as obtained from the t-test with the respective p-values indicated above the letters.

4. DISCUSSION

Rosewood and Teak are economically important timber species, and their natural populations have been indiscriminately logged for years. Future climate change is predicted to cause perceptible changes in the abundance of tropical species (Deutsch et al., 2008), leading to a reduction in the genetic diversity, especially in the peripheral population, as in Thailand, when compared to the centre of the population in Cambodia for Rosewood and India for Teak (Hartvig et al., 2018). A sustainable management will need a long-term conservation of genetic diversity to guarantee undiminished services over time. Light is a key factor affecting plant's growth and development and was the key parameter used to study the growth of Rosewood and Teak seedlings.

4.1 Seedling growth and physiological responses under full sunlight and shade

The growth rate of Rosewood (evergreen) was higher compared to Teak (deciduous), in both the light regimes and even more pronounced when the seedlings were moved from shade to full sunlight (Figures 2(a-c) and 4(a)). The most efficient growth (as indicated by RGR) in Rosewood has been previously reported under a wide range of light intensities (30-100% of full sunlight) (Moonchun et al., 2017) and (75-100%) (Phonguodume et al., 2012)). Sovu et al. (2010) stated that Rosewood is shade tolerant when young but can be light demanding as it matures. However, we confirmed that even as a seedling, Rosewood can both be shade tolerant and light demanding, as indicated by a similar growth rate under 10% and 100% light. For Teak, Moonchun et al. (2017) suggested that 40% of light resulted in optimum growth (with varying light intensity from 10, 20, 40, 60, 80, and 100% of full sunlight), while Nwoboshi (1972) reported that light intensity between 53-75% resulted in optimum growth, However, Teak shade intolerant at any stage of life, as reported by Kaosa-ard (1998) and we report that Teak grew better in full sunlight than in shade.

Light absorption is linked to the number of leaves and leaf area, with a higher leaf number and leaf area leading to more photosynthesis and net growth. In our study, Rosewood had a higher relative leaf number compared to Teak, as it has a compound leaf structure. Being an evergreen/semi-evergreen species, Rosewood does not shed its leaves throughout the year, while Teak, being deciduous with a simple leaf structure, sheds its leaves during the dry months (November to March), leading to a lower relative leaf number. Givnish (2002) reported that the deciduous species tended to have larger leaves so as to harvest maximum sunlight during the growing season, which is not the case with evergreen species. The thinner leaves of Rosewood (high specific leaf number; 180-240 in Rosewood vs. 120-180 g/cm^2 in Teak), led to more light absorption, or better growth (Figure 2(a-b)) and light adaptability (Figure 4(a)).

A relatively lower G_s of the thin-leaved Rosewood (Figure 2(d)) resulted in better light penetration and any increase in leaf temperature was countered by a lower sensitivity to LAVPD (Figure 3), as indicated by the slope of the scatter plot between G_s and LAVPD. Any changes in the driving gradient of atmospheric vapor pressure would cause little to no change to the stomatal closure and photosynthesis rate.

Hence, Rosewood may be resilient to future climate change scenarios. Teak is relatively more sensitive to variable light intensity and atmospheric demand (Figures 3 and 4), which could be due to its deciduous nature and large leaf trait (10 times larger than Rosewood leaflets). Large leaves generally have a thicker boundary layer, causing inefficient heat dissipation under high light intensity (Whitmore, 1998). A higher measured G_s (Figures 2(d) and 4(b)) for Teak could be due to an urge to transpire and reduce its leaf temperature. This response in Teak can be used to indicate any changes in tropical atmospheric conditions, especially when the air is drier, with the response being a rapid closure of the stomata to hotter and drier air.

4.2 Seedlings suddenly exposed to full sunlight after 1 year

In mixed forests with multilayer stories, an over-story comprising of a fast growing species and bamboo would dominate the canopy, resulting in an uneven distribution of light for the seedlings (Ådjers et al., 1995). A sudden change in light conditions would mostly be a result of branch pruning or death of big trees. Any small or large gaps would allow more direct sunlight for the seedlings. In our study, a sudden change in the light conditions from 10% to 100% was investigated to measure the responses of both species simulating a gap opening. The RGR for Teak was low when kept under shade and when suddenly exposed to full sunlight, and was lower than Rosewood (Figure 4(a)). So, Rosewood seedlings had a relatively higher adaptability to variable light conditions and could dominate Teak in terms of growth, when planted at the same time and competing for similar light conditions, in a forest or plantation setting. Therefore, during the seedling stage, Rosewood grows well under shade and sunlight conditions which includes a sudden change from 10% to 100% sunlight when compared to Teak. We also observed that CC and Fv/Fm of both species decreased when exposed to full sunlight and was pronounced in Teak (Figure 4(b)) due to a higher radiation damage. This observation is supported by a previous study reporting that optimum light condition for Teak growth is not under shade or under 100% sunlight but between 40-75% of full sunlight (Moonchun et al., 2017), as intense sunlight resulted in chlorophyll damage. Similar to the findings of Galeano et al. (2019), who indicated that light saturation point, where the photosynthesis rate would reach its maximum in Teak was around 1,217 µmol/m^2/s, which is correlated with a light intensity of 60% in the present study (Figure 1(b)). If Teak receives a light intensity higher than 60%, it would lead to leaf injury in the form of leaf burning and necrosis due to chlorophyll damage.

Reforestation requires species diversity and floristic composition as well as management. Suryanto et al. (2021) suggested that an agroforestry system should incorporate a mixed cropping model, in order to guarantee a sustainable forest regeneration. Teak should be planted at the edge of the area because it requires a higher light intensity (Suryanto et al., 2021). While Rosewood after establishment can grow most efficiently in a gap larger than 64 m^2, due to sufficient direct sunlight for growth (Sovu et al., 2010). Rosewood is considered as an intermediate pioneer species with a high growth rate during early stage of development and can rapidly colonize with only a few seedlings (So, 2000). Also Rosewood behaves as an anisohydric species, maximizing its carbon assimilation at the risk of hydraulic failure. This behaviour is associated with its higher growth during the early stages of establishment (Hung et al., 2020). Thus, Rosewood can both be shade and light tolerant during its early establishment and can become light demanding when nearing maturity, assuring a successful establishment in both the forest and plantation settings.

5. CONCLUSION

Light is a major factor responsible for plant growth and development in every stage of its life. A sudden change from shade to full sunlight resulting from gap opening or transferring nursery seedling to the field can cause damage to Teak leaves relative to those of Rosewood. Also, at all the reported light intensities (100%, 10% or sudden change light conditions), the growth of Rosewood was relatively greater than Teak, as indicated by a higher growth and chlorophyll content, and lower water loss, due to lower stomatal opening. We conclude that Rosewood seedlings can grow better in both shade and under full sunlight conditions and can also adapted well under abrupt changes in light intensity. Teak should not be planted under a shade of 10% of full sunlight or full sunlight, as that would reduce its growth rate.

ACKNOWLEDGEMENTS

This research was funded by Thailand Research Fund (TRF) and Kasetsart University. Authors acknowledge the help of Miss Maratreenung

Seehakrai and Miss Suriwan Moonchan during this work.

REFERENCES

Ådjers G, Hadengganan S, Kuusipalo J, Nuryanto K, Vesa L. Enrichment planting of dipterocarps in logged-over secondary forests: effect of width, direction and maintenance method of planting line on selected *Shorea* species. Forest Ecology and Management 1995;73(1-3):259-70.

Aerts R, Volkaert H, Roongruangsree N, Roongruangsree U-T, Swennen R, Muys B. Site requirements of the endangered rosewood *Dalbergia oliveri* in a tropical deciduous forest in northern Thailand. Forest Ecology and Management 2009;259(1):117-23.

Banerjee SK, Mishra T, Singh AK, Jain A. Impact of plantation on ecosystem development in disturbed coal mine overburden spoils. Journal of Tropical Forest Science 2004;16:294-307.

Deutsch CA, Tewksbury JJ, Huey RB, Sheldon KS, Ghalambor CK, Haak DC, et al. Impacts of climate warming on terrestrial ectotherms across latitude. Proceedings of the National Academy of Sciences 2008;105(18):6668-72.

Elliott S, Navakitbumrung P, Kuarak C, Zangkum S, Anusarnsunthorn V, Blakesley D. Selecting framework tree species for restoring seasonally dry tropical forests in northern Thailand based on field performance. Forest Ecology and Management 2003;184:177-91.

Fan X-X, Xu Z-G, Liu X-Y, Tang C-M, Wang L-W, Han X. Effects of light intensity on the growth and leaf development of young tomato plants grown under a combination of red and blue light. Scientia Horticulturae 2013;153:50-5.

Food and Agriculture Organization (FAO). Global planted forests thematic study: results and analysis. Planted Forests and Trees Working Paper 38 [Internet]. 2006 [cited 2020 Dec 28]. Available from: http://www.fao.org/forestry/site/10368/en.

Galeano E, Vasconcelos TS, de Oliveira PN, Carrer H. Physiological and molecular response to drought stress in teak (*Tecnona grandis* L.f.). PLoS ONE 2019;14(9):e0221571.

Givnish T. Adaptive significance of evergreen vs. deciduous leaves: Solving the triple paradox. Silva Fennica 2002; 36(3):703-43.

Hartvig I, So T, Changtragoon S, Tran HT, Bouamanivong S, Theilade I, et al. Population genetic structure of the endemic rosewoods *Dalbergia cochinchinensis* and *D. oliveri* at a regional scale reflects the Indochinese landscape and life-history traits. Ecology and Evolution 2018;8:530-45.

Hung TH, Gooda R, Rizzuto G, So T, Thammavong B, Tran HT, et al. Physiological responses of rosewoods *Dalbergia cochinchinensis* and *D. oliveri* under drought and heat stresses. Ecology and Evolution 2020;10:10872-85.

Kadambi K. Forestry Bulletin No. 24: Silviculture and Management of Teak. 23rd ed. School of Forestry, Stephen F. Austin State University; 1972. p. 1957-72.

Kaosa-ard A. Overview of problems in Teak plantation establishment. In: Kashio M, White K, editors. Teak for the Future. Bangkok, Thailand: RAP Publication; 1998. p. 49-60.

Kenzo T, Yoneda R, Matsumoto Y. Leaf photosynthetic and growth responses on four tropical tree species to different light conditions in degraded tropical secondary forest, Peninsular Malaysea. Japan Agricultural Research Quarterly 2008; 42(4):299-306.

Khusnul K, Suratno, Asyiah NI, Hariyadi S. Analysis of the effect of several types of shade on the productivity of Robusta coffee. Journal of Physics: Conference Series 2021;1751:012060.

Maikhuri RK, Semwal RL, Rao KS, Singh K, Saxena KG. Growth and ecological impacts of traditional agroforestry tree species in Central Himalaya, India. Agroforestry Systems 2000; 48(3):257-71.

Mapa RB. Effect of reforestation using *Tectona grandis* on infiltration and soil water retention. Forest Ecology and Management 1995;77(1):119-25.

Mishra A, Sharma S, Gupta M. Soil rehabilitation through afforestation: Evaluation of the performance of *Prosopis juliflora*, *Dalbergia sissoo*, and *Eucalyptus tereticornis* plantations in a sodic environment. Arid Land Research and Management 2003;17(3):257-69.

Moonchun S, Leksungnoen N, Uthairatsamee S, Moungsri-muangdee B. Effect of light intensity on growth and photosynthesis related variables of forest tree seedlings. Thai Journal of Forestry 2017;36(2):12-23.

Nwoboshi L. Responses of Teak (*Tectona grandis* L.f.), Idigbo (*Terminalia ivorensis* A chev) and Opepe (*Naclea diderrichii* Mervill) seedlings to various light intensities. Nigerian Journal of Forestry 1972;2(2):48-53.

Phonguodume C, Lee D, Sawathvong S, Park Y, Ho WM, Combalicer E. Effects of light intensities on growth performance, biomass allocation and chlorophyll content of five tropical deciduous seedlings in Lao PDR. Journal of Environmental Science and Management 2012;15:60-7.

Piotto D, Víquez E, Montagnini F, Kanninen M. Pure and mixed forest plantations with native species of the dry tropics of Costa Rica: A comparison of growth and productivity. Forest Ecology and Management 2004;190:359-72.

Popma J, Bongers F. The effect of canopy gaps on growth and morphology of seedlings of rain forest species. Oecologia 1988;75(4):625-32.

Rahman M, Billah M, Rahman MO, Datta D, Ahsanuzzaman M, Islam M. Disentangling the role of competition, light interception, and functional traits in tree growth rate variation in South Asian tropical moist forests. Forest Ecology and Management 2021;483:118908.

Santisuk T, Chayamarit K, Balslev H. Flora of Thailand. Volume 4 Part 3.1. Leguminosae- Papilionoideae. Bangkok, Thailand: The Forest Herbarium, Department of National Parks, Wildlife and Plant Conservation; 2018.

Seemakram W, Suebrasri T, Khaekhum S, Ekprasert J, Aimi T, Boonlue S. Growth enhancement of the highly prized tropical trees siamese rosewood and burma padauk. Rhizosphere 2021;19:100363.

Singh B, Singh G. Biomass partitioning and gas exchange in *Dalbergia sissoo* seedlings under water stress. Photosynthetica 2003;41(3):407-14.

Siriwat P, Nijman V. Online media seizure reports: A tool to monitor CITES implementation in regulating the international rosewood trade. Forest Policy and Economics 2018;97:67-72.

Snook LK, Capitanio R, Tadeo-Noble A. Restoring commercial timber species through silvicultural patch clear-cuts and natural regeneration in Mexico's Maya Forest: Composition and growth 11 years after three treatments. Forest Ecology and Management 2021;493:119206.

So NV. The potential of local tree species to accelerate natural forest succession on marginal grasslands in southern Vietnam.

In: Elliot S, Kerby J, Blakesley D, Hardwick K, Woods K, Anusarnsunthorn V, editors. Forest Restoration for Wildlife Conservation. Chiang Mai: Chiang Mai University; 2000.

Sovu, Tigabu M, Savadogo P, Odén PC, Xayvongsa L. Enrichment planting in a logged-over tropical mixed deciduous forest of Laos. Journal of Forestry Research 2010; 21(3):273-80.

Suryanto P, Sadono R, Yohanifa A, Widyawan MH, Alam T. Semi-natural regeneration and conservation in agroforestry system models on small-scale farmers. Biodiversitas 2021; 22(2):858-65.

Turnbull MH, Doley D, Yates DJ. The dynamics of photosynthetic acclimation to changes in light quantity and quality in three Australian rainforest tree species. Oecologia 1993;94(2): 218-28.

Udayana C, Skarpe C, Solberg SØ, Mathisen KM, Andreassen HP. Soil properties after forest rehabilitation by planting teak and mahogany in Java , Indonesia. Forest Science and Technology 2019;15(4):230-7.

Whitmore TC. An Introduction to Tropical Rain Forests. Oxford, U.K.: Oxford University Press; 1998.

Wydhayagarn C, Elliott S, Wangpakapattanawong P. Bird communities and seedling recruitment in restoring seasonally dry forest using the framework species method in Northern Thailand. New Forests 2009;38:81-97.

Yamashita N, Ishida A, Kushima H, Tanaka N. Acclimation to sudden increase in light favoring an invasive over native trees in subtropical islands, Japan. Oecologia 2000;125:412-9.

Zotz G, Winter K. Short-term photosynthesis measurements predict leaf carbon balance in tropical rain-forest canopy plants. Planta 1993;191(3):409-12.

Characterization of Fluorescent Dissolved Organic Matter in an Affected Pollution Raw Water Source using an Excitation-Emission Matrix and PARAFAC

Mohammad Rangga Sururi[1], Mila Dirgawati[1*], Dwina Roosmini[2], and Suprihanto Notodarmodjo[2]

[1]*Environmental Engineering Study Program, Faculty of Civil and Planning, Institut Teknologi Nasional Bandung, Indonesia*
[2]*Faculty of Civil and Environmental Engineering, Institut Teknologi Bandung, Indonesia*

ARTICLE INFO

Received: 2 Apr 2021
Received in revised: 4 Jun 2021
Accepted: 6 Jun 2021
Published online: 5 Aug 2021
DOI: 10.32526/ennrj/19/2021008

Keywords:
Fluorescence Dissolved Organic Matter/ Tropical/ Raw water source/ PARAFAC

*** Corresponding author:**
E-mail: mila.dirgawati@itenas.ac.id

ABSTRACT

Cikapundung River is the main raw water source for 2-millions inhabitants of Bandung city but has been severely deteriorated due to organic pollution such as cattle manure, domestic, and agriculture wastes. Dissolved Organic Matter (DOM) in raw water can influence the process of water treatment. This study characterized and identified the origins of fluorescent DOM (FDOM) in Cikapundung River. Raw water samples were collected from intake outlets during dry and rainy seasons and analyzed using Fluorescence Excitation Emission Matrix spectroscopy combined with parallel factor (PARAFAC). FDOM origins were identified by Fluorescence-Index (FI) while autochthonous process contribution in water body was determined by Biological-Index (BIX). Chromophoric DOM as UV absorbance at 254 nm (A_{254}) and Chemical Oxygen Demand (COD) were also measured. The FI were 1.82 (dry season) and 1.77 (rainy season), and the BIX were 0.92 (dry season) and 0.65 (rainy season). PARAFAC identified three compounds: water contaminant-like (C1), humic-like (C2) and tryptophan-like (C3) compounds. C2 was predominantly present in the rainy season with a C3/C2 ratio of 0.33. In the dry season, C3 increased substantially with a C3/C2 of 1.60. Strong correlation between C1 and C3 (R=0.86) was evidence that contaminant-like and tryptophan-like compounds were from the same anthropogenic sources. Strong correlation with A_{254} may indicate these identified compounds are aromatics.

1. INTRODUCTION

The main purpose of drinking water treatment plants is to produce drinking water that meets health standards by maximizing the removal of pollutants and pathogens. Rivers in West Java are important raw water sources for drinking water. However, the quality of these rivers have deteriorated due to contamination of organic compounds from anthropogenic activities especially from disposal of domestic and livestock wastes (EPA, 2020).The presence of DOM in raw water may disrupt the performance of drinking water treatment system by increasing the coagulant dosage and increase backwash of filter unit frequency (Jacangelo et al., 1995; Matilainen and Sillanpää, 2010; Ødegaard et al., 2010).

The authorized drinking water company in Bandung City has reported difficulties in treating the raw water during dry season (Sururi et al., 2020). This was indicated by not optimum formation of flock, and more frequent cleaning of secondary treatment units and backwash of rapid sand filter during the dry season than the rainy season. These occurred possibly due to the presence of DOM in the raw water, particularly in tropical countries when the intensity of precipitation may affect the characteristics of DOM in water bodies (Vasyukova et al., 2012). However, the presence of DOM, particularly in polluted raw water bodies and its changes along the water treatment plant (WTP) are not well understood (Ye et al., 2019). Moreover, the majority of drinking water treatment in Indonesia use chlorine-based disinfection because of their low cost and availability (Sururi et al., 2017). In particular, specific fractions of the DOM in the raw water are known as the major precursors for the formation of

Citation: Sururi MR, Dirgawati M, Roosmini D, Notodarmodjo S. Characterization of fluorescent dissolved organic matter in an affected pollution raw water source using an excitation-emission matrix and PARAFAC. Environ. Nat. Resour. J. 2021;19(6):459-467. (https://doi.org/10.32526/ennrj/19/2021008)

carcinogenic disinfection byproducts (DBPs) such as Trihalomethanes (THMs) when chlorine is used as a disinfecting agent (Abouleish and Wells, 2015; Jiang et al., 2017). Therefore, the raw water characteristics combined with chlorination method in the final disinfection stage can potentially produce drinking water that contains harmful THMs. Nonetheless, studies investigating the quantity and characteristics of DOM compound in tropical raw water sources including Indonesian rivers are very limited (Qadafi et al., 2020). The presence of DOM in the raw water is commonly represented as the concentrations of chemical oxygen demand (COD) and biochemical oxygen demand (BOD) including in Indonesia. However, both COD and BOD represent the lability of organic matter and thus inadequately indicate the characteristics of organic matter that may influence the performance of drinking water treatment. This suggests measuring alternative surrogate parameters of DOM that could provide complete information of DOM characteristics is needed.

Studies determining the types of DOM compounds in water body and their origins have gained growing interest worldwide. Recent studies (Hur et al., 2014; Yang et al., 2015) have used the fluorescence of DOM (FDOM) compounds to characterize chromophoric DOM (CDOM) as an alternate of CDOM, the key fraction of DOM which absorbs light over a broad range of ultraviolet-visible wavelengths (Fellman et al., 2010). Recently, FDOM was analyzed by fluorescence spectroscopy with excitation emission matrix and parallel factor analysis (PARAFAC). The composition of FDOM may suggest the origin of DOM whether from terrestrial inputs (allochthonous) or microbial activities in the water body (autochthonous). Among CDOM parameters available, UV absorbance at 254 nm (A_{254}) has been one of the most common CDOM parameters to indicate the presence of humic and aromatic compound.

The purposes of this study were to: (i) identify the origins and FDOM compounds by PARAFAC in tropical raw water source during the dry and rainy seasons; (ii) determine the relationships between the quantity of FDOM and other surrogate parameters of organic such as COD and A_{254} during both seasons. The results of this study can be used as one of the main references to gain better understanding of DOM in tropical drinking water sources and determine the best strategies to produce safe drinking water.

2. METHODOLOGY

2.1 Study area

Cikapundung River is located in Bandung District West Java Province. The upper stream of Cikapundung River has been used as a raw water source to provide drinking water for almost 2 million inhabitants of Bandung Metropolitan City. The upstream area of Cikapundung River is located in Lembang District, inhabited by 197,640 people with a population density of 2,068 people/km^2 in 2019. The air temperature ranges from 19-32°C, and the average rainfall is 295.7 mm with the highest occurring in April (560 mm) while the lowest is in December (60 mm).

The Cikapundung River has a minimum discharge of 0.88 m^3/sec and a maximum discharge of 2.11 m^3/sec. Nearly 600 L/sec raw water is tapped by Bantar Awi Intake and treated at conventional drinking water treatment operated by the local water company. As seen in Figure 1, the water intake is located in natural forestry area (Djuanda National Park) with an area that occupies almost 20% of the catchment of the upper stream area (6,933.30 Ha). The catchment of the upstream area is dominated by anthropogenic activities (81% of the total catchment area) such as agriculture, plantations, cattle manure, tourism, and residential (Sururi et al., 2020). According to the Central Bureau of Statistics, the largest livestock in this area is located along this watershed (BPS KBB, 2019a), accounted by approximately 21,043 cows, 17,918 sheeps, and 526 horses (BPS KBB, 2019b). Cattle wastes were observed in the upper stream of the Cikapundung River which was originated from livestock located ±7 km (Batu Lonceng area) from the intake. The upper Cikapundung has been subjected to domestic wastes pollution since at least 20% of the total inhabitants in the watershed do not have appropriate sanitation facilities (BPS KBB, 2019b).

2.2 Water sampling

The average monthly rainfall intensity in the rainy season ranged from 443 mm/month (November 2019) to 199 mm/month (February 2020) with an average total number of rainy days of 24 days/month. Meanwhile during dry season, the average rainfall intensity and total rainy days was 48 mm/month and 6 days/month (August 2019), respectively. Given these values, raw water samples were collected as grab samples from the outlet of the intake in the dry season: August 14-23, 2019 (n=9); and two sampling periods in the rainy season: 9-17 November 2019 (n=9; period-1), and 28-15 February 2020 (n=9; period-2). Therefore, in total, there were 27 samples/dataset for further analysis which was within the range for minimum input data required for PARAFAC (20-100 samples) as suggested by Stedmon and Bro (2008). 5L-polyethylene bottles were used for the raw water samples. These samples were then stored in a refrigerator at 4ºC. Prior to analysis, the samples were filtered through a membrane of Advantech A045H047A Sterile MCE gridded filter 0.45 µm, 47mm. Other parameters such as pH and temperature were measured onsite, and the measured average pH values were 7.42 in the rainy season and 8.32 in the dry season, and temperature range between 23 and 25ºC.

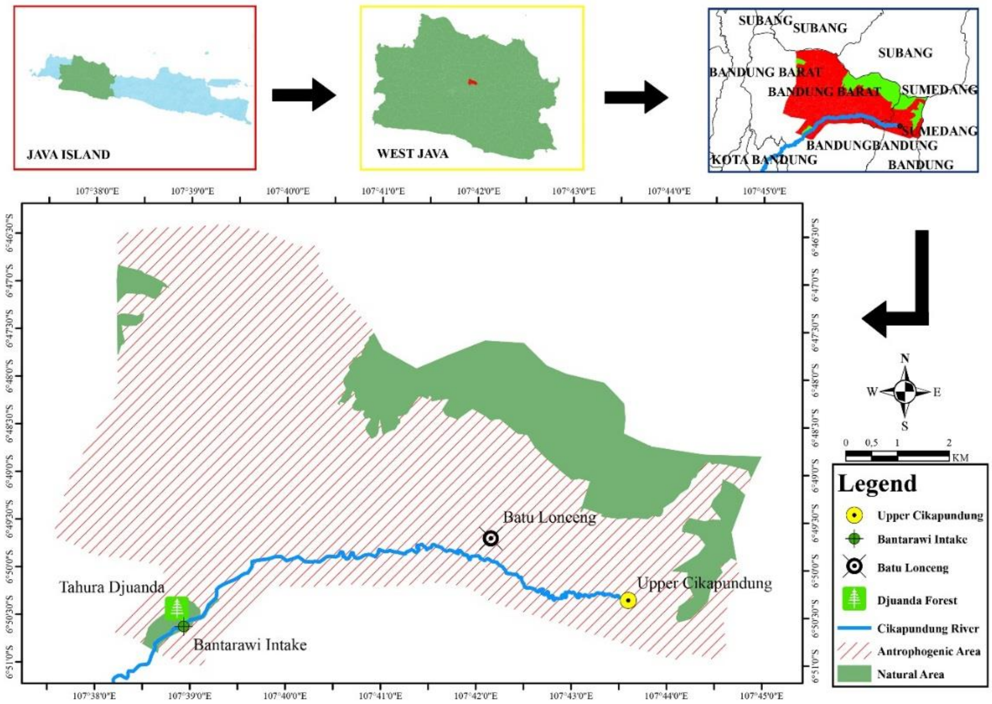

Figure 1. Area of study: Upper stream of Cikapundung River and its Catchment A

2.3 Identification of origin and types of DOM compounds

2.3.1 Spectral measurements

Fluorescence EEMs (FEEMs) were measured with a Shimidzu RF-5301 Spectro fluorophotometer set at emission wavelengths of 250-550 nm and excitation wavelengths range of 220-450 nm, with measurement intervals of 5 nm and 1 nm, respectively. Spectral corrections were applied for both the excitation and emission spectra. The correction procedures include: (1) reduction of inner filter effect using the absorption spectra data, and the fluorescence response of Milli-Q water blank (Murphy et al., 2010); (2) normalization of EEMs to the Raman peak area; and (3) finally removal of the Raman scatter. The correction factors obtained for the inner filter were generated based on the recorded UV-Vis absorbance which was measured at wavelengths of 220-600 nm (Murphy et al., 2010). The Rayleigh effects were then eliminated by replacing the spectra at emission wavelength between two excitation wavelengths in a range of −20 nm to +20 nm. The corresponding values were then set as missing values (Bieroza et al., 2011). The Raman peak area which resulted from these procedures were used for the normalization of the fluorescence intensity and then reported in Raman Units (RU).

2.3.2 Identification origin of DOM

The origin of DOM was identified based on the value of Fluorescence Index (FI) and a representative of algal and microbial versus terrestrial DOM sources (McKnight et al., 2001).The FI was calculated as the ratio of fluorescence intensities of 450 nm emission wavelength measured at 370 nm excitation wavelength to 500 nm at the same excitation wavelength (McKnight et al., 2001). Meanwhile the contribution of autochthonous process in the raw water was identified based on the value of Biological Index (BIX) since BIX values was an indication of the relative importance of biological or microbial DOM (Huguet et al., 2009). The value of BIX was determined as the ratio of intensity of 380 nm to 430 nm emission wavelength which was measured at 310 nm excitation wavelength.

2.3.3 Identification of DOM compound

The FDOM compounds in the raw water were determined statistically by conducting PARAFAC regardless the spectral shapes or number of the FDOM compounds. Briefly, PARAFAC model was developed based on the three key variables: excitation wavelengths, emission wavelengths, and fluorescence intensities as suggested by Stedmon and Bro (2008) using equation below:

$$X_{ijk} = \sum_{f=1}^{f} a_{if}\, b_{jf}\, c_{kf} + \epsilon_{ijk} \quad i = 1, .., I; j = 1, \ldots, J; k = 1, \ldots, K)$$

Where; X_{ijk} is the intensity of fluorescence for sample i^{th} which was measured at j emission wavelength and k excitation wavelength; a_{if} is the f^{th} analyte concentration in sample i; b_{jf} and c_{kf} are the emission and excitation spectra at wavelengths j and k respectively for the analyte f; and e_{ijk} is the noise of residual and variability which was not accounted by the model.

The toolbox from drEEM (decomposition routines for Excitation Emission Matrices) in the MATLAB R2015a (MathWorks) was used for identifying FDOM compounds through PARAFAC. There were 27 EEM (comprised 352 emission and 47 excitation wavelengths for each EEM) which were decomposed into individual components. Split-half validation method was then used to evaluate the results of the PARAFAC for determining valid FDOM compounds. The spectral shapes of individual valid compound were finally compared with those shapes available in the online spectral library of auto-fluorescence (https://openfluor.lablicate.com).

2.4 Measurement of COD and A_{254}

The characteristics of DOM were identified as Chemical Oxygen Demand (COD), and A_{254}. Water samples were filtered by 0.45 μm membrane prior to analysis. COD was analyzed based on the Standard Method protocol 5220C (close reflux method) (APHA, 2005). A_{254} were measured using a spectrophotometer (Shimadzu-1700 UV/Vis with a 1-cm quartz cell) at 254 wavelengths according to the standard method 5910 B (APHA, 2005).

2.5 Correlation analysis

The relationship between each DOM parameters (DOC and A_{254}) and each of the identified compounds was determined based on the results of Pearson correlation analyses using a p-value of 0.05 to determine the significance. A correlation coefficient of >0.65 represented "good" correlation, 0.40-0.64 was "moderate" correlation, ≤0.39 represented "poor" correlation between the pair. T-test analysis was also conducted to indicate the difference of each parameter between the dry and rainy seasons. A t-test value <0.5 was an indicative of statistically significant difference whereas a t-test value >0.5 was interpreted that there were no significant differences between the two seasons (Awad et al., 2016). All statistical analysis was performed using SPSS 19.0 software package: IBM SPSS Statistics.

3. RESULTS AND DISCUSSION

3.1 Origins of FDOM in raw water

The measured ranges of FI and BIX in the raw water (Cikapundung River) during both seasons are summarized in Table 1.

Table 1. BIX and FI values in the raw water during the rainy and dry seasons

Seasons	FI		BIX	
	Range	Mean±SD	Range	Mean±SD
Dry	1.55-3.23	1.82±0.09	0.62-1.33	0.92±0.21
Rainy	1.60-1.95	1.77±0.10	0.48-0.81	0.65±0.12

It was observed that the measured FI average was 1.82 in the dry season and 1.77 in the rainy season, which was consistent with the results of t-test that show insignificant differences between the two seasons. The observed FI were comparable with those in a previous study suggesting FDOM in the raw water sources were from terrestrial and microbial activities (Tang et al., 2019). In this current study, however, the values of FI in the dry was greater than the rainy season, suggesting FDOM that originated from microbial activities was predominant. The results were consistent with the existing land use in the catchment area which is dominated by anthropogenic activities as evident by a large pile of animal waste in the upper stream. The observed results were within the range of FI values for polluted water body such as Han River (1.54-2.07) (Hur et al., 2014), and above the FI values for a natural water body such as Epulu-Congo River during the dry season (1.45) (Spencer et al., 2010). These suggest that the high values of FI in water body was most likely due to the contribution of wastewater discharges as reported by Ye et al. (2019).

The average value of BIX in the dry season was 0.92, greater than the rainy season (0.65) (Table 1), but the results of t-test did not indicate significance differences in the BIX values during both seasons. The results of the rainy season suggest less contribution of autochthonous DOM (Huguet et al., 2009) and terrestrial humic compounds which had entered the water body possibly through rainwater runoff was predominant (Parlanti et al., 2000). However, an increase of BIX during the dry season was likely indicating DOM with autochthonous sources of recently produced organic matter of bacterial origin (Huguet et al., 2009). These BIX values are comparable with those reported by (Hur et al., 2014) for a polluted river (0.58-1.04). Ye et al. (2019) have found that the more polluted the water body, the higher the BIX value. Therefore, the observed BIX during the dry season may indicate an increase in tryptophan compound which had possibly been the result of microorganisms decomposition activity in the cattle waste (Parlanti et al., 2000). Further study regarding the effect of land use on FI and BIX parameters in all segments of Cikapundung River is needed for strengthening the results of current study.

3.2 Type of FDOM compounds and DOM quantity in raw water

The PARAFAC have identified three main compounds in the raw water samples. The split-half validations have shown the spectral of these identified compounds overlapped the excitations and emissions loading of the three compounds in half the data set as well as the entire data set (Figure 2). Direct comparison of the measured EEMs, spectral shapes and position between each of identified FDOM compound with those in the spectral database (library/openfluor.lablicate.com) have resulted in similarities of 90-95%. The fluorescence characteristics of Compound-1 (C1) from this study were very similar to unknown compounds identified by other studies (García et al., 2019; Murphy et al., 2008; Yamashita et al., 2010). Murphy et al. (2006) suggested that the fluorescence characteristic of Compound-1 as an unknown compound and resembled contaminants in water.

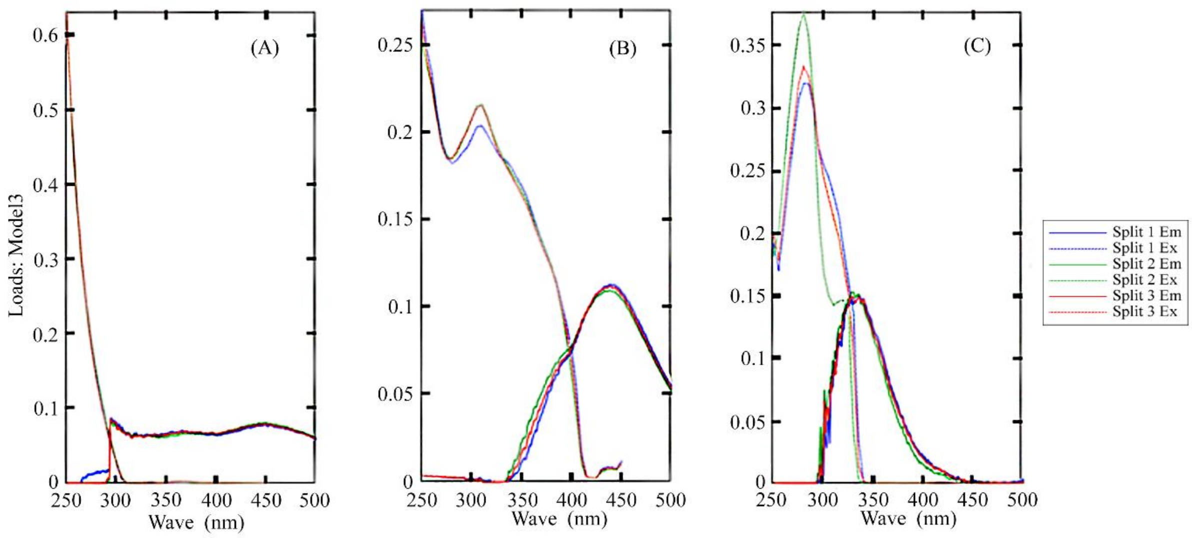

Figure 2. The validation of three-compounds identified by the split half method. Graphs (A-C) show the excitation and emission loadings for individual compound.

Previous studies (Borisover et al., 2011; D'Andrilli et al., 2019; Walker et al., 2009) have found that humic-like compounds were characterized at an excitation maximum of 370-390 nm and an emission maximum of 460-480 nm. Those characteristics closely resembled those found for compound-2 in this current study, suggesting compound-2 (C2) was likely representing humic from the terrestrial origin. The third compound (C3) has similar characteristics to the prior reported fluorescence peak for tryptophan-like compounds particularly tryptophan which were characterized at an excitation maximum of 275 nm and an emission maximum of 350 nm (Cawley et al., 2012; Osburn et al., 2011; Williams et al., 2013). The presence of tryptophan in the raw water was an indication of water contamination by anthropogenic activities (Baker, 2001; Bieroza et al., 2010; Yang et al., 2012). The contour plots of EEM for each compound can be seen in Figure 3.

As seen in Table 2, average COD concentrations during both seasons were above the maximum limit according the national standard (PP 82/2001) for COD concentration in the raw water source (10 mg/L), confirming the raw water source is in polluted condition. The observed COD value was higher than the COD concentration in Baitapuhe River which was considered aerobic (16.86±4.72 mg/L), but lower than the COD concentrations in Xihe River (60±15.73 mg/L) which was considered as anaerobic (Yu et al., 2016). The results, therefore, indicated Cikapundung River was polluted by organic matter but has not reached anaerobic state.

Table 2 also shows higher concentrations of organic aromatic compounds (A_{254}) in the dry season (0.35 cm^{-1}) than the rainy season (0.20 cm^{-1}) was consistent with the result for C1 and C2 quantity which was also greater during the dry season than the rainy season. However, in polluted raw water, this high value of A_{254} during the dry season might be associated with the high values of tryptophan which is also considered as aromatic tryptophan-like compound (Preuße et al., 2000; Stubbins et al., 2014). Therefore, although C2 decreases in the rainy season, the aromatic nature of C1 and C3 were also measured in A_{254}. The results indicate that measuring COD and CDOM (A_{254}) was insufficient to represent the organic presence in the raw water and may cause misinterpretation, leading to inappropriate approaches and strategies for drinking water treatment.

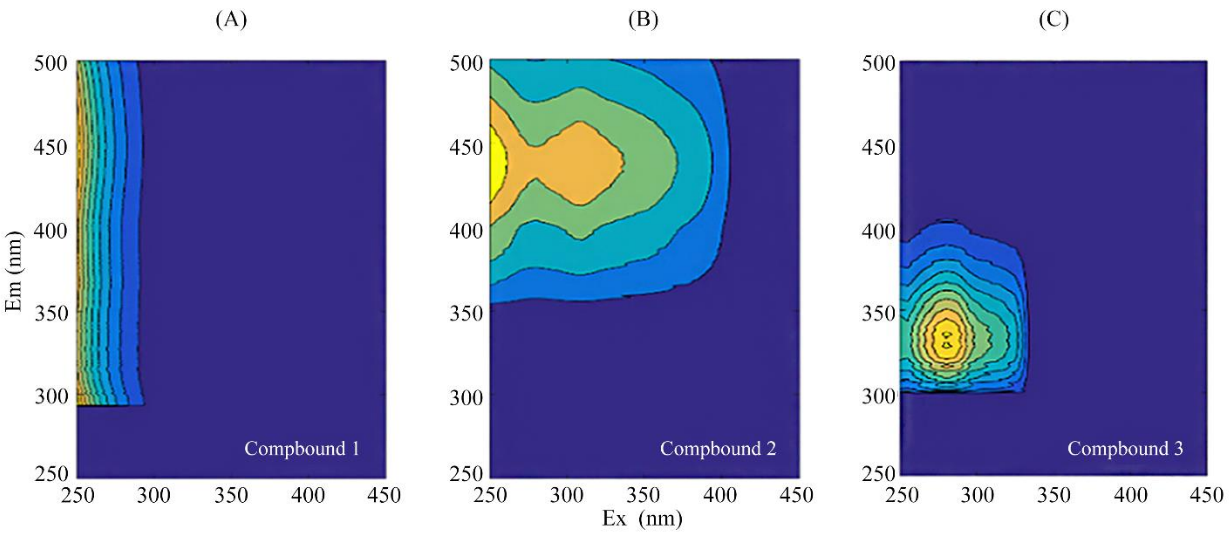

Figure 3. Contour plots of EEM for three valid compounds: (A) compound-1 (C1), (B) compound-2 (C2), and (C) compound-3 (C3) in the raw water samples (sampling period-1)

Table 2. The measured COD, A_{254} and Fmax of FDOM compounds in the dry and rainy seasons

Parameter	Dry (n=9)		Rainy (n=18)	
	Range	Mean±SD	Range	Mean±SD
COD (mg/L)	16.00-38.40	25.18±7.70	12.8-44.8	36.80±9.60
A_{254} (cm^{-1})*	0.21-0.48	0.35±0.08	0.16-0.25	0.20±0.04
C1 (RU)*	0.13-0.19	0.17±0.02	0,01-0,02	0.01±0.005
C2 (RU)	0.05-0.06	0.05±0.03	0,02-0,05	0.03±0.008
C3 (RU)*	0.05-0.14	0.08±0.03	0,01-0.03	0.01±0.008
C3/C2	-	1.60	-	0.33

* indicate there are differences between two seasons (sig<0.05)

There were seasonal variations in the concentrations of each FDOM compound in the raw water as indicated by the corresponding measured maximum intensity values (Fmax) (Table 1). Both the C2- and C3 compounds had maximum concentrations during the dry season. The tryptophan/humic ratio

(C3/C2) was 0.33 during the rainy season, and 1.60 during the dry season. The greater concentrations of the the C3 than C2 during the dry season were similar with those found in a polluted river in England (Baker et al., 2003), adding evidence for the bioavailability and microorganism activities decomposing wastewater in the upper stream of Cikapundung River. The results might be explained by continuous discharges of organic pollutants from anthropogenic activities into the water body throughout the year, but lacking dilution effect of the rainwater during the dry season. This fact added evidence of the consistent results between the identified compounds through PARAFAC and greater values of FI and BIX in the dry season.

The concentration of C2 in the rainy season, on the other hand, was higher than C3 as indicated by the lowest Fmax and both FI and BIX averages during this season. Higher concentrations of humic-like compound indicate that water comprises tannin, lignin, polyphenols and melanin from plants decay (Fellman et al., 2010). The dominance of the terrestial-derived compounds and the occurrence of rainfall during this season might suggest that soil origin-DOM entered the water body through the surface run-off. This higlights the importance of further studies on the dynamics of CDOM in conventional WTP treating raw water from Cikapundung River with differences in DOM composition during the rainy and dry seasons.

3.3 Correlations among PARAFAC components, CDOM absorption and COD

The results of correlation analysis between COD; A_{254} and each of identified FDOM compound during both seasons are summarized in Table 3. The results between A_{254} and each of FDOM compound ($p<0.001$, $R\geq0.60$) demonstrate that the content of aromatic compound well correlated with A_{254}. However, poor correlation between COD and A_{254} as well as between COD and each FDOM compound added evidence that the pollution level of Cikapundung River has not reached anaerobic condition. Yu et al. (2016) have reported good correlation between COD and DOM compound once the water body was in anaerobic condition. The contaminant-like (C1) and tryptophan-like (C3) compounds in the upper stream of Cikapundung River were most likely to be originated from the same anthropogenic activities as shown by strong correlation coefficient between C1 and C3 ($R=0.86$), as suggested by Hur and Cho (2012). The results of t-test also show that C1 significantly differed with C3 in both the dry and rainy seasons. The correlation between A_{254} and all compounds showed that these compounds have aromatic characteristic (Abbt-Braun et al., 2004; Du et al., 2012). Importantly, the observed strong correlation between A_{254} and all identified FDOM compounds suggest it would be inadequate to characterize organic compounds either based on COD or common CDOM parameter such as A_{254} in Cikapundung River. Further study is necessary to add evidence of the potential use of FI and BIX parameters for monitoring the quality of raw water as well as the use of EEM and PARAFAC for characterizing DOM compounds in urban raw water source such as Cikapundung River. This will provide more relevant information to determine appropriate and specific drinking water treatment strategy.

Table 3. Correlation Coefficients between organic compound parameter and identified FDOM compounds

Parameters	COD	A_{254}	C1	C2	C3
COD	1				
A_{254}	0.24	1			
C1	0.15	**0.82***	1		
C2	0.14	**0.69***	**0.80***	1	
C3	-0.08	**0.60***	**0.86***	**0.76***	1

* Significant correlation (p-value<0.01)

4. CONCLUSION

The presence of FDOM compounds in Cikapundung River during the dry season were due to microbial activities which indicate the anthropogenically impacted DOM in Cikapundung River as shown by FI=1.82, BIX=0.92. FDOM compounds were less impacted by anthropogenic activities during rainy season with FI=1.77, BIX=0.65. Identified FDOM compounds by PARAFAC were water contaminant-like (C1), humic-like (C2) and tryptophan-like (C3). C3 was the predominant compound during the dry season (C3/C2=1.60), and the main compound during rainy season was C2 with C3/C2=0.33. A_{254} was well correlated with all FDOM compounds ($R\geq0.60$, $p<0.01$), with the strongest correlation between C1 and A_{254} ($R>0.82$, $p<0.01$). C1 and C3 most likely originated from similar sources ($R=0.86$, $p<0.01$). Characterizing organic compounds solely based on COD and common CDOM parameter (A_{254}) was insufficient to determine the quantity of organic compounds present in surface water.

ACKNOWLEDGEMENTS

The authors would like to acknowledge the Lembaga Penelitian dan Pengabdian Masyarakat (Centre of Research and Community Development) of Institut Teknologi Nasional, Bandung for funding this research (Grant ID:365/B.05/LP2M-Itenas/V/2020), and Prama Setia Putra for the sincere assistance in the data analysis.

REFERENCES

Abbt-Braun G, Lankes U, Frimmel FH. Structural characterization of aquatic humic substances: The need for a multiple method approach. Aquatic Sciences 2004;66(2):151-70.

Abouleish MY, Wells MJ. Trihalomethane formation potential of aquatic and terrestrial fulvic and humic acids: Sorption on activated carbon. Science of The Total Environment 2015; 521:293-304.

American Public Health Association (APHA). Standard Methods for the Examination of Water and Wastewater. Washington DC, USA: American Public Health Association (APHA); 2005.

Awad J, Van Leeuwen J, Chow C, Drikas M, Smernik RJ, Chittleborough DJ, et al. Characterization of dissolved organic matter for prediction of trihalomethane formation potential in surface and sub-surface waters. Journal of hazardous materials 2016;308:430-9.

Baker A. Fluorescence excitation: Emission matrix characterization of some sewage-impacted rivers. Environmental Science and Technology 2001;35(5):948-53.

Baker A, Inverarity R, Charlton M, Richmond S. Detecting river pollution using fluorescence spectrophotometry: Case studies from the Ouseburn, NE England. Environmental Pollution 2003;124(1):57-70.

Bieroza M, Baker A, Bridgeman J. Fluorescence spectroscopy as a tool for determination of organic matter removal efficiency at water treatment works. Drinking Water Engineering and Science 2010;3(1):63-70.

Bieroza M, Baker A, Bridgeman J. Classification and calibration of organic matter fluorescence data with multiway analysis methods and artificial neural networks: An operational tool for improved drinking water treatment. Environmetrics 2011;22(3):256-70.

Borisover M, Laor Y, Saadi I, Lado M, Bukhanovsky N. Tracing organic footprints from industrial effluent discharge in recalcitrant riverine chromophoric dissolved organic matter. Water, Air, and Soil Pollution 2011;222(1-4):255-69.

Badan Pusat Statistika Kabupaten Bandung Barat (BPS KBB). Kecamatan Lembang Dalam Angka 2018. Bandung Barat, Indonesia: BPS KBB; 2019a.

Badan Pusat Statistika Kabupaten Bandung Barat (BPS KBB). Statistik Kesejahteraan Rakyat Kabupaten Bandung Barat 2017. Bandung Barat, Indonesia: BPS KBB; 2019b.

Cawley KM, Ding Y, Fourqurean J, Jaffé R. Characterising the sources and fate of dissolved organic matter in Shark Bay, Australia: A preliminary study using optical properties and stable carbon isotopes. Marine and Freshwater Research 2012;63(11):1098-107.

D'Andrilli J, Junker JR, Smith HJ, Scholl EA, Foreman CM. DOM composition alters ecosystem function during microbial processing of isolated sources. Biogeochemistry 2019;142(2):281-98.

Du E, Cao PR, Sun Y, Gao NY, Wang LP. Application of fluorescence excitation-emission matrices and parafac analysis for indicating the organic matter removal from micro-polluted raw water in water treatment plant. Fresenius Environmental Bulletin 2012;21:4030-9.

Environmental Protection Agency of West Java (EPA). West Java Environmental Performance Document 2019. Bandung, Indonesia: EPA; 2020.

Fellman JB, Hood E, Spencer RG. Fluorescence spectroscopy opens new windows into dissolved organic matter dynamics in freshwater ecosystems: A review. Limnology and Oceanography 2010;55(6):2452-62.

García PE, Queimaliños C, Diéguez MC. Natural levels and photo-production rates of hydrogen peroxide (H_2O_2) in Andean Patagonian aquatic systems: Influence of the dissolved organic matter pool. Chemosphere 2019;217:550-7.

Huguet A, Vacher L, Relexans S, Saubusse S, Froidefond JM, Parlanti E. Properties of fluorescent dissolved organic matter in the Gironde Estuary. Organic Geochemistry 2009; 40(6):706-19.

Hur J, Cho J. Prediction of BOD, COD, and total nitrogen concentrations in a typical urban river using a fluorescence excitation-emission matrix with PARAFAC and UV absorption indices. Sensors 2012;12(1):972-86.

Hur J, Nguyen HV-M, Lee B-M. Influence of upstream land use on dissolved organic matter and trihalomethane formation potential in watersheds for two different seasons. Environmental Science and Pollution Research 2014; 21(12):7489-500.

Jacangelo JG, DeMarco J, Owen DM, Randtke SJ. Selected processes for removing NOM: An overview. Journal - American Water Works Association 1995;87(1):64-77.

Jiang J, Zhang X, Zhu X, Li Y. Removal of intermediate aromatic halogenated DBPs by activated carbon adsorption: A new approach to controlling halogenated DBPs in chlorinated drinking water. Environmental Science and Technology 2017;51(6):3435-44.

Matilainen A, Sillanpää M. Removal of natural organic matter from drinking water by advanced oxidation processes. Chemosphere 2010;80(4):351-65.

McKnight DM, Boyer EW, Westerhoff PK, Doran PT, Kulbe T, Andersen DT. Spectrofluorometric characterization of dissolved organic matter for indication of precursor organic material and aromaticity. Limnology and Oceanography 2001;46(1):38-48.

Murphy KR, Butler KD, Spencer RG, Stedmon CA, Boehme JR, Aiken GR. Measurement of dissolved organic matter fluorescence in aquatic environments: an interlaboratory comparison. Environmental Science and Technology 2010;44(24):9405-12.

Murphy KR, Ruiz GM, Dunsmuir WT, Waite TD. Optimized parameters for fluorescence-based verification of ballast water exchange by ships. Environmental Science and Technology 2006;40(7):2357-62.

Murphy KR, Stedmon CA, Waite TD, Ruiz GM. Distinguishing between terrestrial and autochthonous organic matter sources in marine environments using fluorescence spectroscopy. Marine Chemistry 2008;108(1-2):40-58.

Ødegaard H, Østerhus S, Melin E, Eikebrokk B. NOM removal technologies-Norwegian experiences. Drinking Water Engineering and Science 2010;3(1):1-9.

Osburn CL, Wigdahl CR, Fritz SC, Saros JE. Dissolved organic matter composition and photoreactivity in prairie lakes of the US Great Plains. Limnology and Oceanography 2011; 56(6):2371-90.

Parlanti E, Wörz K, Geoffroy L, Lamotte M. Dissolved organic matter fluorescence spectroscopy as a tool to estimate biological activity in a coastal zone submitted to anthropogenic inputs. Organic Geochemistry 2000;31(12): 1765-81.

Preuße G, Friedrich S, Salzer R. Retention behavior of humic substances in reversed phase HPLC. Fresenius' Journal of Analytical Chemistry 2000;368(2-3):268-73.

Qadafi M, Notodarmojo S, Zevi Y, Maulana YE. Trihalomethane and haloacetic acid formation potential of tropical peat water: Effect of tidal and seasonal variations. International Journal of GEOMATE 2020;18(66):111-7.

Spencer RG, Hernes PJ, Ruf R, Baker A, Dyda RY, Stubbins A, et al. Temporal controls on dissolved organic matter and lignin biogeochemistry in a pristine tropical river, Democratic Republic of Congo. Journal of Geophysical Research: Biogeosciences 2010;115(G3):1-12.

Stedmon CA, Bro R. Characterizing dissolved organic matter fluorescence with parallel factor analysis: A tutorial. Limnology and Oceanography: Methods 2008;6(11):572-9.

Stubbins A, Lapierre JF, Berggren M, Prairie YT, Dittmar T, del Giorgio PA. What's in an EEM? Molecular signatures associated with dissolved organic fluorescence in boreal Canada. Environmental Science and Technology 2014; 48(18):10598-606.

Sururi MR, Notodarmojo S, Roosmini D, Putra PS, Maulana YE, Dirgawati M. An Investigation of a conventional water treatment plant in reducing dissolved organic matter and trihalomethane formation potential from a tropical river water source. Journal of Engineering and Technological Sciences 2020;52(2):271-88.

Sururi MR, Roosmini D, Notodarmojo S. Chromophoric and liability quantification of organic matters in the polluted rivers of Bandung watershed, Indonesia. Proceeding of The 2nd International Conference on Engineering and Technology for Sustainable Development (ICET4SD 2017); 2017 Sept 13-14; Yogjakarta: Indonesia; 2017.

Tang J, Li X, Cao C, Lin M, Qiu Q, Xu Y, et al. Compositional variety of dissolved organic matter and its correlation with water quality in peri-urban and urban river watersheds. Ecological Indicators 2019;104:459-69.

Vasyukova E, Uhl W, Braga F, Simoes C, Baylão T, Neder K. Drinking water production from surface water sources in the tropics: Brasília DF, Brazil. Environmental Earth Sciences 2012;65(5):1587-99.

Walker SA, Amon RM, Stedmon C, Duan S, Louchouarn P. The use of PARAFAC modeling to trace terrestrial dissolved organic matter and fingerprint water masses in coastal Canadian Arctic surface waters. Journal of Geophysical Research: Biogeosciences 2009;114(G4):1-12.

Williams CJ, Frost PC, Xenopoulos MA. Beyond best management practices: pelagic biogeochemical dynamics in urban stormwater ponds. Ecological Applications 2013; 23(6):1384-95.

Yamashita Y, Cory RM, Nishioka J, Kuma K, Tanoue E, Jaffé R. Fluorescence characteristics of dissolved organic matter in the deep waters of the Okhotsk Sea and the northwestern North Pacific Ocean. Deep Sea Research Part II: Topical Studies in Oceanography 2010;57(16):1478-85.

Yang L, Hong H, Guo W, Huang J, Li Q, Yu X. Effects of changing land use on dissolved organic matter in a subtropical river watershed, southeast China. Regional Environmental Change 2012;12(1):145-51.

Yang L, Kim D, Uzun H, Karanfil T, Hur J. Assessing trihalomethanes (THMs) and N-nitrosodimethylamine (NDMA) formation potentials in drinking water treatment plants using fluorescence spectroscopy and parallel factor analysis. Chemosphere 2015;121:84-91.

Ye Q, Zhang Z-T, Liu Y-C, Wang Y-H, Zhang S, He C, Wang J-J. Spectroscopic and molecular-level characteristics of dissolved organic matter in a highly polluted urban river in south China. ACS Earth and Space Chemistry 2019;3(9):2033-44.

Yu H, Song Y, Du E, Yang N, Peng J, Liu R. Comparison of PARAFAC components of fluorescent dissolved and particular organic matter from two urbanized rivers. Environmental Science and Pollution Research 2016; 23(11):10644-55.

Biosynthesis of Silver Nanoparticles Using Orange Peel Extract for Application in Catalytic Degradation of Methylene Blue Dye

Cathleen Simatupang[1], Vinod K Jindal[2], and Ranjna Jindal[1*]

[1]*Department of Civil and Environmental Engineering, Faculty of Engineering, Mahidol University, Nakhon Pathom 73170, Thailand*
[2]*Department of Chemical Engineering, Faculty of Engineering, Mahidol University, Nakhon Pathom 73170, Thailand*

ARTICLE INFO

Received: 12 May 2021
Received in revised: 8 Jul 2021
Accepted: 12 Jul 2021
Published online: 25 Aug 2021
DOI: 10.32526/ennrj/19/202100088

Keywords:
Biosynthesis/ Orange peel extract/ Silver nanoparticles/ Central composite design/ Methylene blue dye

*** Corresponding author:**
E-mail: ranjna.jin@mahidol.ac.th

ABSTRACT

Interest in the biosynthesis of silver nanoparticles (AgNPs) has been steadily increasing primarily due to their numerous applications in various fields, low-cost, use of non-toxic environmentally-friendly materials and easy implementation. This study focused on the biosynthesis of AgNPs using orange peel extract (OPE), optimization of process conditions, and application in catalytic degradation of methylene blue (MB) dye used in the textile industry. A central composite design in response surface methodology resulted in optimum conditions of 0.0075 g dry peel/mL for OPE concentration, pH of 11 and 1.5 mM silver nitrate concentration. The optimum conditions for the response variables corresponded to the peak absorbance of 0.79 and SPR wavelength of 403.8 nm in UV-vis spectra, and minimum particle size of 12.9 nm. In addition, peak absorbance and SPR wavelength appeared to be related to the size of the AgNPs. A full-factorial design for the catalytic degradation of MB dye by the biosynthesized AgNPs for 1 h indicated the maximum influence of AgNPs compared to the concentrations of MB dye and $NaBH_4$ in decreasing order. The MB dye was reduced rapidly with $NaBH_4$ in the presence of AgNPs due to their catalytic action. The findings of the study show the potential of OPE for the biosynthesis of AgNPs with excellent catalytic activity for the treatment of MB dye in industrial effluent.

1. INTRODUCTION

Dyes are a major class of synthetic organic compounds released by many industries including paper, plastic, leather, food, and cosmetics. (Husain, 2010; Zollinger, 1987). Methylene blue (MB) is widely used in manufacturing of paints and printing inks, paper and plastics (Nasuha et al., 2010). Dyes lead to the formation of harmful by-products in industrial wastewater that ultimately cause significant damage to the aquatic environment (Sabouri et al., 2020). Conventional water treatment methods are not very effective for the degradation of dyes due to their stable and complex structure. Therefore, new techniques are needed to remove such contaminants from the wastewater or convert them into harmless products.

Nanotechnology has attracted much interest due to the wide range of potential applications such as catalysis, imaging, biological product development, drug delivery, antimicrobial activity, and pollution prevention. (Khodadadi et al., 2017; Ndolomingo et al., 2020; Jamkhande et al., 2019). Among a large number of materials used in nanotechnology, silver nanoparticles (AgNPs) have gained prominence due to their excellent properties and good catalytic activity (Bhattarai et al., 2018; Rostami-Vartooni et al., 2016) and can be synthesized by physical, chemical, and biological methods (Xu et al., 2020; Shanmuganathan et al., 2019). Biological methods are considered superior to the physical and chemical methods due to their simplicity, low cost and eco-friendliness (Patil et al., 2012; Menon et al., 2019).

The biosynthesis of AgNPs using plant extracts both as reducing and stabilizing agents offers distinct advantages of nontoxicity, simplicity, and cost-effectiveness (Ahmad et al., 2019; Zhang et al., 2020). The effects of parameters such as plant extract concentration, silver nitrate ($AgNO_3$) concentration,

Citation: Simatupang C, Jindal VK, Jindal R. Biosynthesis of silver nanoparticles using orange peel extract for application in catalytic degradation of methylene blue dye. Environ. Nat. Resour. J. 2021;19(6):468-480. (https://doi.org/10.32526/ennrj/19/202100088)

temperature, and time on the biosynthesized AgNPs have been studied using the response surface methodology (RSM) (Heydari and Zaryabi, 2018; Biswas and Mulaba-Bafubiandi, 2016; Chinnasamy et al., 2017; Nikaeen et al., 2020).

The application of AgNPs in catalytic dye degradation has been reported in the presence of $NaBH_4$ (Bonnia et al., 2016; Indana et al., 2016; Saha et al., 2017; Suvith and Philip, 2014) and when used alone (Vanaja et al., 2014; Bhakya et al., 2015; Jyoti and Singh, 2016; Vidhu and Philip, 2014). The size of AgNPs appears to affect their catalytic activity in dye degradation (Suvith and Philip, 2014; Jana et al., 2000).

Orange is a popular citrus fruit product with a global production of about 48.8 million tons in 2015-2016 (Bátori et al., 2017). In Thailand, tangerine is the most important type of citrus fruit contributing about 76% of total production (Sethpakdee, 1997). Orange peels are rich in alcoholic compounds, flavonoids and proteins (Ozturk et al., 2018; Gupta et al., 2014) and thus orange peel extract (OPE) can reduce Ag^+ and stabilize AgNPs (Kaviya et al., 2011; Kahrilas et al., 2014; Saratale et al., 2018).

The information on the biosynthesis of AgNPs using OPE for catalytic degradation of MB dye based on the design of experiments in RSM, to our knowledge, has not been reported. Therefore, the overall objective of this study was to determine the optimum conditions for the biosynthesis of AgNPs with OPE using a central composite design (CCD) in RSM for application in catalytic degradation of MB dye. Subsequently, the relative significance of the process parameters in catalytic dye degradation was investigated using a full-factorial design.

2. METHODOLOGY

2.1 Orange peel extract preparation

Fresh orange peels were washed with distilled water, cut into small pieces, and oven dried at 93°C for 60 min. A blender was used to produce fine powder passing through a 20-mesh screen. A 5 g sample of dried peel was mixed with 100 mL of distilled water at 60ºC using a magnetic stirrer for 10 min. The peel extract was subsequently cooled, filtered and stored at 4°C until further use. The concentration of OPE was expressed as g dry peel/mL.

2.2 Biosynthesis of AgNPs

A 10 mM stock solution of $AgNO_3$ (analytical grade, Sigma-Aldrich) in deionized water (DI) and OPE with 0.05 g/mL concentration were prepared in advance, and diluted to produce AgNPs as needed. The pH of OPE was adjusted using 1 mM KOH solution prior to the addition of $AgNO_3$ solution and DI water according to the experimental design to make up the 20 mL volume. All experiments were carried out at room temperature under bright day light conditions.

2.3 AgNPs Characterization

The AgNPs in suspension were characterized by a UV-vis spectrophotometer (GENESYS 10s) in the 350-550 nm range for peak absorbance and characteristic surface plasmon resonance (SPR) wavelength. The baseline spectra were obtained for the OPE at specific concentrations used in the tests. A dilution factor of 50 was used to determine UV-vis spectra of all test samples. The size distribution of AgNPs was determined by dynamic light scattering (DLS) using Malvern Zetasizer 7 based on 10 repeated measurements.

2.4 Catalytic dye degradation

Stock solutions of 10 mM MB dye and 1 M $NaBH_4$ were prepared and diluted as needed. The chemicals used were of analytical grade. The dye degradation was investigated for 1 h in a 20 mL mixture prepared by adding MB dye, $NaBH_4$, AgNPs solutions and DI water based on the reduction in absorbance at a 663 nm wavelength in the UV-vis spectra using the following equation (Raj et al., 2020).

$$\text{Dye degradation (\%)} = \frac{A_0 - A_t}{A_0} \times 100\ \% \qquad (1)$$

Where; A_0 is absorbance of the MB dye solution at the start of experiment and A_t is the absorbance after reaction time t, respectively.

Additional experiments were performed to identify the individual and combined effects of 1 mM $NaBH_4$ and 1 mL AgNPs solutions on the reduction of 0.5 mM MB dye for 180 min by adjusting the sample volume to 20 mL with DI water.

2.5 Experimental design

In the biosynthesis of AgNPs, the independent variables included OPE concentration, $AgNO_3$ concentration, and pH, while AgNPs size, peak absorbance, and SPR wavelength represented response variables. A central composite design (CCD) with eight factorial, six axial and six center point experimental runs was used. The coded and actual values of independent variables and their levels are shown in Table 1.

In dye degradation, the effect of initial dye concentration, $NaBH_4$ concentration, and the volume of AgNPs solution was investigated using a full-factorial design with eight factorial and two center point experiments. Table 2 shows the coded and actual values of each variables.

Table 1. Coded and actual values of independent variables for the biosynthesis of AgNPs.

Variables	Coded levels				
	-1.682	-1	0	1	1.682
OPE conc. (X_1) (g/mL)	0.0008	0.0025	0.005	0.0075	0.0092
pH (X_2)	5.64	7	9	11	12.4
$AgNO_3$ conc. (X_3) (mM)	0.16	0.5	1	1.5	1.84

Table 2. Coded and actual values for dye degradation.

Variables	Coded levels		
	-1	0	1
Dye Conc. (X_1) (g/mL)	0.000031985	0.0001759	0.00031985
$NaBH_4$ (X_2) (mM)	1	5.5	10
AgNPs conc. (X_3) (mM)	0.1	0.5	0.9

All experiments were replicated twice and the mean value of the response was used in statistical analysis for developing the models.

2.6 Statistical analysis

A second-order polynomial model (Equation 2) was fitted to experimental data using regression analysis in MS Excel.

$$Y = \beta_0 + \sum_{i=1}^{3} \beta_i . X_i + \sum_{i=1}^{3} \beta_{ii} . X_i^2 + \sum_{i=1}^{2} \sum_{j=i+1}^{3} \beta_{ij} . X_i . X_j \quad (2)$$

Where; Y is the response variable; β_o is the constant, β_i, β_{ii}, and β_{ij} are coefficients; X_i, X_j are the independent variables. Subsequently, the optimum conditions for the biosynthesis of AgNPs were determined from the developed models using Excel Solver.

3. RESULTS AND DISCUSSION

3.1 Biosynthesis of AgNPs

Figures 1 and 2 present typical results from the biosynthesis of AgNPs using a 1.5 mM $AgNO_3$ solution, OPE concentration of 0.0075 g/mL, and pH of 11. The change of the solution color from yellowish to light brown within 15 to 30 min indicated the formation of nanoparticles (Figure 1). Similar findings have been reported in many studies (Jyoti and Singh, 2016; Saha et al., 2017). The change in color occurred due to the bioreduction of aqueous Ag^+ ions into AgNPs accompanied by SPR (Vanaja et al., 2014; Bonnia et al., 2016). In Figure 2, a plot of absorbance vs. wavelength shows the characteristic SPR wavelength peak for AgNPs at around 410 nm resulting in an intense change of color. Various experimental runs in CCD resulted in similar UV-vis spectra and exhibited a wide variation in peak absorbance and SPR wavelength. It has been reported that the SPR wavelength peak and width may be influenced by the changes in the size and shape of the nanoparticles (Evanoff and Chumanov, 2005; Wiley et al., 2006). In general, the size distributions of AgNPs based on the DLS analysis exhibited a unimodal peak (Figure 3) with average particle size in the range of 1-50 nm.

(a) (b)

Figure 1. Change in color of OPE after formation of colloidal AgNPs: (a) before; (b) after.

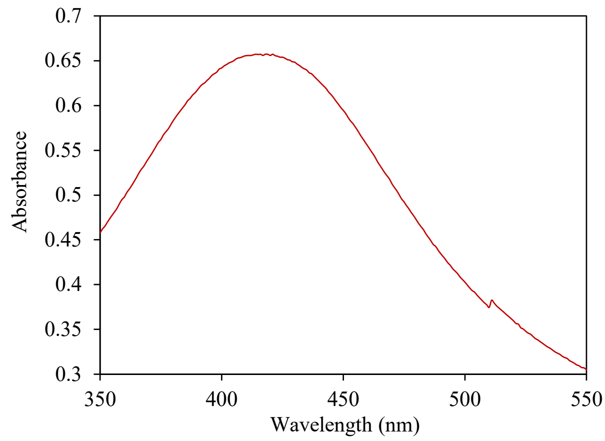

Figure 2. UV-visible absorbance spectrum of the biosynthesized AgNPs.

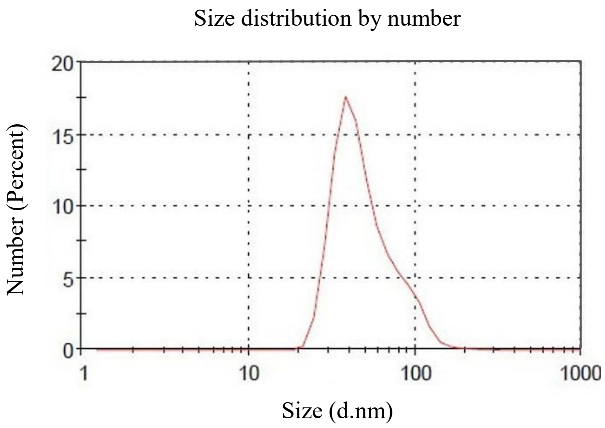

Figure 3. A typical plot of AgNPs size distribution from DLS (Malvern Zetasizer v7.02).

3.2 Models for biosynthesis of AgNPs based on CCD

Equations 3 to 5 present the regression models in coded units for the three response variables based on the experimental runs (Table 3). The coefficients of determination (R^2) for the developed models ranged from 0.735 to 0.923. The coefficients of the predictor terms in the developed models indicated their respective contributions for the estimation of response variables.

3.3 Model evaluation and optimization

Equations 3-5 indicated that among the indicator variables, pH had the most important effect on the biosynthesis of AgNPs. The contributions of interactions and quadratic terms were relatively small in all models. The influence of each independent variable on the normalized absorbance spectra was evaluated by considering its minimum and maximum values while keeping the other two independent variables at their mean values. An additional test in which all independent variables were set at their mean values was also included for comparison. Thus, sample nos. 9, 10, and 15 in Table 3 were selected for the OPE concentration. Figure 4 shows that a significant shift of SPR wavelength resulted towards red with a decrease in OPE concentration indicating the formation of larger AgNPs. In comparison, the change in normalized peak absorbance was relatively small.

The effect of pH on the biosynthesis of AgNPs (samples nos. 11, 12, and 15 in Table 3) is shown in Figure 5. A low pH of about 5.6 resulted in larger particle size and a higher pH of about 12.4 produced smaller AgNPs as indicated by the shift in SPR wavelength peaks (Figure 5). The pH has been reported to influence the size and shape of the AgNPs during biosynthesis due to the changes in binding and electrostatic repulsion ability of biomolecules present in the solution (Andreescu et al., 2007; Hasan et al., 2018) where high pH leads to the smaller nanoparticle sizes (Vanaja et al., 2014).

Likewise, the effect of $AgNO_3$ concentration was evaluated using sample nos. 13, 14, and 15 in Table 3 as shown in Figure 6. An increase in the $AgNO_3$ concentration resulted in a decrease of SPR wavelength from 438 to 430 nm and an increase in absorbance from 0.187 to 0.572 (Table 3), indicating the formation of smaller nanoparticles with a corresponding increase in their concentration.

The trends presented in Figures 4-6 and the corresponding experimental values in Table 3 indicate that increasing values of three process variables resulted in an increase in peak absorbance and a decrease in both SPR wavelength and nanoparticles size. Table 4 presents the optimum conditions for the biosynthesis of AgNPs as determined by the models (equations 3-5) resulting in maximum absorbance, minimum SPR wavelength and minimum particle size. The optimum conditions, based on overall considerations, included an OPE concentration of about 0.0075 g/mL, pH of 11 and $AgNO_3$ concentration of 1.5 mM for the biosynthesis of AgNPs to ensure maximum concentration of AgNPs based on the smallest particle size.

$$Y_1 = 0.432 + 0.067\,X_1 + 0.1178\,X_2 + 0.088\,X_3 - 0.0264\,X_1X_2 + 0.0246\,X_1X_3 + 0.0197X_2X_3 - 0.00057\,X_1^2 + 0.0461\,X_2^2 - 0.0064\,X_3^2 \quad (R^2=0.923) \tag{3}$$

$$Y_2 = 424.822 - 5.737\,X_1 - 8.849X_2 + 0.625X_3 + 0.25X_1X_2 + 0.75\,X_1X_3 + 0.75X_2X_3 - 2.996\,X_1^2 - 2.819X_2^2 + 1.2448\,X_3^2 \quad (R^2=0.735) \tag{4}$$

$$Y_3 = 32.0328 - 5.449\ X_1 - 14.59\ X_2 + 3.762\ X_3 - 0.444\ X_1X_2 - 5.637\ X_1X_3 + 1.720X_2X_3 + 4.282\ X_1^2 - 0.531\ X_2^2 - 2.249\ X_3^2\ \ (R^2=0.859) \quad (5)$$

Where; Y_1=peak absorbance, Y_2=SPR wavelength (nm), Y_3=AgNPs size (nm), X_1=OPE conc. (g/mL), X_2=pH, and X_3=$AgNO_3$ conc. (mM).

Table 3. Experimental and predicted values of response variables in biosynthesis of AgNPs.

Run No.	Coded variables			Absorbance		SPR wavelength (nm)		AgNPs size based on number (nm)	
	X_1	X_2	X_3	Expt.	Pred.	Expt.	Pred.	Expt.	Pred.
1	-1 -2.5	-1 -7	-1 -0.16	0.32	0.24	430	436	50.8	45.45
2	1 -7.5	-1 -11	-1 -1.5	0.34	0.33	414	422	46.19	46.71
3	-1 -2.5	1 -7	-1 -0.16	0.49	0.44	408	416	14.04	13.71
4	1 -7.5	1 -11	-1 -1.5	0.57	0.52	402	404	25.32	13.2
5	-1 -2.5	-1 -7	1 -0.16	0.33	0.33	428	434	48.43	60.81
6	1 -7.5	-1 -11	1 -1.5	0.53	0.52	424	424	38.93	39.52
7	-1 -2.5	1 -7	1 -0.16	0.66	0.61	418	418	36.21	35.95
8	1 -7.5	1 -11	1 -1.5	0.77	0.79	406	408	7.28	12.89
9	-1.68 -0.8	0 -9	0 -1	0.24	0.32	434	426	57.01	53.31
10	1.68 -9.2	0 -9	0 -1	0.55	0.55	410	407	31.64	34.98
11	0 -5	-1.68 -5.64	0 -1	0.34	0.37	440	432	59.78	55.07
12	0 -5	1.68 -12.4	0 -1	0.72	0.76	405	402	1.64	5.98
13	0 -5	0 -9	-1.68 -0.16	0.19	0.27	438	427	48.95	19.33
14	0 -5	0 -9	1.68 -1.84	0.57	0.57	430	429	42.76	31.99
15	0 -5	0 -9	0 -1	0.48	0.43	422	425	28.75	32.03
16	0 -5	0 -9	0 -1	0.46	0.43	415	425	33.26	32.03
17	0 -5	0 -9	0 -1	0.39	0.43	431	425	32.41	32.03
18	0 -5	0 -9	0 -1	0.43	0.43	425	425	29.44	32.03
19	0 -5	0 -9	0 -1	0.42	0.43	425	425	35.95	32.03
20	0 -5	0 -9	0 -1	0.44	0.43	429	425	32.3	32.03

*X_1 (mg/mL)=OPE conc.; X_2=pH; X_3=$AgNO_3$ conc. Actual values are shown in parentheses.

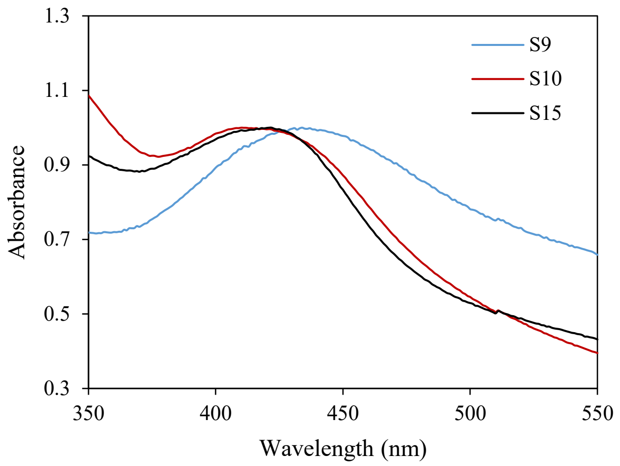

Figure 4. Absorbance spectra of AgNPs biosynthesized with different OPE concentration.

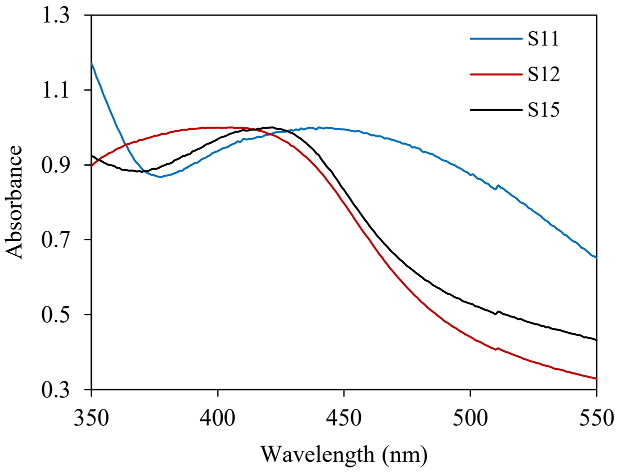

Figure 5. Absorbance spectra of AgNPs biosynthesized with different pH.

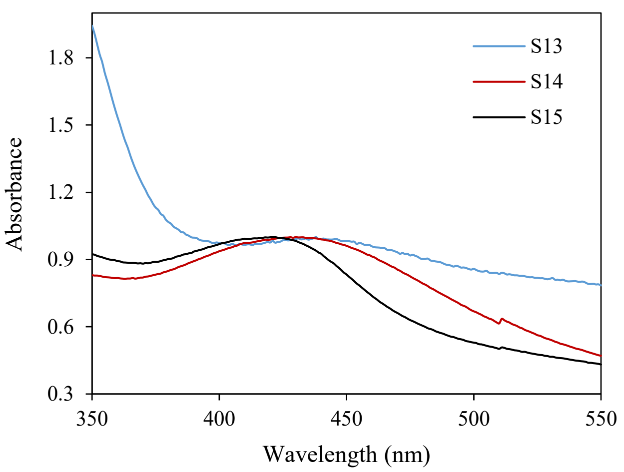

Figure 6. Absorbance spectra of AgNPs biosynthesized with different $AgNO_3$ concentration.

The optimum conditions for the biosynthesis of AgNPs using OPE reported in the literature are in the range of 1-4 mM $AgNO_3$ concentration and 4.5-9 pH to form particle sizes in 5- 46 nm range (Basavegowda and Lee, 2013; Kahrilas et al., 2014; De Barros Santos et al., 2015; Dutta et al., 2020; Saratale et al., 2018). The results obtained in this study (Table 4) appear to agree with the past studies and correspond to the smallest size of AgNPs and maximum concentration in solution.

3.4 Surface plots for particle size and peak absorbance for biosynthesis of AgNPs

The plot in Figure 7(a) shows peak absorbance as a function of OPE concentration and pH, with $AgNO_3$ concentration held constant at the mean value for AgNPs biosynthesis. An increase in both OPE concentration and pH resulted in an increase in the peak absorbance of AgNPs solution in the respective ranges of the experimental variables. Similar trends for the variation in peak absorbance were also observed in Figure 7(b) and Figure 7(c) for the effect of $AgNO_3$ concentration and pH, and $AgNO_3$ and OPE concentrations, respectively.

Table 4. Optimum conditions for the biosynthesis of AgNPs.

Response variable	Coded and actual values			Optimum value
	X_1	X_2	X_3	
Absorbance	1 (0.0075)	1 (11)	1 (1.5)	0.79
SPR wavelength (nm)	1 (0.0075)	1 (11)	-0.854 0.427	403.8
Mean particle size (nm)	1 (0.0075)	1 (11)	1 (1.5)	12.89

Figure 8 presents the effects of OPE concentration, pH and $AgNO_3$ concentration on the average size of AgNPs. The smallest particle size was produced at higher pH in combination with lower concentrations of OPE or $AgNO_3$ as shown in Figure 8 (a) and Figure 8 (b), respectively. However, lower concentrations of $AgNO_3$ and higher concentrations of OPE resulted in smaller nanoparticles size as shown in Figure 8 (c). The surface plots in Figures 7 and 8 clearly indicate that the process variables followed identical trends resulting in maximum absorbance and minimum nanoparticle size, respectively.

3.5 Relationship between peak absorbance, SPR wavelength and AgNPs size

Figures 9 and 10 present the mean size of biosynthesized AgNPs as a function of peak absorbance and SPR wavelength, respectively. As observed in Figures 9 and 10, a decrease in peak absorbance in association with an increase in the particle size or an increase in the SPR wavelength has been similarly reported in the literature (Gupta et al., 2002; Fleger and Rosenbluh, 2009). Thus a red-shift in SPR wavelength in UV-vis spectra indicates an increase in the size of AgNPs. Many empirical relationships for estimating the size of gold and AgNPs in colloidal suspension have been proposed for fast and easy characterization (Haiss et al., 2007; Ashkarran and Bayat, 2013; Dalal et al., 2019).

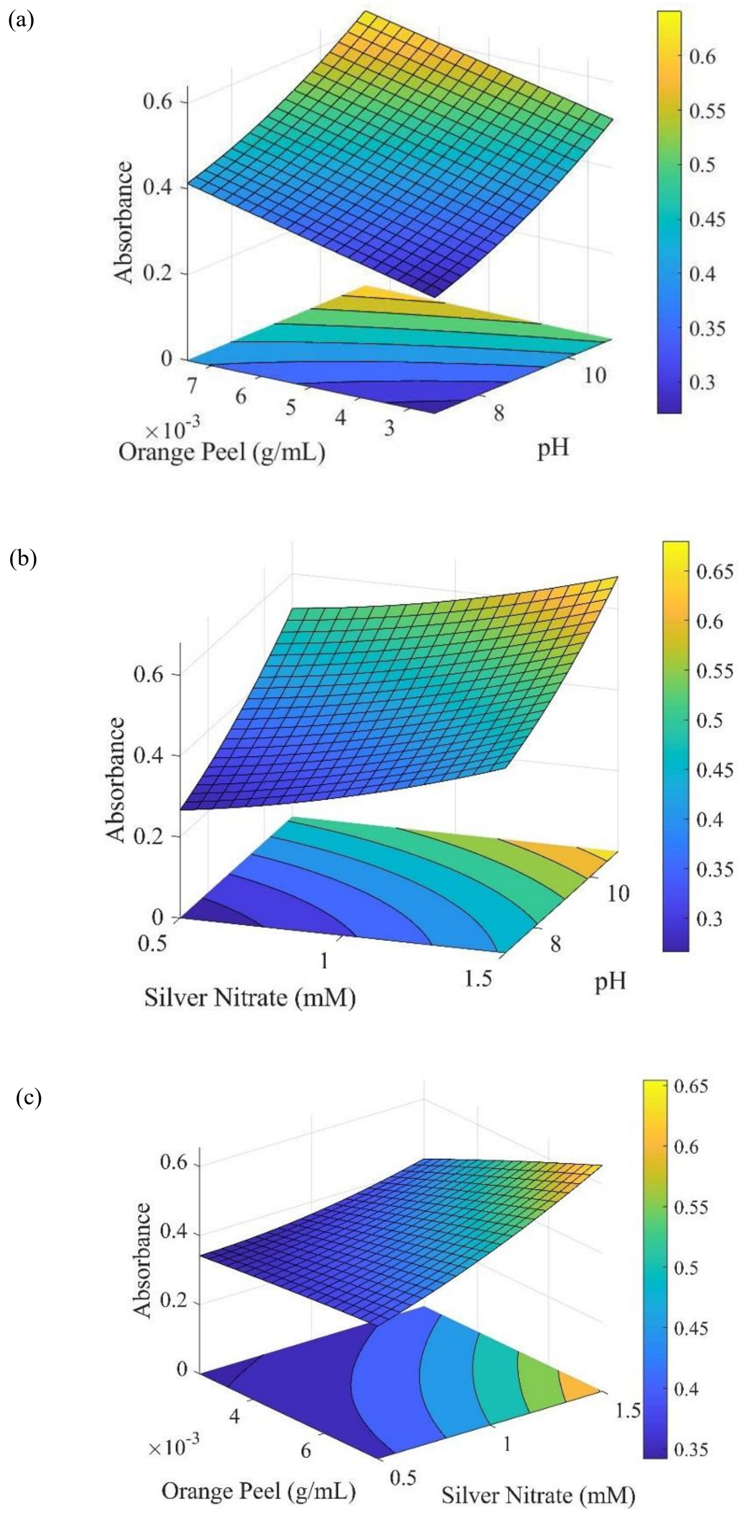

Figure 7. Surface plots showing absorbance as a function of OPE concentration and pH (a), $AgNO_3$ concentration and pH (b), and OPE concentration and $AgNO_3$ concentration (c).

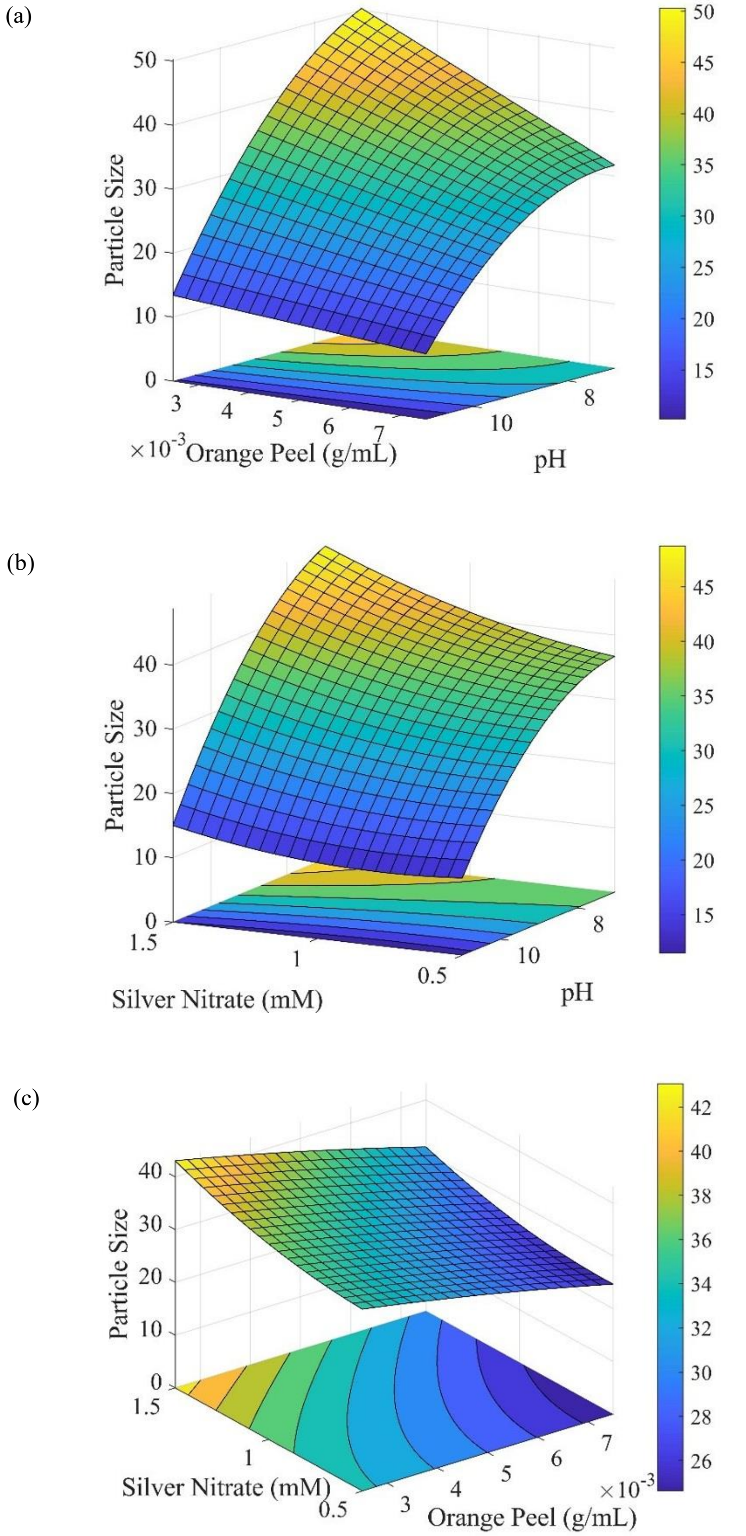

Figure 8. Surface plots showing AgNPs size as a function of OPE concentration and pH (a), $AgNO_3$ concentration and pH (b), and OPE concentration and $AgNO_3$ concentration (c).

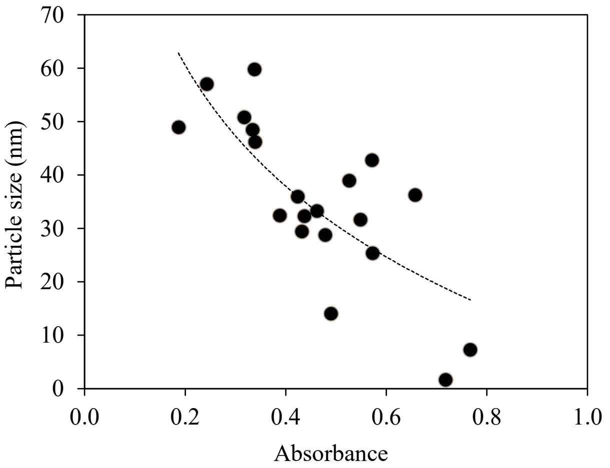

Figure 9. Relationship between AgNPs size and peak absorbance in UV-vis spectra.

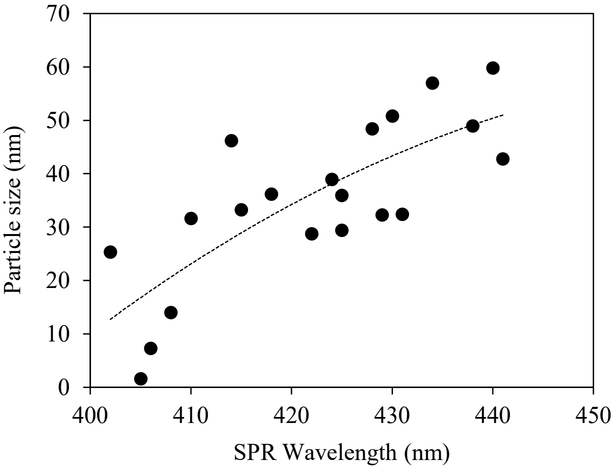

Figure 10. Relationship between AgNPs size and SPR wavelength in UV-vis spectra

3.6 Effect of AgNPs on MB dye reduction

There are many studies on the reduction of MB dye by $NaBH_4$ in the presence of AgNPs. However, the information on the relative significance of the individual concentrations of MB dye, $NaBH_4$ and AgNPs in catalytic dye reduction is not available.

Table 5 presents the results from a full-factorial experimental design for MB dye degradation by $NaBH_4$ and AgNPs. The following relationship was developed in coded units using Equation 2 without the inclusion of quadratic terms.

$$\text{Dye degradation (\%)} = 93.70 + 2.357 X_1 - 2.822 X_2 - 0.146 X_3 + 1.874 X_1X_2 + 0.920 X_1X_3 - 0.352 X_2X_3 \quad (R^2 = 0.89) \tag{6}$$

The coefficients in the fitted model (Equation 6) indicate the independent contributions of the main factors and their interactions in MB dye degradation and can be ranked from high to low as follows.

$$X_2 > X_1 > X_1X_2 > X_1X_3 > X_2X_3 > X_3$$

These results showed that AgNPs (X_2) contributed the most to catalytic MB dye degradation, followed by dye concentration (X_1) and their interactions (X_1X_2 and X_1X_3). In contrast, $NaBH_4$ (X_3) contributed the least with minor effects of its interaction with AgNPs (X_2) and dye concentration (X_1).

Figure 11 shows the pictorial view of MB dye degradation in 20 mL vials with an initial concentration of 0.5 mM in the presence of 1 mM $NaBH_4$ and 1 mL AgNPs solution. The MB dye changed from its natural state dark color to light blue in the first 5 min and turned light yellowish after about 50 min. However, the MB dye degradation without $NaBH_4$ under similar conditions showed only a slight visible change in the color of the MB dye even after a 180 min reaction time without AgNPs (Figure 12).

Table 5. Catalytic reduction of MB in presence of $NaBH_4$ and AgNPs.

RUN	Code			A_0	A_t=60 min	MB dye degradation	
	X_1	X_2	X_3			Expt. (%).	Pred. (%).
1	-1 (0.0319)	-1 (1)	-1 (0.1)	0.22	0.01	95.45	96.78
2	1 (0.319)	-1 (1)	-1 (0.1)	3.048	0.12	96.06	95.91
3	-1 (0.03190	1 (1)	-1 (0.1)	0.288	0.034	88.19	88.04
4	1 (0.319)	1 (1)	-1 (0.1)	2.115	0.141	93.33	94.66

*X_1(mg/mL) = MB dye conc.; X_2 = AgNPs; X_3 = $NaBH_4$ conc.

Table 5. Catalytic reduction of MB in presence of $NaBH_4$ and AgNPs (cont.).

RUN	Code			A_0	A_t=60 min	MB dye degradation	
	X_1	X_2	X_3			Expt. (%).	Pred. (%).
5	-1 (0.0319)	-1 (1)	1 (0.9)	0.264	0.012	95.45	95.3
6	1 (0.319)	-1 (1)	1 (0.9)	2.793	0.09	96.78	98.11
7	-1 (0.0319)	1 (10)	1 (0.9)	0.224	0.036	83.93	85.26
8	1 (0.319)	1 (10)	1 (0.9)	2.987	0.128	95.71	95.56
9	0 (0.1759)	0 (5.5)	0 (0.5)	1.651	0.067	95.94	93.7
10	0 (0.1759)	0 (5.5)	0 (0.5)	1.721	0.066	96.17	93.7

*X_1(mg/mL) = MB dye conc.; X_2 = AgNPs; X_3 = $NaBH_4$ conc.

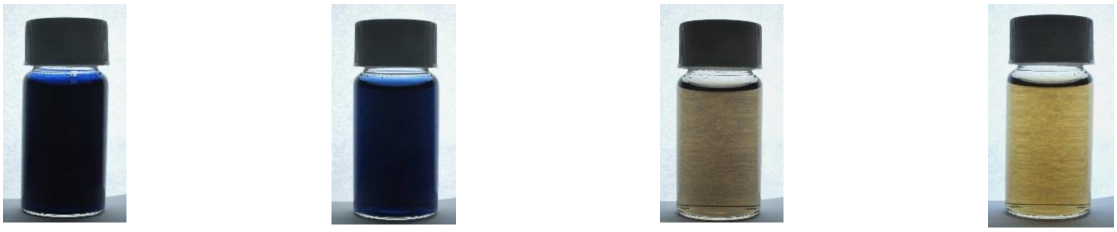

t=0 min t=5 min t=20 min t=50 min

Figure 11. Change in color during MB dye degradation in presence of $NaBH_4$.

t=0 min t=5 min t=30 min t=180 min

Figure 12. Change in color during MB dye degradation in absence of $NaBH_4$.

The pictorial trends for dye degradation in Figures 11 and 12 are presented quantitatively in Figure 13. Though there was a sharp reduction in dye concentration initially when using the AgNPs alone, the addition of $NaBH_4$ further expedited the dye reduction process.

A rapid degradation of MB dye within 2-10 min has been reported with the addition of AgNPs in a mixture of MB dye and $NaBH_4$ (Indana et al., 2016; Saha et al., 2017). On the other hand, longer times were needed for MB dye degradation in the absence of $NaBH_4$ (Santhanalakshmi and Venkatesan, 2011; Vanaja et al., 2014). Several studies have indicated that catalytic degradation of MB dye takes place at the surface of AgNPs (Vidhu and Philip, 2014; Jyoti and Singh, 2016; Saha et al., 2017). AgNPs act as an efficient catalyst through the electron transfer between $NaBH_4$ acting as a donor and MB dye as acceptor. Thus, the reduction of MB dye by $NaBH_4$ increases in the presence of AgNPs. In addition, the smaller size of AgNPs may promote the catalytic activity due to the availability of large surface area (Suvith and Philip, 2014; Bonnia et al., 2016).

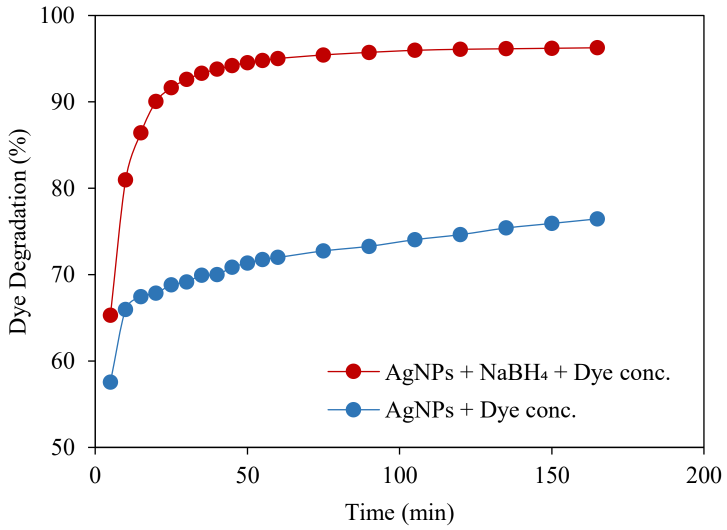

Figure 13. Catalytic MB dye degradation with time in presence of AgNPs and $NaBH_4$.

4. CONCLUSION

The biosynthesis of AgNPs could be carried out using OPE without requiring toxic chemicals. Models based on the CCD in RSM identified the effects of OPE concentration, pH and $AgNO_3$ concentration on the peak absorbance and SPR wavelength in UV-vis spectra, and particle size as response variables. The pH had the maximum influence on the formation of AgNPs compared to the OPE and $AgNO_3$ concentration. The optimum conditions (OPE concentration of 0.0075 g/mL, pH of 11 and $AgNO_3$ concentration of 1.5 mM) resulted in the mean particle size, SPR wavelength and absorbance of about 12.9 nm, 403.8 nm and 0.79, respectively. AgNPs had a major influence on the MB dye degradation compared to the initial dye concentration and $NaBH_4$. This was confirmed by the quick discoloration of MB dye by AgNPs alone and in combination with $NaBH_4$. Results showed that AgNPs biosynthesized by OPE offer an inexpensive and eco-friendly treatment method for catalytic reduction of MB dye in industrial effluent.

ACKNOWLEDGEMENTS

The authors would like to express their sincere appreciation to the Department of Civil and Environmental Engineering, Faculty of Engineering, Mahidol University, Salaya campus for making available the laboratory facilities.

REFERENCES

Ahmad S, Munir S, Zeb N, Ullah A, Khan B, Ali J, et al. Green nanotechnology: A review on green synthesis of silver nanoparticles - an ecofriendly approach. International Journal of Nanomedicine 2019;14:5087-107.

Andreescu D, Eastman C, Balantrapu K, Goia DV. A simple route for manufacturing highly dispersed silver nanoparticles. Journal of Materials Research 2007;22(9):2488-96.

Ashkarran AA, Bayat A. Surface plasmon resonance of metal nanostructures as a complementary technique for microscopic size measurement. International Nano Letters 2013;3:50.

Basavegowda N, Lee YR. Synthesis of silver nanoparticles using Satsuma mandarin (*Citrus unshiu*) peel extract: A novel approach towards waste utilization. Materials Letters 2013; 109:31-3.

Bátori V, Jabbari M, Åkesson D, Lennartsson PR, Taherzadeh MJ, Zamani A. Production of pectin-cellulose biofilms: A new approach for citrus waste recycling. International Journal of Polymer Science 2017;2017:9732329.

Bhakya S, Muthukrishnan S, Sukumaran M, Muthukumar M, Kumar ST, Rao MV. Catalytic degradation of organic dyes using synthesized silver nanoparticles: A green approach. Journal of Bioremediation and Biodegredation 2015;6(5): 1000312.

Bhattarai B, Zaker Y, Bigioni TP. Green synthesis of gold and silver nanoparticles: Challenges and opportunities. Current Opinion in Green and Sustainable Chemistry 2018;12:91-100.

Biswas S, Mulaba-Bafubiandi AF. Optimization of process variables for the biosynthesis of silver nanoparticles by *Aspergillus wentii* using statistical experimental design. Advances in Natural Sciences: Nanoscience and Nanotechnology 2016;7(4):045005.

Bonnia NN, Kamaruddin MS, Nawawi MH, Ratim S, Azlina HN, Ali ES. Green biosynthesis of silver nanoparticles using 'Polygonum Hydropiper' and study its catalytic degradation of methylene blue. Procedia Chemistry 2016;19:594-602.

Chinnasamy C, Tamilselvam P, Karthik V, Karthick B. Optimization, and characterization studies on green synthesis of silver nanoparticles using response surface methodology. Advances in Natural and Applied Sciences 2017;11(4): 214-22.

Dalal N, Boruah BS, Neoh A, Biswas R. Correlation of surface plasmon resonance wavelength (SPR) with size and concentration of noble metal nanoparticles. Annals of Reviews and Research 2019;5(2):555658.

De Barros Santos E, Madalossi NV, Sigoli FA, Mazali IO. Silver nanoparticles: Green synthesis, self-assembled nanostructures, and their application as SERS substrates. New Journal of Chemistry 2015;39(4):2839-46.

Dutta T, Chattopadhyay AP, Ghosh NN, Khatua S, Acharya K, Kundu S, et al. Biogenic silver nanoparticle synthesis and stabilization for apoptotic activity; insights from experimental and theoretical studies. Chemical Papers 2020;74:4089-101.

Evanoff Jr DD, Chumanov G. Synthesis and optical properties of silver nanoparticles and arrays. ChemPhysChem 2005;6(7): 1221-31.

Fleger Y, Rosenbluh M. Surface plasmons and surface enhanced Raman spectra of aggregated and alloyed gold-silver nanoparticles. Research Letters in Optics 2009;2009:475941.

Gupta R, Dyer MJ, Weimer WA. Preparation and characterization of surface plasmon resonance tunable gold and silver films. Journal of Applied Physics 2002;92(9):5264-71.

Gupta M, Gularıa P, Sıngh D, Gupta S. Analysis of aroma active constituents, antioxidant, and antimicrobial activity of *C. sinensis*, *Citrus limetta* and *C. limon* fruit peel oil by GC-MS. Bioscıences Biotechnology Research Asia 2014;11(2):895-9.

Haiss W, Thanh NT, Aveyard J, Fernig DG. Determination of size and concentration of gold nanoparticles from UV-Vis spectra. Analytical Chemistry 2007;79(11):4215-21.

Hasan M, Ullah I, Zulfiqar H, Naeem K, Iqbal A, Gul H, et al. Biological entities as chemical reactors for synthesis of nanomaterials: Progress, challenges, and future perspective. Materials Today Chemistry 2018;8:13-28.

Heydari S, Zaryabi MH. Response surface methodology for optimization of green silver nanoparticles synthesized via *Phlomis cancellata* bunge extract. Analytical and Bioanalytical Chemistry Research 2018;5(2):373-86.

Husain Q. Peroxidase mediated decolorization and remediation of wastewater containing industrial dyes: A review. Reviews in Environmental Science and Bio/Technology 2010;9(2):117-40.

Indana MK, Gangapuram BR, Dadigala R, Bandi R, Guttena V. A novel green synthesis and characterization of silver nanoparticles using gum tragacanth and evaluation of their potential catalytic reduction activities with methylene blue and Congo red dyes. Journal of Analytical Science and Technology 2016;7(1):1-9.

Jana NR, Wang ZL, Pal T. Redox catalytic properties of palladium nanoparticles: Surfactant and electron donor-acceptor effects. Langmuir 2000;16(6):2457-63.

Jamkhande PG, Ghule NW, Bamer AH, Kalaskar MG. Metal nanoparticles synthesis: An overview on methods of preparation, advantages and disadvantages, and applications. Journal of Drug Delivery Science and Technology 2019; 53:101174.

Jyoti K, Singh A. Green synthesis of nanostructured silver particles and their catalytic application in dye degradation. Journal of Genetic Engineering and Biotechnology 2016; 14(2):311-7.

Kahrilas GA, Wally LM, Fredrick SJ, Hiskey M, Prieto AL, Owens JE. Microwave-assisted green synthesis of silver nanoparticles using orange peel extract. ACS Sustainable Chemistry and Engineering 2014;2(3):367-76.

Kaviya S, Santhanalakshmi J, Viswanathan B, Muthumary J, Srinivasan K. Biosynthesis of silver nanoparticles using citrus sinensis peel extract and its antibacterial activity. Spectrochimica Acta Part A: Molecular and Biomolecular Spectroscopy 2011;79(3):594-8.

Khodadadi B, Bordbar M, Nasrollahzadeh M. *Achillea millefolium* L. extract mediated green synthesis of waste peach kernel shell supported silver nanoparticles: Application of the nanoparticles for catalytic reduction of a variety of dyes in water. Journal of Colloid and Interface Science 2017;493:85-93.

Menon S, KS SD, Agarwal H, Shanmugam VK. Efficacy of biogenic selenium nanoparticles from an extract of ginger towards evaluation on anti-microbial and antioxidant activities. Colloid and Interface Science Communications 2019;29:1-8.

Nasuha N, Hameed BH, Din AT. Rejected tea as a potential low-cost adsorbent for the removal of methylene blue. Journal of Hazardous Materials 2010;175(1-3):126-32.

Ndolomingo MJ, Bingwa N, Meijboom R. Review of supported metal nanoparticles: Synthesis methodologies, advantages, and application as catalysts. Journal of Materials Science 2020;55(15):6195-241.

Nikaeen G, Yousefinejad S, Rahmdel S, Samari F, Mahdavinia S. Central composite design for optimizing the biosynthesis of silver nanoparticles using plantago major extract and investigating antibacterial, antifungal and antioxidant activity. Scientific Reports 2020;10(1):1-6.

Ozturk B, Parkinson C, Gonzalez-Miquel M. Extraction of polyphenolic antioxidants from orange peel waste using deep eutectic solvents. Separation and Purification Technology 2018;206:1-13.

Patil RS, Kokate MR, Kolekar SS. Bioinspired synthesis of highly stabilized silver nanoparticles using *Ocimum tenuiflorum* leaf extract and their antibacterial activity. Spectrochimica Acta Part A: Molecular and Biomolecular Spectroscopy 2012; 91:234-8.

Raj S, Singh H, Trivedi R, Soni V. Biogenic synthesis of AgNPs employing *Terminalia arjuna* leaf extract and its efficacy towards catalytic degradation of organic dyes. Scientific Reports 2020;10:9616.

Rostami-Vartooni A, Nasrollahzadeh M, Alizadeh M. Green synthesis of seashell supported silver nanoparticles using *Bunium persicum* seeds extract: Application of the particles for catalytic reduction of organic dyes. Journal of Colloid and Interface Science 2016;470:268-75.

Sabouri MR, Sohrabi MR, Moghaddam AZ. A novel and efficient dyes degradation using bentonite supported zero-valent iron-based nanocomposites. Chemistry Select 2020;5(1):369-78.

Saha J, Begum A, Mukherjee A, Kumar S. A novel green synthesis of silver nanoparticles and their catalytic action in reduction of methylene blue dye. Sustainable Environment Research 2017; 27(5):245-50.

Santhanalakshmi J, Venkatesan P. Mono and bimetallic nanoparticles of gold, silver and palladium-catalyzed NADH oxidation-coupled reduction of Eosin-Y. Journal of Nanoparticle Research 2011;13(2):479-90.

Saratale RG, Shin HS, Kumar G, Benelli G, Ghodake GS, Jiang YY, et al. Exploiting fruit byproducts for eco-friendly nanosynthesis: *Citrus × clementina* peel extract mediated fabrication of silver nanoparticles with high efficacy against microbial pathogens and rat glial tumor C6 cells. Environmental Science and Pollution Research 2018; 25(11):10250-63.

Sethpakdee R. Citrus production in Thailand. Taipei: Food and Fertilizer Technology Center; Extension Bulletin No. 437 [Internet]. 1997 [cited 2021 Jan 20]. Available from: http://swfrec.ifas.ufl.edu/hlb/database/pdf/00001303.pdf.

Shanmuganathan R, Karuppusamy I, Saravanan M, Muthukumar H, Ponnuchamy K, Ramkumar VS, et al. Synthesis of silver nanoparticles and their biomedical applications: A comprehensive review. Current Pharmaceutical Design 2019; 25(24):2650-60.

Suvith VS, Philip D. Catalytic degradation of methylene blue using biosynthesized gold and silver nanoparticles. Spectrochimica Acta Part A: Molecular and Biomolecular Spectroscopy 2014;118:526-32.

Vanaja M, Paulkumar K, Baburaja M, Rajeshkumar S, Gnanajobitha G, Malarkodi C, et al. Degradation of methylene blue using biologically synthesized silver nanoparticles. Bioinorganic Chemistry and Applications 2014;2014:742346.

Vidhu VK, Philip D. Catalytic degradation of organic dyes using biosynthesized silver nanoparticles. Micron 2014;56:54-62.

Wiley BJ, Im SH, Li ZY, McLellan J, Siekkinen A, Xia Y. Maneuvering the surface plasmon resonance of silver nanostructures through shape-controlled synthesis. Journal of Physical Chemistry B 2006;110(32):15666-75.

Xu L, Wang YY, Huang J, Chen CY, Wang ZX, Xie H. Silver nanoparticles: Synthesis, medical applications, and biosafety. Theranostics 2020;10(20):8996-9031.

Zhang D, Ma XL, Gu Y, Huang H, Zhang GW. Green synthesis of metallic nanoparticles and their potential applications to treat cancer. Frontiers in Chemistry 2020;8:799.

Zollinger H. Color Chemistry: Syntheses, Properties, and Applications of Organic Dyes and Pigments. New York, USA: Wiley-VCH; 1987.

GIS-Based Flood Susceptibility Mapping Using Statistical Index and Weighting Factor Models

Worawit Suppawimut*

Department of Geography, Faculty of Humanities and Social Sciences, Chiang Mai Rajabhat University, Thailand

ARTICLE INFO

Received: 12 May 2021
Received in revised: 8 Jul 2021
Accepted: 12 Jul 2021
Published online: 25 Aug 2021
DOI: 10.32526/ennrj/19/2021003

Keywords:
Flood susceptibility/ Hazard mapping/ Statistical index/ San Pa Tong District/ Bivariate statistics

*** Corresponding author:**
E-mail: worawit_sup@cmru.ac.th

ABSTRACT

Floods are one of the most devastating natural hazards, causing deaths, economic losses, and destruction of property. Flood susceptibility maps are an essential tool for flood mitigation and preparedness planning. This study mapped flood susceptibility using statistical index (SI) and weighting factor (WF) models in San Pa Tong District, Chiang Mai Province, Thailand. The conditioning factors used to perform flood susceptibility mapping were elevation, slope, aspect, curvature, topographic wetness index, stream power index, rainfall, distance from rivers, stream density, soil drainage, land use, and road density. The flood data were randomly classified as training data for mapping (70% of data) and testing data for model validation (30% of data). The results revealed that the SI and WF models classified 49.49% and 51.74% of the study area, respectively, as very highly susceptible to flooding. In the WF model, the factors with the greatest influence were land use, soil drainage, and elevation. The validation of the models using the area under the curve revealed that the success rates of the SI and WF models were 91.80% and 93.06%, while the prediction rates were 92.05% and 93.52%, respectively. The results from this study can be useful for local authorities in San Pa Tong District for flood preparedness and mitigation.

1. INTRODUCTION

Flooding is the most devastating category of natural disaster, affecting people and properties around the world (Paul et al., 2019; Samanta et al., 2018), with an average of 71.9 million people reported as affected by flooding annually (CRED, 2020). In the monsoon-dominated tropical and subtropical regions of the world, flooding occurs frequently and across wide areas (Khaing et al., 2021). In Asia, flooding is one of the most destructive natural disasters, with the highest proportion (79.9%) of the total population affected by floods globally (CRED, 2020). In Thailand, floods are one of the most destructive natural disasters. In 2011, the country suffered the worst floods in more than half a century; these floods inundated more than six million hectares of land in 66 provinces and affected more than 13 million people. The estimated damage and losses totaled approximately USD 46.5 billion (World Bank, 2012).

Flood occurrence is affected by various factors. Heavy rainfall is one of the main factors, leading to the rapid accumulation and release of runoff waters from upstream to downstream areas (Kongmuang et al., 2020). Climate change also causes flood occurrences with rising frequency and magnitude (Khaing et al., 2021; Tehrany et al., 2019), while human activities such as urbanization and deforestation can also increase flooding incidence rates (Cabrera et al., 2019; Paul et al., 2019). In flood-prone areas, flood risk can be assessed to prevent damage to residential areas, agriculture, public properties, etc. (Paul et al., 2019; Samanta et al., 2018). Flood susceptibility mapping is an essential tool for flood preparedness and mitigation, in particular, planning using reliable information can help support communities and government authorities to precisely implement flood protection strategies.

Various approaches have been applied for flood susceptibility mapping. Hydrological models have been developed by various researchers such as SWAT (Igarashi et al., 2019) and HEC-RAS (Khaing et al., 2021; Rahmati et al., 2016). Although hydrological model can predict and simulate flood hazard, there are

Citation: Suppawimut W. GIS-based flood susceptibility mapping using statistical index and weighting factor models. Environ. Nat. Resour. J. 2021;19(6):481-493. (https://doi.org/10.32526/ennrj/19/2021003)

some limitations such as the requirement of vast data budget, unavailability of large-scale data and time consuming for preparation and calibration of parameters (Cabrera et al., 2019; Hoang et al., 2020). In the few past decades, geographic information system (GIS) and remote sensing (RS) have made remarkable contributions in flood hazard mapping (Rahmati et al., 2016; Samanta et al., 2018). Several techniques have been applied with GIS and RS, including analytical hierarchy process (AHP) (Hoang et al., 2020; Khaing et al., 2021; Rahmati et al., 2016), frequency ratio (FR) (Anucharn, 2019; Cao et al., 2016; Samanta et al., 2018; Tehrany et al., 2019), logistic regression (LR) (Tehrany et al., 2019), weight of evidence (WoE) (Tehrany et al., 2017), statistical index (SI) (Cao et al., 2016; Khosravi et al., 2016; Tehrany et al., 2019), and artificial neural network (ANN) (Anucharn, 2019; Kia et al., 2012). The results of the research mentioned above, demonstrate slightly variance from place to place and each type of model is still necessary to be examined. Thus, testing and valuation of these models can provide optimal and more reliable results.

Statistical index (SI) modeling has been applied to various hazard mapping efforts and has performed efficiently with acceptable results (Khosravi et al., 2016). It has been widely used in mapping landslide susceptibility (Budha et al., 2016; Pourghasemi et al., 2013) and has also been applied to flood susceptibility mapping (Khosravi et al., 2016; Tehrany et al., 2019). However, the main limitation of SI is the lack of consideration of the relationship between the causative factors themselves which needs further research. The weighting factor (WF) method has been applied widely in the field of landslide studies (Yalcin, 2008), however, its use is still lacking in the field of flood susceptibility mapping (Khosravi et al., 2016). Additionally, some causative factors have not been applied to the WF model to measure their impact on flood occurrence such as aspect and road density. Given this context, a comparative study of the SI and WF models may contribute to the assessment of flood susceptibility.

This research, therefore, aimed to perform flood susceptibility mapping of the San Pa Tong District, Chiang Mai, which suffered from flooding in 2005, 2009, 2010, and 2011, by applying SI and WF models and to examine the performance of these two models. This research also aimed to find the most influential factors for flood occurrence in the study area. The study results can be useful for local administrators to minimize the consequences of future floods, and, furthermore, these research methods can provide guidelines for further research.

2. METHODOLOGY

2.1 Study area

The study area is the San Pa Tong District, Chiang Mai Province, in northern Thailand. It is located between latitudes 18°30′ and 18°43′ N and longitudes 98°48′ and 98°57′E, covering an area of approximately 173.45 km^2 (Figure 1). The altitude ranges between 239 m and 640 m above sea level, with a mountainous area in the north and lowlands covering the central and the southern parts of the area. There are three main rivers in San Pa Tong, namely the Ping River, Khan River, and Mae Wang River. Due to the area's topographic and hydrological characteristics, San Pa Tong is flood-prone and has been frequently affected by floods. The main causes of flooding in the area are the high intensity of rainfall and runoff from the upper catchments flowing to the lower areas in the south. Regarding the flood data of 2005, 2009, 2010, and 2011, 59.49 km^2 of San Pa Tong has been recorded as a flooded area (Suppawimut, 2020). In this context, the San Pa Tong District was, therefore, selected as the study area.

2.2 Data collection

The historic flood data was collected from multi-source satellite imagery from 2005 to 2019 including RADARSAT, COSMO, and THAICHOTE, operated by the Geo-Informatics and Space Technology Development Agency (GISTDA). In this study, the flood inventory was prepared based on the floods that occurred in 2005, 2009, 2010, and 2011. Flood raster data were randomly classified as training data (70%) and testing data (30%) (Figures 2 and 3). The conditioning factor data were acquired from secondary data sources and government organizations. The digital elevation model (DEM) data were derived from the Advanced Spaceborne Thermal Emission and Reflection Radiometer (ASTER) with 30 m × 30 m resolution and was obtained from the Earthdata website (https://earthdata.nasa.gov). The DEM was used to extract the topographic factors, namely slope, aspect, curvature, topographic wetness index (TWI), and stream power index (SPI). The other sources of data were as follows: rainfall data from the Upper Northern Region Irrigation Hydrology Center; land use data of 2018 and soil drainage data from the Land Development Department; road data from Nostra Map; and river and stream data derived from 1:50,000 topographic maps.

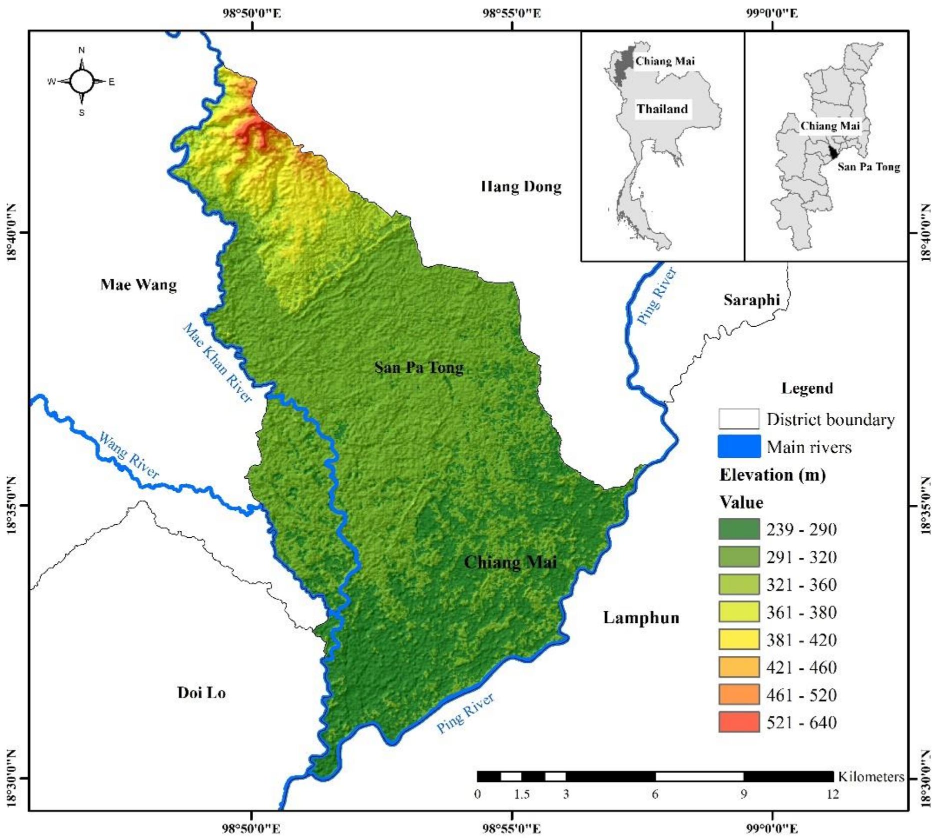

Figure 1. Map of the study area

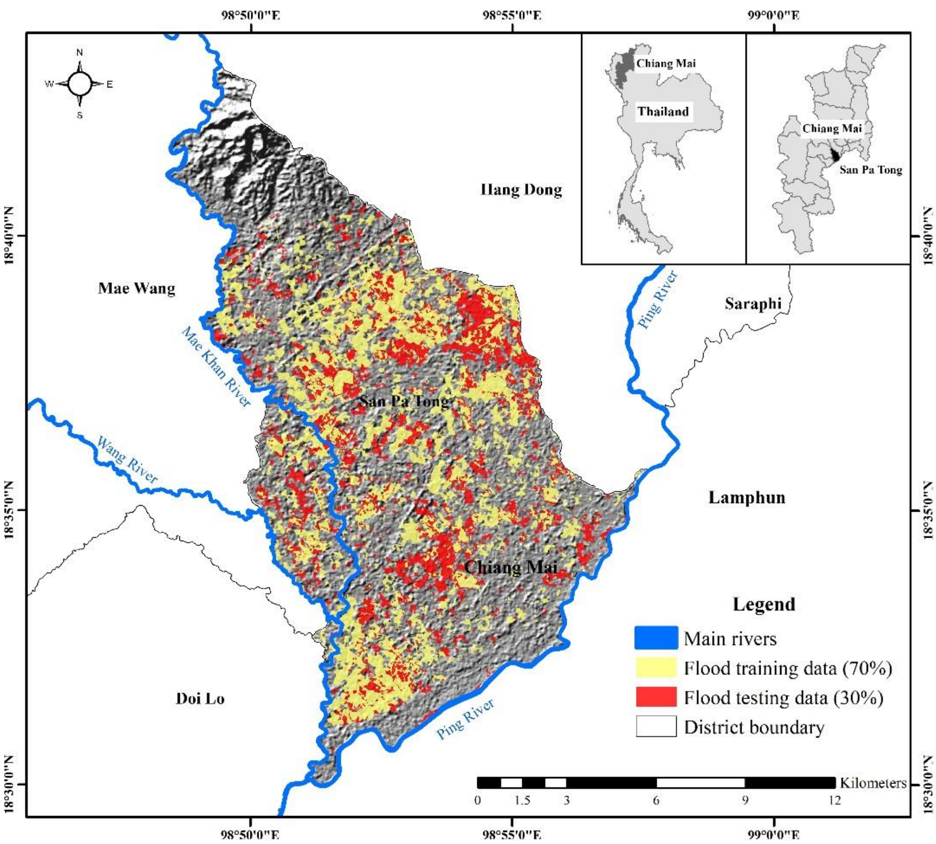

Figure 2. Map of the study area with training and testing data

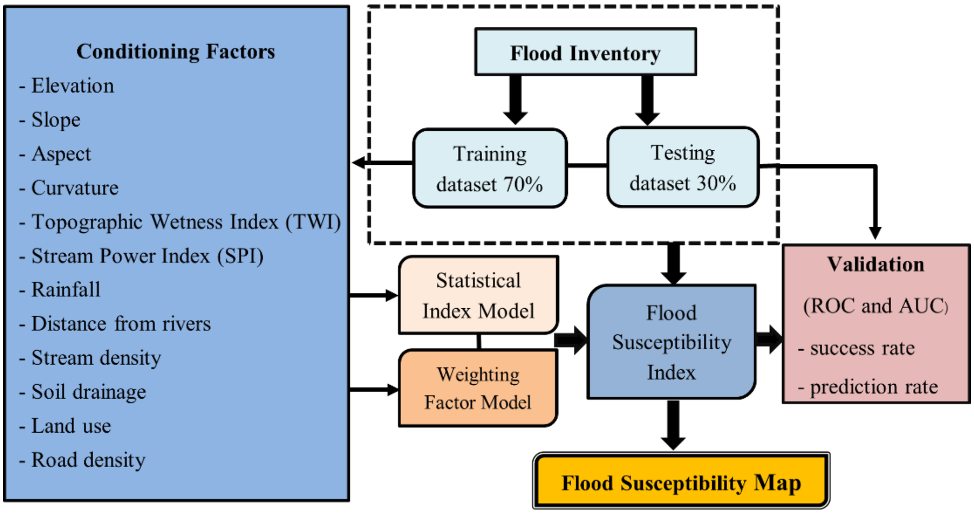

Figure 3. Flow chart of the research methodology

2.3 Flood conditioning factors

Flood conditioning factor data is essential for examining the relationships between the causative factors and flood occurrence (Khosravi et al., 2016). In this study, 12 conditioning factors were considered for flood susceptibility mapping based on the literature (Anucharn, 2019; Khosravi et al., 2016; Kongmuang et al., 2020; Paul et al., 2019; Tehrany et al., 2017; Tehrany et al., 2019), namely elevation, slope, aspect, curvature, TWI, SPI, rainfall, distance from rivers, stream density, soil drainage, land use, and road density (Figures 3 and 4). All conditioning factors were used to perform the flood susceptibility mapping. Each factor was prepared in raster format at a spatial resolution of 30 m × 30 m and was classified using the natural breaks method. Figure 3 shows a flowchart of the research methodology, and Table 1 shows the class values and the characteristics of the conditioning factors.

2.4 Flood susceptibility mapping

2.4.1 Statistical index model

The SI model is a bivariate statistical analysis (BSA) introduced by van Westen et al. (1997). It has been applied to various natural hazard studies, including landslides (Budha et al., 2016; Pourghasemi et al., 2013), floods (Khosravi et al., 2016; Tehrany et al., 2019), and flash floods (Cao et al., 2016). For SI, the weighted value of a conditioning class is calculated as the natural logarithm of flood existence in each class of a conditioning factor divided by the total flood density for the study as expressed in Equation 1 (Tehrany et al., 2019):

$$W_{ij} = \ln\left(\frac{D_{ij}}{D}\right) = \ln\left[\left(\frac{N_{ij}}{S_{ij}} / \frac{N}{S}\right)\right] \qquad (1)$$

Where; W_{ij} is the weight given to class i of the factor j, D_{ij} is the flood density in class i of the factor j, D is the total flood density of the study area, N_{ij} is the number of flood pixels in class i of the factor j, S_{ij} is the total number of pixels in class i of the factor j, N is the total number of flood pixels, and S is the total number of pixels in the study area.

The conditioning factors were reclassified using the W_{ij} values. Then, the classified factors were combined using the raster calculator to calculate the flood susceptibility index (FSI). The FSI can be described by the following equation:

$$FSI_{SI} = \sum_{j=1}^{n} W_{ij} \qquad (2)$$

Where; FSI_{SI} is the flood susceptibility index of the SI model, W_{ij} is the weight given to class i of the factor j, and n represents the number of conditioning factors.

2.4.2 Weighting factor model

The weighting factor model is a modified version of the SI model (Oztekin and Topal, 2005; Yalcin, 2008; Khosravi et al., 2016). Weights are derived for the conditioning factors to determine their influence on flood occurrence. TSI values are calculated by multiplying the SI values by the number of flood pixels in the same conditioning class, then, the values of all conditioning classes for a particular factor are summed (Oztekin and Topal, 2005). The weighting factor values for each conditioning factor are calculated, ranging from 1 to 100, using the following equations (Yalcin, 2008; Khosravi et al., 2016):

$$TSI_{value} = \sum_{i=1}^{n} SI \times S.pixel \quad (3)$$

$$W_{wf} = \frac{(TSI_{value}) - (MinTSI_{value})}{(MaxTSI_{value}) - (MinTSI_{value})} \times 100 \quad (4)$$

Where; TSI is the total weighting index value of pixels in the conditioning class for each factor, $MinTSI_{value}$ and $MaxTSI_{value}$ are the minimum and maximum values of the total weighting index value among all conditioning factors, respectively, and W_{wf} is the weighting factor value for each conditioning factor.

To calculate the flood susceptibility index value using the WF model, the W_{ij} weighting value (i.e., W_{ij} of the SI method) of the conditioning class is multiplied by the weighting factor value. The FSI of the WF model is then calculated using the following equation:

$$FSI_{WF} = \sum_{i=1}^{n} SI \times WF \quad (5)$$

Where; FSI_{WF} is the flood susceptibility index of the WF model, SI is the weighting value of the conditioning class, and WF is the weighting factor value of each conditioning factor.

2.4.3 Validation of the model

The receiver operating characteristic (ROC) and the area under the curve (AUC) metrics were used to evaluate the performance of the results of the SI and WF methods. ROC and AUC methods are widely used in natural hazard research (Khosravi et al., 2016; Tehrany et al., 2019). Both susceptibility map results were compared with training data and testing data. The calculated AUC values represent the success rate and prediction rate performance for training data and testing data, respectively. The AUC has a value range from 0-1, where 1 indicates the highest accuracy; if the AUC is closer to 1, the map results are considered more precise and reliable (Tehrany et al., 2019). The AUC value can be classified as follows: weak (0.5-0.6), moderate (0.6-0.7), good (0.7-0.8), very good (0.8-0.9), or excellent (0.9-1.0) (Pourghasemi et al., 2013; Yesilnacar, 2005).

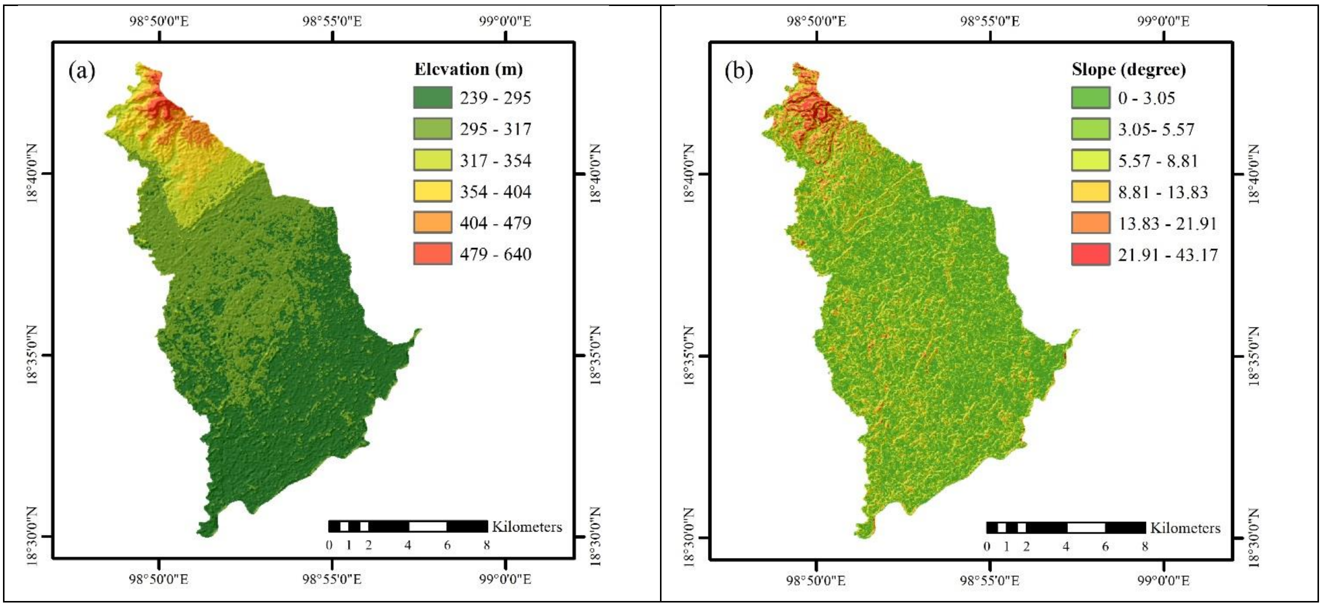

Figure 4. Conditioning factors: (a) elevation, (b) slope, (c) aspect, (d) curvature, (e) TWI, (f) SPI, (g) rainfall, (h) distance from rivers, (i) stream density, (j) soil drainage, (k) land use, and (l) road density

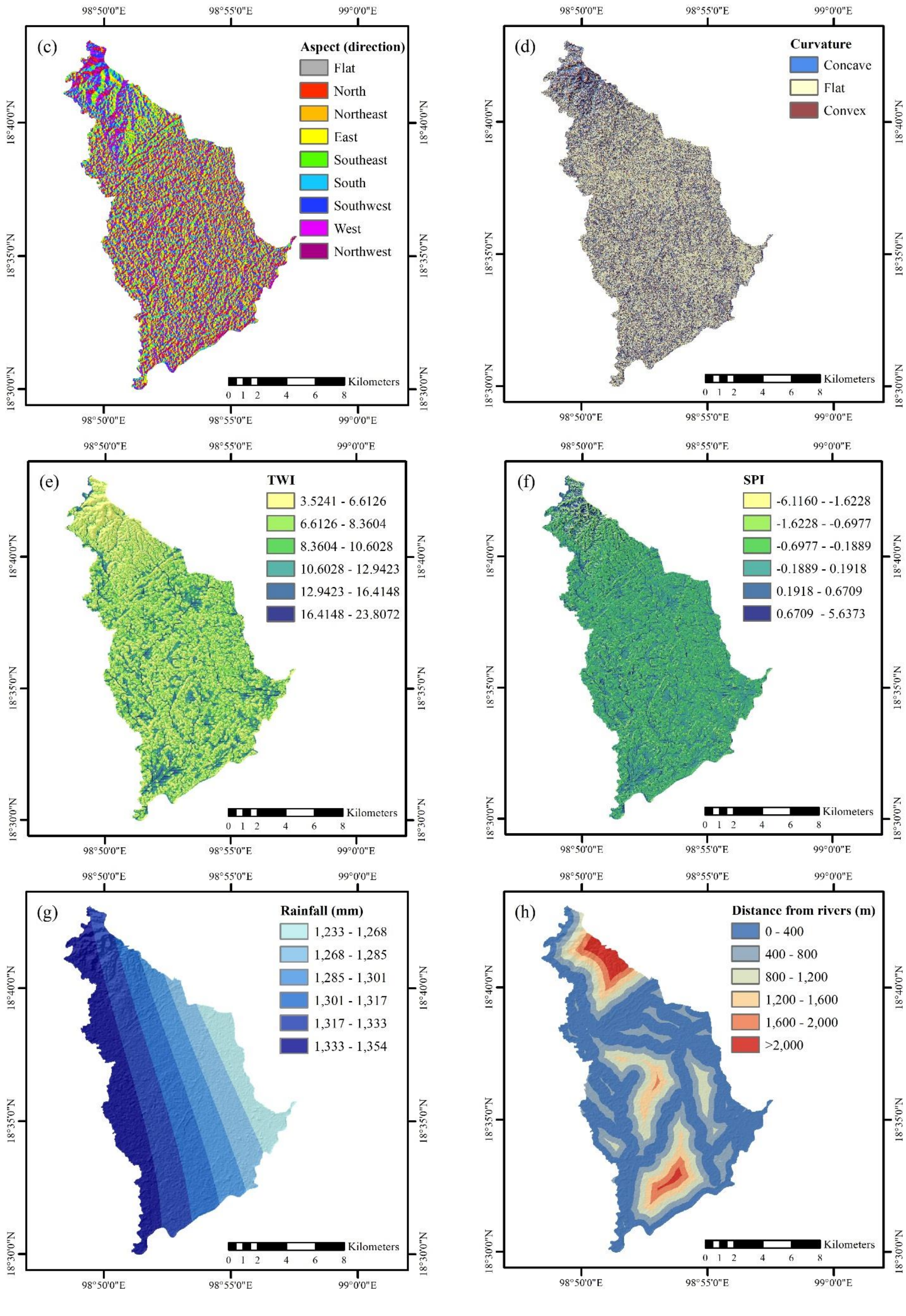

Figure 4. Conditioning factors: (a) elevation, (b) slope, (c) aspect, (d) curvature, (e) TWI, (f) SPI, (g) rainfall, (h) distance from rivers, (i) stream density, (j) soil drainage, (k) land use, and (l) road density (cont.)

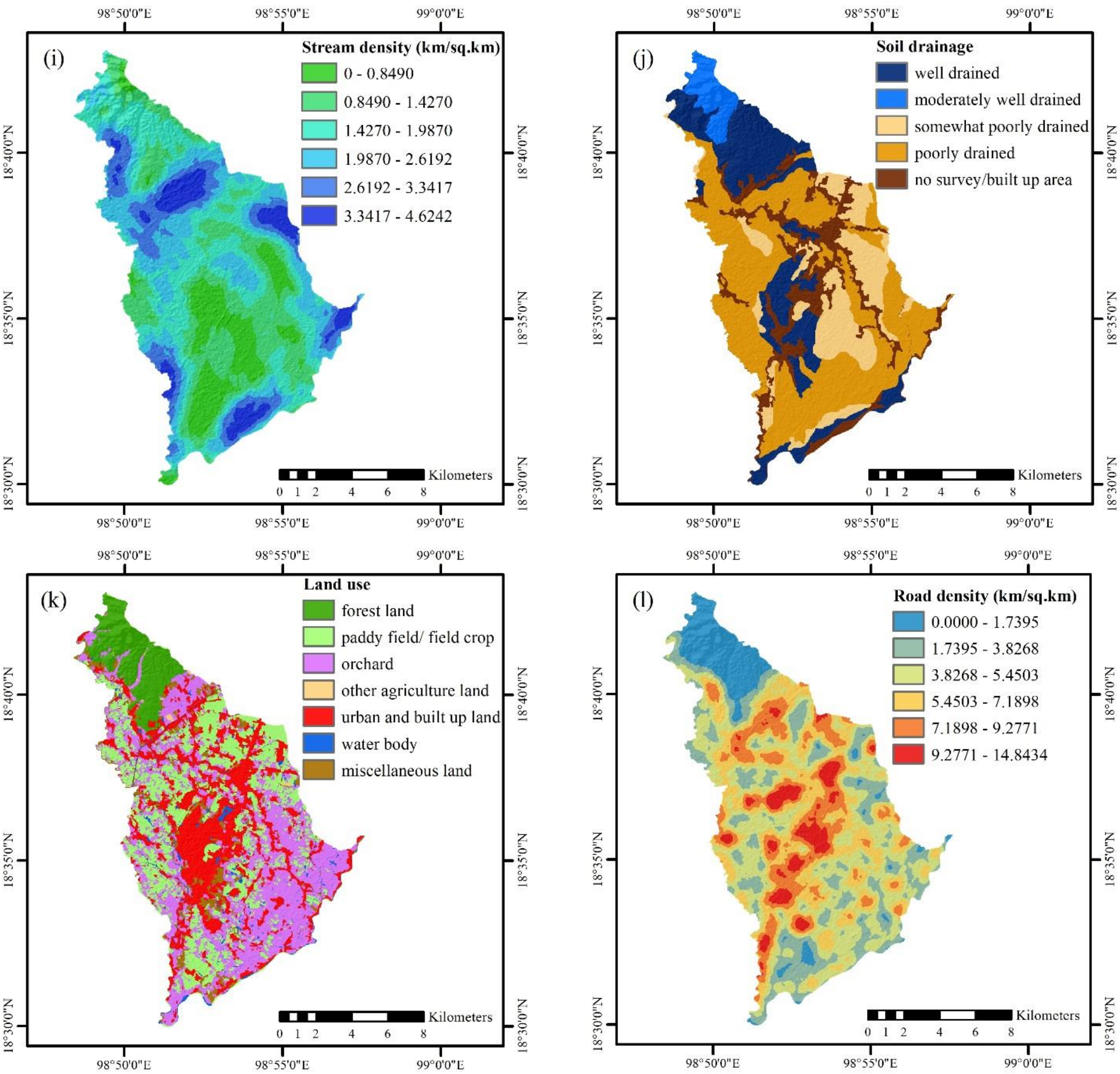

Figure 4. Conditioning factors: (a) elevation, (b) slope, (c) aspect, (d) curvature, (e) TWI, (f) SPI, (g) rainfall, (h) distance from rivers, (i) stream density, (j) soil drainage, (k) land use, and (l) road density (cont.)

3. RESULTS AND DISCUSSION

3.1 Flood susceptibility mapping using SI model

The results of using the SI model to calculate the weight of each flood conditioning factor class represent the correlation with flood occurrence and are presented in Table 1. A positive weight for the conditioning class indicates a high correlation with flood occurrence, whereas a negative weight means a low correlation. Each conditioning class of 12 factors was reclassified using its SI weight (W_{ij}) and was used to calculate the flood susceptibility index (FSI), as expressed in Equation (6). FSI values from the SI model were reclassified into five susceptibility classes (very low, low, moderate, high, and very high) using the geometrical interval classifier in ESRI ArcGIS 10.5 software.

$$FSI_{SI} = SI_{elevation} + SI_{slope} + SI_{aspect} + SI_{curvature} + SI_{TWI} + SI_{SPI} + SI_{rainfall} + SI_{distance\ to\ river} + SI_{stream\ density} + SI_{soil\ drainage} + SI_{land\ use} + SI_{road\ density} \quad (6)$$

The SI results presented in Figure 5 (a) show that about 49.49% of the study area is classified as very high susceptibility. The proportions of the study area classified as high, moderate, low, and very low susceptibility are 23.35%, 23.21%, 3.71%, and 0.24%, respectively (Table 1). The very highly susceptible areas are found in the west, the east, and the south, while the very low susceptibility regions are mostly found in the northern area.

3.2 Flood susceptibility mapping using WF model

The WF model showed the weight of each conditioning factor as an influence on flooding, as shown in Table 1. The advantage of the WF approach is its consideration of the different weights among the factors. The results showed that land use, soil drainage, and elevation are the most influential factors, with WF weights of 100, 82.61, and 75.77, respectively (Table 1). This indicates the importance of these factors and their necessity for flood susceptibility mapping research. The remaining conditioning factors are, in order of influence: road density, slope, distance from rivers, TWI, SPI, stream density, rainfall, aspect, and curvature. In contrast, the study of Khosravi et al. (2016) in the Haraz watershed of Iran found that the most influential factors were distance from rivers, elevation, and TWI.

Table 1. Calculation of weight values of SI and WF models

Conditioning factors	Conditioning classes	No. pixels	Percentage of area	No. of flood pixels	Percentage of flood	SI(W_{ij})	TSI	WF
Elevation (m)	239-295	91,113	47.2764	21,527	51.3305	0.0823	1,771	75.77
	295-317	71,637	37.1708	18,885	45.0308	0.1918	3,623	
	317-354	13,411	6.9587	1,194	2.8471	-0.8937	-1067	
	354-404	9,366	4.8598	332	0.7916	-1.8146	-602	
	404-479	5,467	2.8367	0	0.0000	0.0000	0	
	479-640	1,730	0.8977	0	0.0000	0.0000	0	
Slope (degree)	0-3.0544	66,718	34.6184	16,253	38.7548	0.1129	1,834	26.41
	3.0544-5.5710	65,599	34.0378	15,426	36.7829	0.0776	1,196	
	5.5710-8.8112	37,982	19.7080	7,832	18.6752	-0.0538	-422	
	8.8112-13.8323	15,086	7.8278	2,181	5.2005	-0.4089	-892	
	13.8323-21.9126	5,310	2.7552	241	0.5747	-1.5675	-378	
	21.9126 43.1662	2,029	1.0528	5	0.0119	-4.4808	-22	
Aspect (direction)	Flat	363	0.1884	93	0.2218	0.1633	15	1
	North	23,113	11.9928	5,391	12.8547	0.0694	374	
	Northeast	21,506	11.1590	5,061	12.0678	0.0783	396	
	East	22,893	11.8786	5,237	12.4875	0.0500	262	
	Southeast	26,306	13.6496	5,771	13.7608	0.0081	47	
	South	27,207	14.1171	5,844	13.9349	-0.0130	-76	
	Southwest	24,598	12.7633	4,925	11.7435	-0.0833	-410	
	West	22,754	11.8065	4,600	10.9686	-0.0736	-339	
	Northwest	23,984	12.4447	5,016	11.9605	-0.0397	-199	
Curvature	-6.7778-(-)0.5312	41,911	21.7466	8,731	20.8188	-0.0436	-381	1
	-0.5312-0.4449	109,325	56.7262	24,574	58.5960	0.0324	797	
	0.4449-5.6667	41,488	21.5272	8,633	20.5851	-0.0447	-386	
Topographic Wetness Index (TWI)	3.5241-6.6126	66,549	34.5307	11,639	27.7529	-0.2185	-2,543	11.35
	6.6126-8.3604	54,317	28.1838	12,026	28.6757	0.0173	208	
	8.3604-10.6028	28,472	14.7735	6,490	15.4752	0.0464	301	
	10.6028-12.9423	29,072	15.0848	7,742	18.4606	0.2020	1,564	
	12.9423-16.4148	11,321	5.8742	3,244	7.7352	0.2752	893	
	16.4148-23.8072	2,993	1.5530	797	1.9004	0.2019	161	
Stream Power Index (SPI)	-6.1160-(-)1.6228	2,549	1.3226	103	0.2456	-1.6837	-173	8.85
	-1.6228-(-)0.6977	19,349	10.0397	3,441	8.2050	-0.2018	-694	
	-0.6977-(-)0.1889	4,7245	24.5143	10,627	25.3398	0.0331	352	
	-0.1889-0.1918	91,143	47.2920	21,136	50.3982	0.0636	1,345	
	0.1918-0.6709	28,111	14.5861	6,003	14.3140	-0.0188	-113	
	0.6709-5.6373	4,327	2.2452	628	1.4974	-0.4050	-254	

Table 1. Calculation of weight values of SI and WF models (cont.)

Conditioning factors	Conditioning classes	No. pixels	Percentage of area	No. of flood pixels	Percentage of flood	SI(W_{ij})	TSI	WF
Rainfall (mm)	1,233-1,267	18,887	9.8000	4,152	9.9003	0.0102	42	1.27
	1,267-1,285	25,591	13.2786	5,501	13.1170	-0.0122	-67	
	1,285-1,301	29,372	15.2404	6,946	16.5625	0.0832	578	
	1,301-1,317	34,939	18.1290	6,864	16.3670	-0.1022	-702	
	1,317-1,333	41,908	21.7451	9,747	23.2415	0.0665	649	
	1,333-1,353	42,027	21.8068	8,728	20.8117	-0.0467	-408	
Distance from rivers (m)	0-400	101,742	52.7916	23,400	55.7967	0.0554	1,295	13.82
	400-800	43,241	22.4367	9,238	22.0278	-0.0184	-170	
	800-1,200	23,561	12.2253	5,127	12.2252	0.0000	0	
	1,200-1,600	13,067	6.7802	2,895	6.9030	0.0180	52	
	1,600-2,000	6,466	3.3551	1,162	2.7708	-0.1913	-222	
	>2,000	4,647	2.4112	116	0.2766	-2.1653	-251	
Stream density (km/km^2)	0-0.8490	24,481	12.7026	6,208	14.8028	0.1530	950	5.66
	0.8490-1.4270	44,644	23.1647	8,726	20.8069	-0.1073	-937	
	1.4270-1.9870	48,947	25.3975	9,299	22.1732	-0.1358	-1,262	
	1.9870-2.6192	38,946	20.2082	9,571	22.8218	0.1216	1,164	
	2.6192-3.3417	22,452	11.6498	4,847	11.5575	-0.0080	-39	
	3.3417-4.6242	13,254	6.8772	3,287	7.8378	0.1307	430	
Soil drainage	Well drained	40,767	21.1530	4,632	11.0449	-0.6498	-3,010	82.61
	Moderately well drained	8,301	4.3072	4	0.0095	-6.1128	-24	
	Somewhat poorly drained	32,827	17.0332	9,324	22.2328	0.2664	2,484	
	Poorly drained	81,629	42.3554	22,746	54.2372	0.2473	5,624	
	No survey/built up area	29,200	15.1512	5,232	12.4756	-0.1943	-1,017	
Land use	Forest land	18,150	9.4176	592	1.4116	-1.8979	-1,124	100
	Paddy field/ field crop	48,414	25.1209	18,062	43.0683	0.5391	9,737	
	Orchard	64,831	33.6393	10,908	26.0098	-0.2572	-2,806	
	Other agricultural land	741	0.3845	120	0.2861	-0.2954	-35	
	Urban and built-up land	46,179	23.9612	9,502	22.6573	-0.0560	-532	
	Water body	4,191	2.1746	646	1.5404	-0.3448	-223	
	Miscellaneous land	10,218	5.3019	2,108	5.0265	-0.0533	-112	
Road density (km/km^2)	0-1.7395	18,578	9.6397	1,025	2.4441	-1.3722	-1,407	39.28
	1.7395-3.8268	35,663	18.5047	9,959	23.7470	0.2494	2,484	
	3.8268-5.4503	57,787	29.9843	13,429	32.0211	0.0657	883	
	5.4503-7.1898	43,113	22.3703	8,985	21.4245	-0.0432	-388	
	7.1898-9.2771	27,452	14.2442	6,344	15.1271	0.0601	382	
	9.2771-14.8434	10,131	5.2567	2,196	5.2363	-0.0039	-9	

The FSI from the WF model was calculated using both SI and WF weights, as shown in equation (7), and was categorized into five classes using the geometrical interval classifier method (Figure 5 (b)). Land classified as very highly susceptible occupies 51.74% of the study area, followed by 26.18%, 18.54%, 2.87%, and 0.66% of the area classified as high, moderate, low, and very low susceptibility, respectively. The WF model yields a greater area classified as very high or high susceptibility, accounting for 78.92% of the study area, compared to 72.84% according to the SI model (Table 1).

As Figures 5 (a) and (b) show, low and very low susceptibility areas are mainly in areas of high elevation. However, the very high and high susceptibility areas from the SI and WF models are partly different. The high susceptibility areas of the WF map cover a greater extent than those in the SI map and mainly dominate the southeast of the study area located in low elevations with poor drainage conditions. The results indicate that the weighting values of the conditioning factors play an important role in obtaining the flood susceptibility mapping while the SI model relies on a calculation with the equal weight of the conditioning factors (Khosravi et al., 2016).

$$\begin{aligned}\mathrm{FSI_{WF}} = {} & (\mathrm{SI_{elevation}} \times 75.77) + (\mathrm{SI_{slope}} \times 26.41) + \\ & (\mathrm{SI_{aspect}} \times 1) + (\mathrm{SI_{curvature}} \times 1) + (\mathrm{SI_{TWI}} \times 11.35) + \\ & (\mathrm{SI_{SPI}} \times 8.85) + (\mathrm{SI_{rainfall}} \times 1.27) + \\ & (\mathrm{SI_{dist.\ from\ river}} \times 13.82) + (\mathrm{SI_{stream\ density}} \times 5.66) + \\ & (\mathrm{SI_{soil\ drainage}} \times 82.61) + (\mathrm{SI_{land\ use}} \times 100) + \\ & (\mathrm{SI_{road\ density}} \times 39.28)\end{aligned} \tag{7}$$

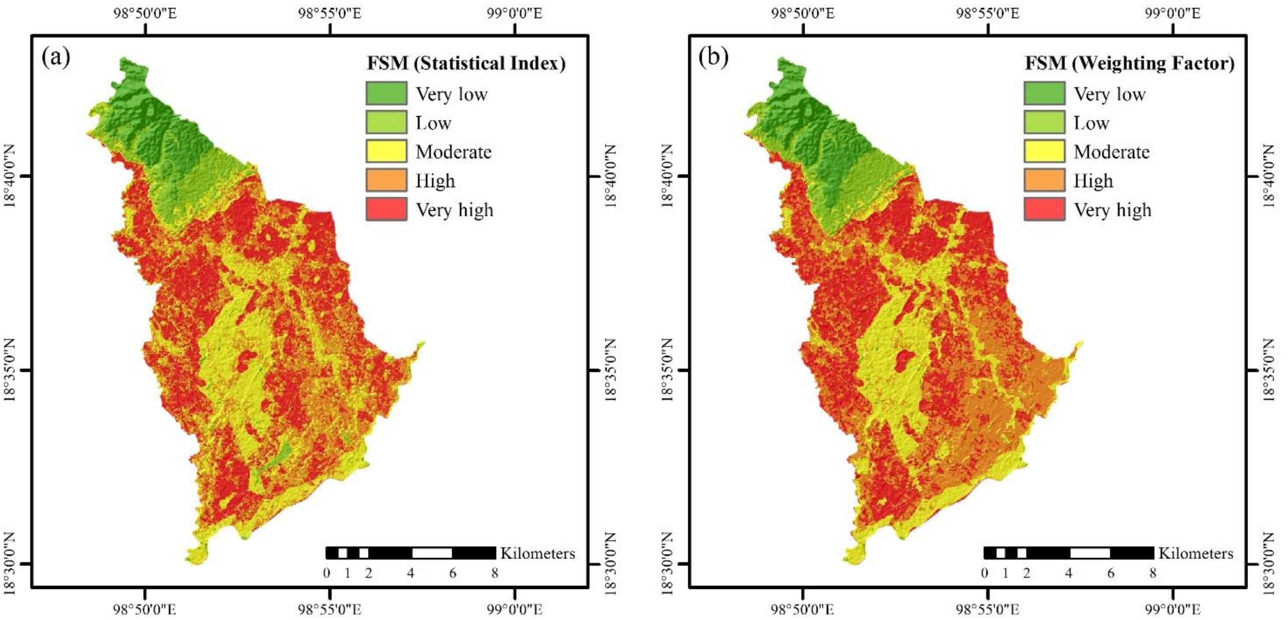

Figure 5. Flood susceptibility mapping: (a) SI model, (b) WF model

3.3 Validation of the models

The results from the SI and WF models were compared with the training data (70%) and testing data (30%) using the ROC curve and the AUC value methods. Figures 6 (a) and (b) show the ROC curves of the success and prediction rates of both results. The success rates of the SI and WF models were 91.80% and 93.06%, respectively. The prediction rate is widely used to clarify the predictability of future flood occurrences (Paul et al., 2019); the prediction rate values were 93.53% for the WF model and 92.05% for the SI model. Therefore, the results show that the WF model performed slightly better than the SI model for mapping flood-susceptible areas in San Pa Tong. However, both models provided excellent outcomes, with AUC values higher than 90% (Khosravi et al., 2016; Yesilnacar, 2005). A similar pattern of results was obtained by Khosravi et al. (2016), who found excellent results with SI and WF, and Cao et al. (2016), who also obtained a high prediction rate result using the SI model.

Additionally, the recurring flood data were utilized and compared with the results from SI and WF models. Figures 7 (a) and (b) show an excellent correlation between the recurring flood areas and the results from both SI and WF models. Comparatively, the WF model performed more accurately with 82.12% of the recurring flood areas falling into the very high susceptibility class, compared to 77.06% from the SI model (Table 2). The results also revealed that no recurring flood area was in the very low susceptibility class for either the SI or WI model. Based on the validation results, both models can be considered effective approaches for mapping flood susceptibility in other geographic areas.

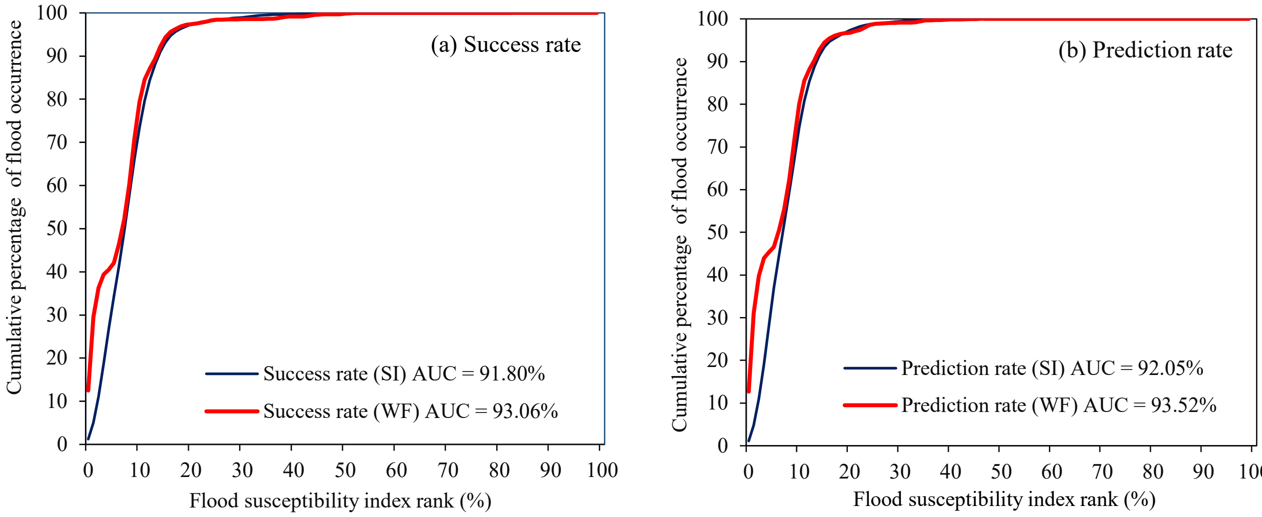

Figure 6. Validation using ROC and AUC: (a) success rate and (b) prediction rate

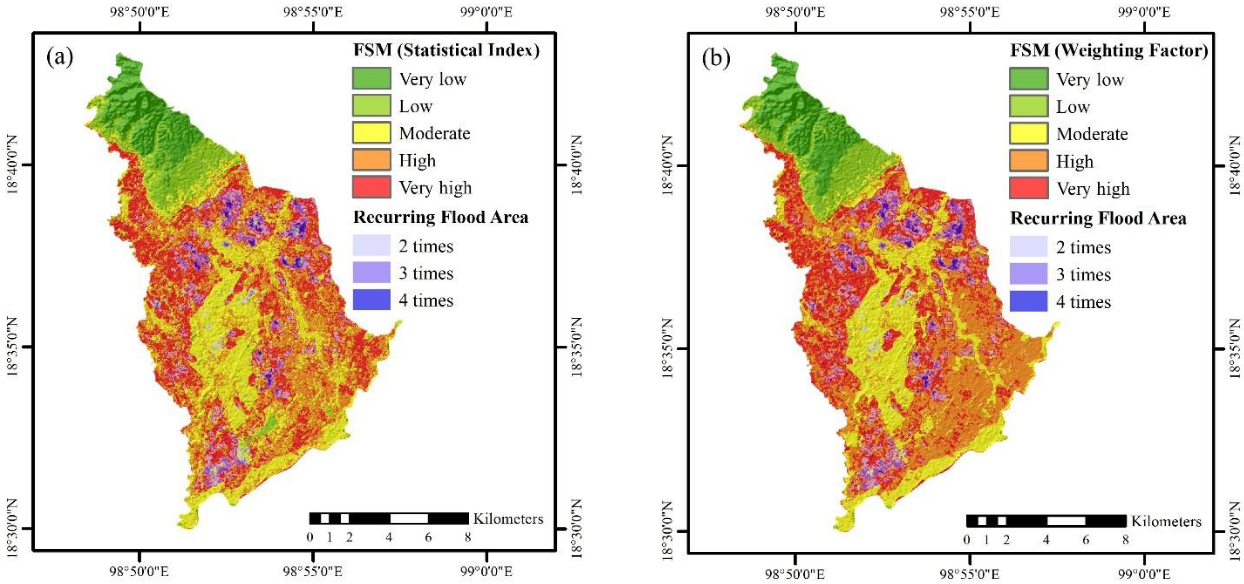

Figure 7. Flood susceptibility mapping using SI (a) and WF (b) models and recurring flood areas from 2005 to 2019

Table 2. Computation of the recurring flood area and flood susceptibility class

Model	Susceptibility class	Recurring flood area (km^2)				Percentage (%)
		2 times	3 times	4 times	Total	
SI	Very low	0.00	0.00	0.00	0.00	0.00
	Low	0.11	0.01	0.00	0.12	0.70
	Moderate	1.42	0.55	0.08	2.06	11.93
	High	1.40	0.32	0.06	1.78	10.30
	Very High	8.18	4.05	1.06	13.29	77.06
	Total	11.11	4.94	1.20	17.24	100.00
WF	Very low	0.00	0.00	0.00	0.00	0.00
	Low	0.06	0.01	0.00	0.07	0.39
	Moderate	0.96	0.17	0.01	1.14	6.62
	High	1.43	0.36	0.08	1.87	10.87
	Very High	8.65	4.40	1.10	14.16	82.12
	Total	11.11	4.94	1.20	17.24	100.00

3.4 Suggestion for further research

In terms of the results of this study, each conditioning factor has a different impact on flood occurrence, depending on the geographic context of the area. Thus, statistical models comparing the influencing factor are highly important (Kia et al., 2012). The DEM is also an essential component of these models and plays an important role in flood hazard research (Cabrera et al., 2019); the effects of flood susceptibility mapping using a different spatial resolution of DEM data might also therefore be investigated. Although both SI and WF results showed excellent and effective outcomes, there are some limitations in this study to be considered. Socio-economic factors could be integrated into the method as demonstrated by Hoang et al. (2020) and Khaing et al. (2021). Further conditioning factors could also be investigated, such as the Normalized difference vegetation index (NDVI), lithology, and land-use changes. For further research, FSM using statistical and machine learning models such as weight of evidence, artificial neural networks, logistic regression, and support vector machines could be considered (Anucharn, 2019; Paul et al., 2019; Tehrany et al., 2017; Tehrany et al., 2019). Moreover, integrating hydrological models and GIS-based technique is also a suggested point for further study (Khaing et al., 2021; Rahmati et al., 2016).

4. CONCLUSION

Flood susceptibility mapping is an essential tool for flood preparation. Identification of susceptible areas using reliable methods can help to reduce flood damage. This research applied SI and WF models for flood susceptibility mapping in the San Pa Tong District, Chiang Mai, Thailand, and compared their performance, in addition to investigating the most influential factors for flood occurrence in the study area. Flood data were randomly divided into training and testing data. Then, 12 conditioning factors, namely elevation, slope, aspect, curvature, TWI, SPI, rainfall, distance from rivers, stream density, soil drainage, land use, and road density were used to compare with training data and calculate the correlation with flood occurrence. The results from the SI and WF models revealed that very highly susceptible areas covered an estimated 49.49% and 51.74% of the study area, respectively. Regarding the WF results, the most influential factors were land use, soil drainage, and elevation, while the aspect and curvature were the least significant factors in determining flood susceptibility. ROC and AUC were then used to evaluate the success rate and the prediction rate of the SI and WF models. The results revealed that WF shows a better success rate than the SI model, with AUC values of 93.06% and 91.80%, respectively. WF also performed better, with a prediction rate of 93.52% compared to 92.05% for SI. In summary, both WF and SI results were shown as acceptable and reliable methods, with excellent performance rates for flood susceptibility mapping. The results of this research can be used to help planners implement flood preparedness and to minimize the impacts of future floods.

ACKNOWLEDGEMENTS

The author would like to express gratitude to GISTDA, the Upper Northern Region Irrigation Hydrology Center, and the Land Development Department for supporting the collection of the research data. The author is grateful to the Department of Geography, Faculty of Humanities and Social Sciences, Chiang Mai Rajabhat University for supporting the research facilities. Lastly, the author gratefully acknowledges the anonymous reviewers and the editor for their constructive comments and valuable suggestions which have helped to improve the quality of this manuscript.

REFERENCES

Anucharn T. A comparison the most appropriate method for flood susceptibility map in Khlong Nathawi Subwatershed, Songkhla Province. Journal of King Mongkut's University of Technology North Bangkok 2019;29(4):612-29 (in Thai).

Budha PB, Rai P, Katel P, Khadka A. Landslide hazard mapping in Panchase Mountain of Central Nepal. Environment and Natural Resources Journal 2020;18(4):387-99.

Cabrera JS, Lee HS. Flood risk assessment for Davao Oriental in the Philippines using geographic information system-based multi-criteria analysis and the maximum entropy model. Journal of Flood Risk Management 2020;13(2):e12607.

Cao C, Xu P, Wang Y, Chen J, Zheng L, Niu C. Flash flood hazard susceptibility mapping using frequency ratio and statistical index methods in coalmine subsidence areas. Sustainability 2016;8(9):948.

Center for Research on the Epidemiology of Disasters (CRED). Natural disaster 2019: Now is the time to not give up [Internet]. 2020 [cited 2020 Nov 10]. Available from: https://emdat.be/natural-disasters-2019-now-time-not-give/.

Hoang DV, Tran HT, Nguyen TT. A GIS-based spatial multi-criteria approach for flash flood risk assessment in the Ngan Sau-Ngan Pho mountainous river basin, North Central of Vietnam. Environment and Natural Resources Journal 2020;18(2):110-23.

Igarashi K, Koichiro K, Tanaka N, Aranyabhaga N. Prediction of the impact of climate change and land use change on flood discharge in the Song Khwae District, Nan Province, Thailand. Journal of Climate Change 2019;5(1):1-8.

Khaing TW, Tantanee S, Pratoomchai W, Mahavik N. Coupling flood hazard with vulnerability map for flood risk assessment: A case study of Nyaung-U Township in Myanmar. Greater Mekong Subregion Academic and Research Network International Journal 2021;15:127-38.

Khosravi K, Pourghasemi HR, Chapi K, Bahri M. Flash flood susceptibility analysis and its mapping using different bivariate models in Iran: A comparison between Shannon's entropy, statistical index, and weighting factor models. Environmental Monitoring and Assessment 2016;188(12): 656.

Kia MB, Pirasteh S, Pradhan B, Mahmud AR, Sulaiman WNA, Moradi A. An artificial neural network model for flood simulation using GIS: Johor River Basin, Malaysia. Environmental Earth Sciences 2012;67(1):251-64.

Kongmuang C, Tantanee S, Seejata K. Urban flood hazard map using GIS of Muang Sukhothai District, Thailand. Geographia Technica 2020;15(1):143-52.

Oztekin B, Topal T. GIS-based detachment susceptibility analyses of a cut slope in limestone, Ankara-Turkey. Environmental Geology 2005;49(1):124-32.

Paul GC, Saha S, Hembram TK. Application of the GIS-based probabilistic models for mapping the flood susceptibility in Bansloi sub-basin of Ganga-Bhagirathi River and their comparison. Remote Sensing in Earth Systems Sciences 2019;2:120-46.

Pourghasemi HR, Moradi HR, Aghda SMF. Landslide susceptibility mapping by binary logistic regression, analytical hierarchy process, and statistical index models and assessment of their performances. Natural Hazards 2013;69(1):749-79.

Rahmati O, Zeinivand H, Besharat M. Flood hazard zoning in Yasooj region, Iran, using GIS and multi-criteria decision analysis. Geomatics, Natural Hazards and Risk 2016;7(3): 1000-17.

Samanta S, Pal DK, Palsamanta B. Flood susceptibility analysis through remote sensing, GIS and frequency ratio model. Applied Water Science 2018;8(2):66.

Suppawimut W. Spatial analysis of recurrent flood in San Pa Tong District, Chiang Mai Province. Proceedings of the 6th Conference on Research and Creative Innovations; 2020 Sep 2-3; Rajamangala University of Technology Lanna, Chiang Mai: Thailand; 2020 (in Thai).

Tehrany MS, Shabani F, Jebur MN, Hong H, Chen W, Xie X. GIS-based spatial prediction of flood prone areas using standalone frequency ratio, logistic regression, weight of evidence and their ensemble techniques. Geomatics, Natural Hazards and Risk 2017;8(2):1538-61.

Tehrany MS, Kumar L, Jebur MN, Shabani F. Evaluating the application of the statistical index method in flood susceptibility mapping and its comparison with frequency ratio and logistic regression methods. Geomatics, Natural Hazards and Risk 2019;10(1):79-101.

World Bank. Thai Flood 2011, Rapid Assessment for Resilient Recovery and Reconstruction Planning. World Bank; 2012.

van Westen CJ, Rengers N, Terlien MTJ, Soeters R. Prediction of the occurrence of slope instability phenomenal through GIS-based hazard zonation. Geologische Rundschau 1997; 86:404-14.

Yalcin A. GIS-based landslide susceptibility mapping using analytical hierarchy process and bivariate statistics in Ardesen (Turkey): Comparisons of results and confirmations. Catena 2008;72(1):1-12.

Yesilnacar EK. The Application of Computational Intelligence to Landslide Susceptibility Mapping in Turkey [dissertation]. Melbourne, Australia: University of Melbourne; 2005.

Blended Amendments: A Sustainable Approach for Managing Nutrient Deficiency in Rice Fields

Madhumita Ghosh Datta*

Department of Environmental Science, Tezpur University, Napaam, Sonitpur, Assam, India

ARTICLE INFO

Received: 4 Mar 2021
Received in revised: 15 Jul 2021
Accepted: 19 Jul 2021
Published online: 1 Sep 2021
DOI: 10.32526/ennrj/19/202100032

Keywords:
Rice/ Soil properties/ Chemical fertilizer/ Blended organic amendments

*** Corresponding author:**
E-mail: madhutzp@gmail.com

ABSTRACT

The application of chemical fertilizer provides absorbable soluble macronutrients for increasing rice yield while reducing the availability of micronutrients and occasionally halting nitrogen mineralisation in the soil. To lessen some of these undesirable effects of chemical fertilization, an effort has been made to prepare blended soil organic amendments by mixing organic materials like rice straw, dried cow-dung and compost prepared from eco-friendly wastes from the kitchen, backyard garden and dried cow-dung mixed in the ratio 1:2:2. Such prepared amendments were applied in the rice field by growing three high-yielding rice cultivars *Dikhow*, *Chandrama* and *Naveen*, in three different rice cropping seasons, pre-monsoon (*Ahu)*, monsoon *(Sali)* and summer *(Boro*) during 2015-2016 and 2016-2017 for studying soil properties, crop growth and yield. The key finding of the investigation was that the soil amended with chemical fertilizer showed improvement in soil moisture compared to unamended soil in all three rice fields. However, chemically fertilized soil exhibited lower amounts of available phosphorus, available potassium, diethylenetriaminepentaacetic acid (DTPA) extracted iron and copper in *Ahu* field, DTPA extracted iron, copper and zinc in *Sali* field and immobilizing nitrogen in *Boro* field than blended amendments. Overall, chemical fertilizer + rice straw displayed more available nitrogen and yield in *Ahu* field, whereas, chemical fertilizer + dried cow dung showed the highest amount of zinc and copper along with the highest yield in *Sali* rice field and chemical fertilizer+compost had better moisture and soil organic carbon amounts with an ideal acidic pH supporting maximum yield in *Boro* rice field.

1. INTRODUCTION

Rice is a staple food for half of the world's population regardless of their economic status (Mackill et al., 2012). It supplies more than 27% of daily calories in developing countries while creating a gargantuan need for its production (Carrijo et al., 2017; Naresh et al., 2018). This increasing demand for rice production is attained by growing more rice-rice crop sequences, diversifying the rice ecosystem through irrigation, and managing nutrients in rice fields (Singh et al., 2002).

The nutrients of the rice soil have increased by the application of fertilizer in rice soil which rose during the latter half of the twentieth century following the introduction of high-yielding rice varieties (Khush, 1999; Davies, 2003). These varieties have 20% more grain production than traditional varieties and are more responsive to chemical fertilizers. But overuse of chemical fertilizers to get high yield triggers environmental issues like increased greenhouse gas emission, groundwater contamination, and surface water eutrophication (Cai et al., 2018). It also causes soil degradation by altering the natural microflora and increasing soil acidity, nutrient imbalances, micronutrient deficiencies (Singh, 2000; Leip et al., 2014; Lehmann and Kleber, 2015; Gunina and Kuzyavok, 2015; Dimkpa and Bindraban, 2016; Elemike et al., 2019), thus, reducing the availability of nutrients for plant uptake for effective plant functioning and biomass accumulation (Faisal and Farooq, 2019). Moreover, a reduction in the concentration of iron and zinc in rice soil affects uniform grain maturity and productivity.

Organic materials gathered from the neighbouring locality of a rice field have a share in improving soil properties (Arunrat et al., 2020). The

Citation: Datta MG. Blended amendments: A sustainable approach for managing nutrient deficiency in rice fields. Environ. Nat. Resour. J. 2021;19(6):494-502. (https://doi.org/10.32526/ennrj/19/202100032)

immediate positive effects of the application of organic materials are soil aggregation and increasing the moisture content, and long-term benefits on micronutrient and organic carbon storage (Hans et al., 2018) on complete decomposition. The application of too much organic materials in the soil produces toxic effects arising from the reduced metabolic intermediates on the degradation of these materials (Liang et al., 2003). In reality, organic materials solely may not meet the rice plants' requirements due to the comparatively low nutrient contents and the gradual release of plant nutrients (Elemike et al., 2019). So, an approach used for sustainable rice cultivation is to apply organic materials blended with chemical fertilizer. Such organic materials like rice straw and dried cow dung provide recalcitrant carbon and nutrients, whereas compost derived only from biodegradable organic material provides humified carbon, supports carbon sequestration and soil formation.

There are reports on the use of organic materials with chemical fertilizer in rice fields which emphasise the increase in yield, dissolved organic carbon, microbial biomass carbon, different soil organic carbon fractions like humic acid, fulvic acids, and reducing greenhouse gases emission (Moscatelli et al., 2005; Bharali et al., 2018; Iqbal et al., 2020). But studies to specify nutrients variation at harvest stage by cultivating high-yielding varieties in acidic sandy soil in a sub-tropical type of climate are limited. The application of blended amendments in rice fields improve soil fertility and ultimately increases the yield of high-yielding rice varieties. So, the objectives of this study were (1) to assess the effect of blended amendments on soil properties like soil temperature, soil moisture, soil pH, soil organic carbon, available nitrogen, available phosphorus, available potassium and DTPA extracted iron, copper, manganese and zinc; (2) to determine the combined effect of blended amendments on plant height, yield, and partial factor productivity at harvest. The influence of chemical and blended amendments investigated by growing high-yielding three rice cultivars *Dikhow*, *Chandrama* and *Naveen*, in three different rice cropping seasons in *Ahu* (pe-monsoon), *Sali* (monsoon) and *Boro* (summer) during 2015-2016 and 2016-2017.

2. METHODOLOGY

2.1 Study area, amendments applied and field design

The study was carried out in the Tezpur University campus Napaam comes under the Sonitpur district of Assam, India. The site is at 26º37′59″ N latitude and 92º47′59″ E longitude at an elevation of 74 m above sea level and falls under the North Bank Plains Agroclimatic zone of Assam. The site experiences a humid and subtropical climate and has more or less hot wet summers and dry winters. The climatic data of the experimental years are in Figure 1. The pre-monsoon rice (*Ahu*) variety of *Dikhow* (Parents: Heera and Ananda; duration of the variety: 90-100 days), monsoon rice (*Sali)* variety of *Chandrama* (ARC6650 and CR94-721-3; duration of the variety: 135-140 days) and summer rice (*Boro*) variety *Naveen (*Parents: Sattari and Jaya; duration of the variety: 115-130 days) were taken for performing the field experiments. *Dikhow* is a short-duration variety growing well in flooded soil conditions, and *Chandrama and Naveen* are semi-dwarf varieties that grow both in *Sali* and *Boro* seasons. The investigation was carried out from March 2015 to June 2016 and similar experiment was redone again at the same field in following year 2016-2017. A plot size of 4 m^2 was done with four replicates in randomised block design with six amendments (Figure 2), T1-No application of amendments, T2-mineral fertilizer (NPK), T3-NPK+ rice straw (5 ton/ha), T4-NPK+dried cow dung (5 ton/ha), T5-NPK+dried cow dung (10 ton/ha) and T6-NPK+compost (2.5 ton/ha) (Table 1). The chemical fertilizer NPK was applied in the form of urea (N), superphosphate (P_2O_5) and muriate of potash (K_2O) at the rate of 40:20:20 kg/ha for *Ahu* and 60:20:40 for *Sali* and 60:30:30 for *Boro* rice cropping seasons. The amendments with the recommended dose of chemical fertilizer were incorporated in the field at the final puddling for even mingling, maintaining a gap of 50 cm between two plots to prevent intermixing of the amendments. Here, only 50% of urea is applied at this stage and the remaining 50% is applied after transplantation. The rice straw is the harvested straw of previous rice cultivation, chopped into 5cm pieces. The cow dung mixed with urine was dried under the sun and ground into a fine granular texture. The compost was made using kitchen wastes, garden wastes, and dried cow dung in the ratio of 1:2:2 by compositing in a dug-up soil for two months before application. Nitrogen supplied through organic materials is positively linked to mineralizable nitrogen but varies with texture, groundwater level and land use. However, no such predictive value is introduced into fertilizer recommendation schemes (Rose et al., 2011). Hence, the quantity of organic materials is selected based on cost, handiness, accessibility and

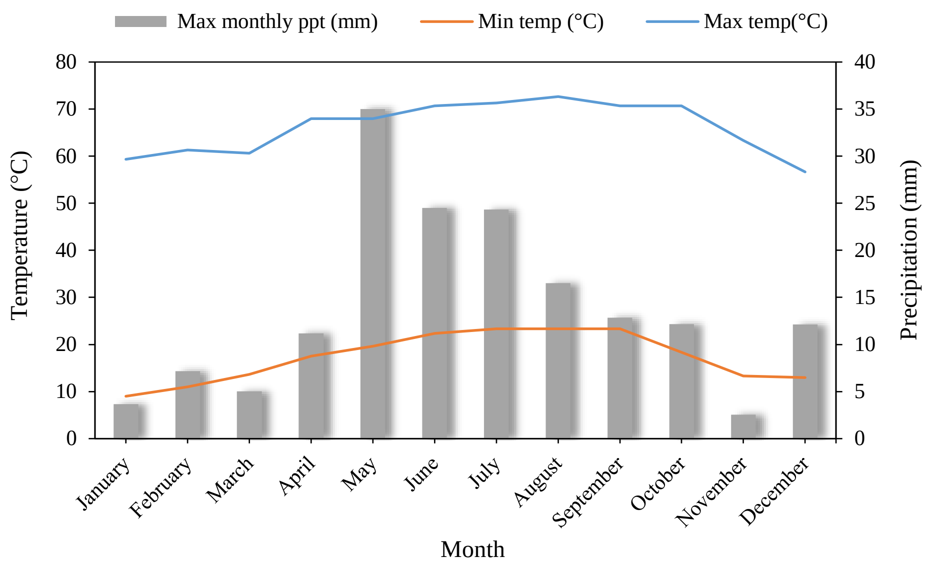

Figure 1. Monthly maximum temperature, monthly minimum temperature, and Monthly maximum precipitation with mean values recorded for 2015-2017

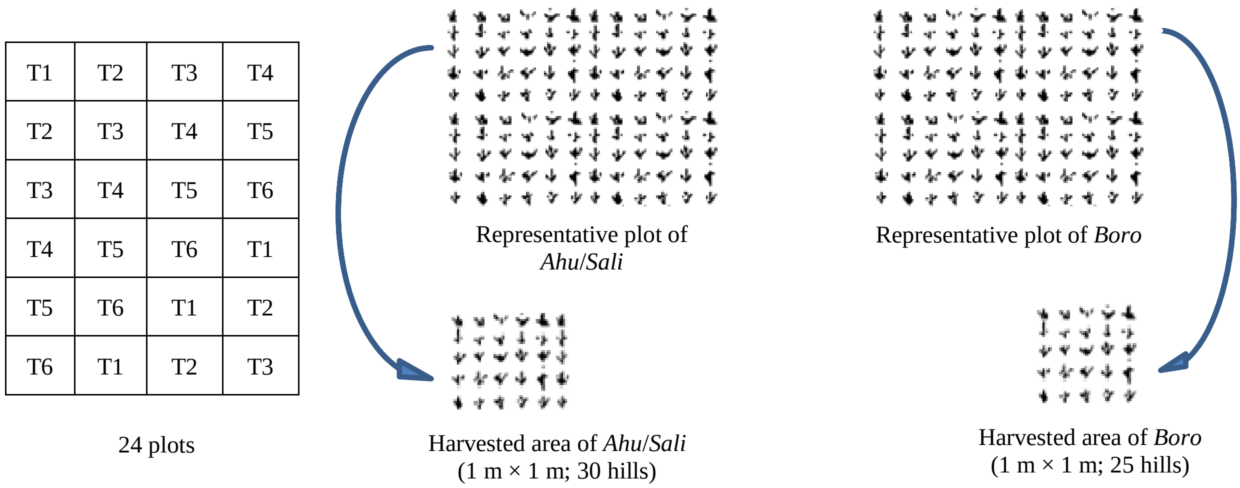

Figure 2. Schematic representation of field layout RBD-(Randomised Block Design) of *Ahu*, *Sali* and *Boro*

Table 1. The detail of amendments presented in Tabular format

Amendment	Nature of the amendment
T1	No amendment
T2	NPK (recommended dose)
T3	NPK + crop residues (5 ton/ha)
T4	NPK + farmyard manure (5 ton/ha)
T5	NPK + farmyard manure (10 ton/ha)
T6	NPK + compost (2.5 ton/ha)

Recommended dose of NPK: *Ahu* (40:20:20), *Sali* (60:20:40) and *Boro* (60:30:30)

availability. In the current experiment, the crop residue in the form of straw supplied 1 Mg carbon (5 ton) per ha was blended with urea (<200 kg). As most of the carbon supplied through cow dung in the tropical climate are mineralised, two rates of cow dung addition were chosen, 5 ton/ha and 10 ton/ha, to facilitate grain yield, increase soil nutrients and soil organic carbon quantity. Whereas the amount of compost was maintained at 2.5 ton/ha as it can immediately supply plant available nutrients. Rice straw (C:N=49.70 and moisture content=12.7%), dried cow dung (C:N=14.02 and moisture content=46.94%) and compost (C:N=10.28 and moisture content=35.49%) were applied in *Ahu*, *Sali* and *Boro* rice ecosystems for two years of cropping cycles. Since the crops of *Ahu* and *Sali* are rain supported (rainfed), no irrigation is required after the establishment of the crop as advised by the Government of Assam. However, for soaking land before the preparatory tillage and the final puddling, irrigation has been applied. The water management adopted for *Boro* rice is in the scheme of flooding-dry-re-flooding. The irrigation was done in plots to maintain 5 cm of standing water and at an interval of three days till panicle initiation. Fertilizer dose, spacing and other agronomic practices were retained for two consecutive years according to the package of practice issued by the Government of Assam, India.

2.2 Soil sample and crop growth analysis

Soil samples collected randomly were examined before crop growth and at harvest to determine the influence of the amendments on soil moisture by gravimetric method, pH by pH meter, soil temperature by soil thermometer, total carbon (TC) and total nitrogen (TN) by CHN analyser (model: 2400 series2, USA) and values (TC/TN) were divided to get C:N ratio, soil organic carbon oxidisable at 24 N sulphuric acid by Walkley and Black (1937) method. Available nitrogen, available phosphorus and available potassium were determined as per Page et al. (1982), and 0.005 N Diethyletriaminepenta acetic acid (DTPA) extracted micronutrients (copper, iron, manganese, zinc) by mass spectrophotometer. Plant height at harvest was measured from the base of the stem to the tip of the panicle with a measuring tape from the field itself. The matured grains containing 10% moisture were gathered for the calculation of yield. The partial factor productivity (PFP_N, kg grain/kg N applied) was calculated from grain yield with N use divided by applied N amount (Guo et al., 2017).

$$\mathrm{PFPN} = \frac{\text{kg grain}}{\text{kg N applied}}$$

2.3 Statistical analysis

The data were pooled from two experimental years and were analysed statistically using the SPSS 15.0 software package. The one-way ANOVA compares the values of amendments T2 to T6 with unamended T1. The least significant difference and Tukey's Honest difference tests estimate the significant difference at $p<0.05$ level. The least significant difference rejects the blended amendments that do not affect soil properties in Table 2 whereas, Tukey's Honest difference finds the difference among the plant height, yield, and PFP_N in Table 3.

3. RESULTS

3.1 Soil properties

The physico-chemical properties of soil of the three experimental fields were done before the crop cultivation. From the analysis it was found that soil was sandy, slightly acidic having pH varying from 5.40 to 5.67 with a bulk density of 1.34 kg/m^3, porosity 37.04%, water holding capacity 47.01% and with low organic carbon content (11.3-18.5 g/kg). The availability of nitrogen is low (113.56-238 kg/ha) due to occurrence of leaching in humid climates whereas available phosphorus varies from 12.50 kg/ha to13.90 kg/ha. The soil also experiences available potassium in the range of 70.65 kg/ha to 86.17 kg/ha with low organic carbon and zinc.

3.2 Effects of blended amendments on soil properties, plant growth and yield

In *Ahu* rice field, excluding soil temperature, all other soil properties differed slightly from each other among amendments with T2 showing the lowest available potassium, DTPA extracted iron and copper. The amendment T5 presented the highest value for DTPA extracted iron, zinc and copper (Table 2). The T3 and T1 plots had the highest and the lowest plant height (Figure 3). The *Ahu* fields had the lowest partial factor productivity of nitrogen in comparison to other rice fields with T6 (11.17±0.00 kg/kg) showing the highest values while T5 had the lowest values (8.45±0.00 kg/kg). The lowest nitrogen utilisation efficiency resulted in the lowest rice production and shows no significant difference among the amendments; T3 exhibiting the highest yield (13.50±0.02 Q/ha) and T1 the lowest yield (8.70±0.00 Q/ha).

In response to amendments in *Sali* rice fields, soil organic carbon and available nitrogen showed significant differences among the soil parameters. The soil nutrients, such as available phosphorus, DTPA extracted iron and zinc at harvest were more in blended amendments (T3-T6) than T2. Also, T2 recorded the lowest value of iron, zinc and copper, while T4 showed the highest value of iron and manganese. T5 recorded the highest value for zinc, copper, and yield (53.65±0.01 Q/ha). The T1 plots showed the lowest plant height (111.40±0.70 cm) and the lowest yield (40.00±0.01 Q/ha).

Table 2. Variation of soil properties at harvest stage indicated by mean under amendments from data pooled for two years

Cropping season	Amendment	ST (ºC)	SM (%)	pH	SOC (g/kg)	C:N	AN (kg/ha)	AP (kg/ha)	AK (kg/ha)	Fe (mg/kg)	Zn (mg/kg)	Mn (mg/kg)	Cu (mg/kg)
Pre-monsoon (*Ahu*)	T1	32	34.28	5.73	16.05	7.03	213.40	12.19	80.15	18.93	1.00	3.42	1.82
	T2	32	35.70	5.47	18.25	5.45	222.90	11.59	70.01	18.72	1.09	3.76	1.81
	T3	32	36.64	5.39	18.85	2.10	254.87*	10.10	71.40	19.85	1.18	3.74	2.00
	T4	32	37.98	5.39	16.70	3.48	238.67	13.25	80.97	20.04	1.25	3.80	1.91
	T5	32	34.87	5.34	18.90	2.16	240.87	12.31	79.16	20.52	1.46	3.78	2.10
	T6	32	35.15	5.44	17.05	2.35	234.76	13.81	71.72	19.22	1.24	3.32	1.87
Monsoon (*Sali*)	T1	31	28.21	5.73	12.30	29.50	242.50	13.19	85.15	19.94	1.51	3.52	1.86
	T2	31	30.26	5.44	11.70*	14.08	266.50	12.59	78.01	19.78	1.19	3.81	1.88
	T3	31	29.04	5.38	13.60	11.59	295.50*	12.10	76.40	20.87	1.22	3.84	2.01
	T4	31	28.59	5.39	13.30	11.23	285.00*	14.25	83.97	22.05	1.35	3.89	1.98
	T5	31	31.26	5.33	11.80*	13.66	287.50*	14.31	80.17	21.51	1.56	3.84	2.13
	T6	31	30.85	5.43	0.98*	16.07	262.50	14.81	71.73	21.43	1.34	3.35	1.88
Summer (*Boro*)	T1	33	29.55	4.91	11.71	2.08	225.00	10.91	79.79	15.08	0.78	9.31	2.41
	T2	33	34.58	4.78	14.39	1.77	284.83*	11.43	114.94	19.24*	0.88	11.38	2.51
	T3	33	34.01	4.72	14.85	2.44	304.00*	13.01	102.55	20.02*	0.88	11.66	2.47
	T4	33	33.77	4.97	13.21	2.19	308.83*	10.72	94.98*	20.38*	0.88	11.65	2.53
	T5	33	32.25	4.92	15.64*	2.28	294.00*	12.32	119.25	22.01*	0.97	11.78	3.05
	T6	33	38.88*	5.16	16.94*	2.34	308.50*	11.34	93.35	21.38*	0.92	11.82	2.73

Note: Values marked with (*) are significantly different from the corresponding values under T1 by least significant difference test at $p<0.05$. ST-Soil temperature, SM-Soil moisture, C:N-carbon:nitrogen, SOC-Soil organic carbon, AN- Available Nitrogen, AP-Available phosphorus, AK-Available potassium, Fe-Iron, Zn-Zinc, Mn-Manganese and Cu-Copper

Table 3. Variation of crop growth at harvest stage indicated by mean under amendments from data pooled for two years

Cropping season	Amendments	Plant height (cm)	Yield (Q/ha)	PFP_N (kg/kg)
Pre-monsoon (*Ahu*)	T1	83.66±1.60	8.70±0.00	-
	T2	93.00±1.00	9.80±0.00	11.13±0.00
	T3	108.50±1.26*	13.50±0.02	11.06±0.01
	T4	102.80±1.75	10.30±0.01	9.76±0.00
	T5	106.60±1.78	10.40±0.20	8.45±0.00
	T6	103.00±2.64	10.05±0.02	11.17±0.00
Monsoon (*Sali*)	T1	111.40±0.70	40.00±0.01	-
	T2	119.75±0.35*	46.00±0.01	34.85±0.00
	T3	116.23±0.14*	50.00±0.01*	30.12±0.00
	T4	119.00±0.57*	52.00±0.02*	35.45±0.00
	T5	120.00±0.44*	53.00±0.01*	32.33±0.00
	T6	121.50±0.28*	49.00± 0.01*	36.13±0.00
Summer (*Boro*)	T1	80.36±0.31	32.72±3.10	-
	T2	106.40±0.30*	46.08±4.31	52.28±0.04
	T3	93.43±0.64*	43.41±4.06	35.2±0.04
	T4	98.43±0.31*	43.62±4.14	41.71±0.4
	T5	107.83±0.44*	47.47±2.51	38.22±0.02
	T6	104.50±0.28*	53.34±2.10	56.15±0.02

Values are means±standard error with (*) under the same column are significantly different from the corresponding value of T1 of a growth stage at 5% level of probability by Tukey honest difference test. PFP_N -Partial factor productivity

A significant variation in the value of soil properties of *Boro* rice fields at the harvest stage was observed (Table 2). The T6 exhibited the highest soil moisture, pH, soil organic carbon and manganese whereas, T1 exhibited the lowest soil organic carbon, available nitrogen, available potassium, iron, zinc, manganese and copper. In addition, available phosphorus and available potassium concentrations in T6 soil increased as compared to T2. This may be due to the fact that T6 plots received nutrients both from chemical fertilization and compost. The plant height was the highest in (T5) whereas the lowest in (T1). Also, the lowest yield of 32.72±3.10 Q/ha was found in T1 and the highest yield of 53.34±2.10 Q/ha and PFP_N of 56.15±0.02kg/kg was recorded in T6 (Table 3).

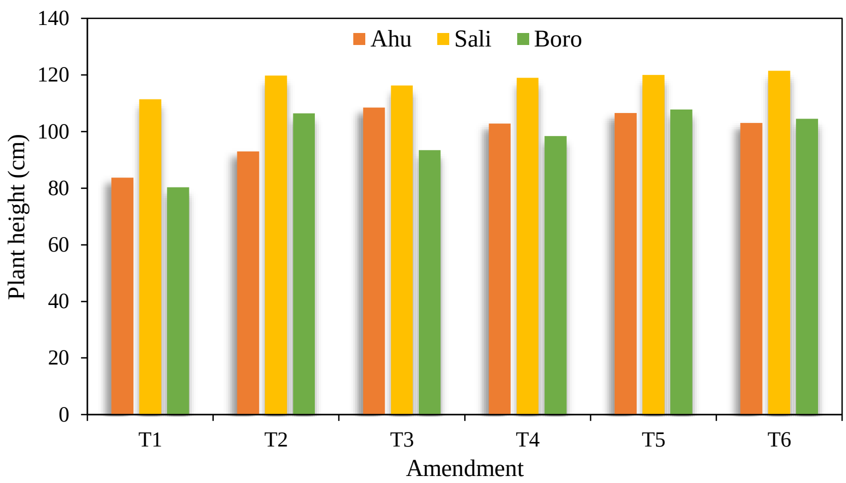

Figure 3. A comparison of rice plant growth at harvest of each amendment in each cropping season

4. DISCUSSION

The agriculture method depends on chemical fertilizer with damaging effects on soil quality, crop yield, and environment (Moe et al., 2019; Naher et al., 2019; Chandini et al., 2019). The amelioration of nutrient status, carbon transformations, and maintaining soil structure for sustainable crop production are key research topics (Kibblewhite et al., 2007; Al-Khuzai and Al-Juthery, 2020). Thus, the objective of this study was to determine the effect of blended amendments on soil properties, plant height, yield, and partial factor productivity in the acidic sandy soil of the sub-tropical climatic region.

At harvest, soil samples analysed from three rice fields exhibited that chemical fertilized plots had a deficiency in nutrients while T3-T6 containing blended amendments prevented a reduction in macro and micronutrients in varying proportions. Soil temperature, soil moisture, and pH influence microbial activity to conserve native soil organic matter enhancing soil organic carbon quantity across the blended amendments with T5, T3, and T6 showed the highest amount in *Ahu*, *Sali*, and *Boro* fields at the time of harvest. Soil organic carbon is an indicator of soil quality (Ngatia et al., 2021). Overall, the untreated soil (T1) took in the lowest soil moisture among the amendments in all three cropping seasons at the harvest stage. Thus, the application of amendments (inorganic or organic) provides easy access to nutrients favouring microbial growth and turnover, increasing moisture availability, promoting a positive soil environment for plant growth, and eventually enhancing rice yield (Dhaliwal et al., 2019). The pH of T2-T6 was lower than T1 except for T6 under *Boro* cropping seasons. The plants' growth in T2-T6 dropped the soil pH under amendments in three cropping cycles as hydrogen ions discharged in soil by microbial decomposition from applied nitrogen fertilizer were consumed in nitrate formation. These might be the reason for lower soil pH in T2-T6 than an unfertilized soil T1. The T6 of *Boro* cropping seasons picked up the hydrogen ions formed during irrigation and nitrogen fertilizer solubilisation. Thus, lowering the pH to 5.15 was favourable for the rice plant's growth. The amendments immobilised the nitrogen in the soil in *Ahu* and *Boro* cropping cycle. This nitrogen is mineralised by heterotrophic microbes only on the death of these organisms. The process of mineralisation being slow would lead to a residual effect. At the same time, the amount of nitrogen will decrease in succeeding cultivation. A plant requires nitrogen for making amino acids, proteins, and cells. When there is a nitrogen deficiency in the soil, the growth of plants stops. However, when nitrogen is abundantly available, its concentration in plant tissue after transplanting increases and gradually decreases towards maturity. There is the proper development of rice plants if there is an adequate supply of nitrogen at all growth stages for prolific tillering, satisfactory panicle formation, good seed setting, and proper filling of those grains (Djaman et al., 2018).

On the whole, the concentration of micronutrients extracted by DTPA followed the order Fe>Mn>Cu>Zn. The amount removed by DTPA can be implicitly related to the amount taken by plants. Shukla and Behera, (2019) reported that 36.50% of the soil of India is deficient in available zinc, 12.80% in iron, 7.10% in manganese and 4.20% in copper. The dried cow dungs an effective micronutrients provider like iron, zinc, copper and manganese in the T5 among the amendments in *Ahu* cropping season. But rice yield under blended amendments with *Dikhow* crop variety was at par with NPK or even decreased under additional organic input. Although organic materials mixed with chemical fertilizer as blended amendment input increases micronutrients quantities, a large amount of organic material should be avoided to maintain crop yield. Therefore, in order to identify the best strategies for increasing rice productivity in the *Ahu* ecosystems, a few more field experiments are needed.

The nitrogen utilisation was better in *Sali* and *Boro* fields than *Ahu* field, T6 producing the highest efficiency in *Sali* and *Boro* fields. Thus, better nitrogen utilisation efficiency can be attributed to variation in weather conditions and average rainfall more during this period of the cropping season. The availability of nutrients increases with the addition of blended amendments, and they also promote the decomposition rate of native soil organic nitrogen. In addition, these blended amendments enhanced rice productivity by improving the nitrogen supply capacity from vegetative parts of plants to grains. The emergence of widespread micronutrient deficiencies is a constraint on productivity. A balanced supply of NPK and micronutrients is necessary for crop growth, yield, and nitrogen utilisation efficiency. Other reports have established the positive effects of micronutrients on rice yield and nitrogen utilisation efficiency, and the positive effects varied with the type of rice and nutrient (Li et al., 2019; Nadeem and Farooq, 2019). The high-yielding cultivar takes away nutrients from the soil besides utilizing mineral fertilizers and lowers micronutrients from the rice soil through leaching. However, regular use of dried cow-dung or other organic supplies stops the reduction of extractable micronutrient levels from the rice soil of India reported by Pal et al. (2015). In submerged fields, zinc is the most commonly deficient micronutrient, while the iron is the most usual toxic micronutrient. As in flooded conditions, biochemical characteristics of soil change to reductive nature, making zinc less available and more of iron to rice plants. The application of chemical fertilizer+dried cow dung in the right amount partially mitigates the problems.

Nutrients are already present in the soil. The rice plants still need more macronutrients in amount from chemical fertilizers, particularly for higher yields. If chemical fertilizer replaces blended amendments consisting of chemical fertilizer and organic materials, the breakdown of such material produces definite organic acids, which lower the pH of the soil to a favourable acidic pH range and ultimately increased the availability of nutrients for the plants. Various investigators like Linquist et al. (2007), Moe et al. (2019), Bhardwaj et al. (2020), and Datta and Devi (2020) have reported that organic material increased the availability of a maximum number of nutrients. There is a positive association between organic material and nutrient elements and presumably by providing soluble complexing mediators that delay their fixation in the soil. The North Bank plain zone part of the agroecosystem, with high rainfall and the mean temperature, is found favourable for rice cultivation throughout the year except for winter where the temperature is low. So, mostly monsoon and summer crops of rice are grown during the months from May to November. The *Boro* rice system showed the maximum yield among the three ecosystems. This higher production in the summer season is attributed to more soil organic matter, higher solar radiation, better water control (irrigation), fertilizer responsive rice varieties. Thus, seasonal weather conditions influence crop production.

5. CONCLUSION

The results reveal that chemical fertilization of rice soil increases the soil moisture more than unamended soil for all three rice fields. But chemical fertilized soil showed the lowest amount of available phosphorus, available potassium, DTPA extracted iron and copper in *Ahu* field, DTPA extracted iron, copper, and zinc in *Sali* field, and immobilizing nitrogen in *Boro* field. The chemical fertilizer+rice straw (T3) showed the highest available nitrogen and yield in the *Ahu* rice field whereas, the chemical fertilizer+dried cow dung (T5) showed the most zinc, copper, and rice yield in the *Sali rice* field and the chemical fertilizer+compost (T6) had better moisture and soil organic carbon and an ideal acidic pH sustaining maximum yield attainment in the *Boro* rice field. On the whole, after the addition of blended amendments to acidic sandy soil, there is an increase in soil organic carbon and other soil nutrients with a positive effect on rice yield.

ACKNOWLEDGEMENTS

This research has no funding. I am sincerely thankful to Department of Environmental Science of Tezpur University for providing the laboratory facilities and experimental areas for conducting the research.

REFERENCES

Al-Khuzai AHG, Al-Juthery HWA. Effect of DAP fertilizer source and nano fertilizers (silicon and complete) spray on some growth and yield indicators of rice (*Oryza sativa* L. cv. Anber 33). Proceedings of the IOP Conference Series: Earth and Environmental Science 2020;553:012008.

Arunrat N, Kongsurakan P, Sereenonchai S, Hatano R. Soil organic carbon in sandy paddy fields of Northeast Thailand: A review. Agronomy 2020;10(8):ID1061.

Bharali A, Baruah KK, Baruah SG, Bhattacharyya P. Impacts of integrated nutrient management on methane emission, global warming potential and carbon storage capacity in rice grown in a northeast India soil. Environmental Science and Pollution Research 2018;25:5889-901.

Bhardwaj AK, Rajwar D, Basak N, Bhardwaj N, Chaudhari SK, Bhaskar S, et al. Nitrogen mineralization and availability at critical stages of rice (*Oryza sativa*) crop, and its relation to soil biological activity and crop productivity under major nutrient management systems. Journal of Soil Science and Plant Nutrition 2020;20:1238-48.

Cai A, Zhang W, Xu M, Wang B, Wen S, Shah SAAJ. Soil fertility and crop yield after manure addition to acidic soils in South China. Nutrient Cycling in Agroecosystems 2018;111(1):61-72.

Carrijo DR, Lundy ME, Linquist BA. Rice yields and water use under alternate wetting and drying irrigation: A meta-analysis. Field Crops Research 2017;203:173-80.

Chandini, Kumar R, Kumar R, Prakash O. The impact of chemical fertilizers on our environment and ecosystem. In: Kumar R, Kumar R, Prakash O, editors. Research Trends in Environmental Sciences. India: AkiNik Publication; 2019. p. 69-86.

Datta MG, Devi A. Prospect of application of amendments in a summer rice field: Upholding soil properties via inorganic blended amendments. Communications in Soil Science and Plant Analysis 2020;51(15):1991-2000.

Davies WP. An historical perspective from the green revolution to the gene revolution. Nutrition Reviews 2003;61(6):124-34.

Djaman K, Mel VC, Ametonou FY, El-Namaky R, Diallo MD, Koudahe K. Effect of nitrogen fertilizer dose and application timing on yield and nitrogen use efficiency of irrigated hybrid rice under semi-arid conditions. Journal of Agricultural Science and Food Research 2018;9(2):1000223.

Dimkpa CO, Bindraban PS. Fortification of micronutrients for efficient agronomic production: A review. Agronomy and Sustainable Development 2016;36(1):ID7(1-27).

Dhaliwal SS, Naresh RK, Mandal A, Singh R, Dhaliwal MK. Dynamics and transformations of micronutrients in agricultural soils as influenced by organic matter build-up: A review, Environmental and Sustainability Indicators 2019; 1-2:100007.

Elemike EE, Uzoh IM, Onwudiwe DC, Babalola OO. The role of nanotechnology in the fortification of plant nutrients and improvement of crop production. Applied Sciences 2019;9(3):ID499(1-32).

Faisal N, Farooq M. Application of micronutrients in rice-wheat cropping system of South Asia. Rice Science 2019;26(6): 356-71.

Gunina A, Kuzyakov Y. Sugars in soil and sweets for microorganisms: Review of origin, content, composition and fate. Soil Biology and Biochemistry 2015;90:87-100.

Guo J, Hu X, Gao L, Xie K, Ling N, Shen Q, et al. The rice production practices of high yield and high nitrogen use efficiency in Jiangsu, China. Scientific Reports 2017;7:2101.

Hans X, Xu C, Dungait JAJ, Bol R, Wang X, Wu W, et al. Straw incorporation increases crop yield and soil organic carbon sequestration but varies under different natural conditions and farming practises in China: A system analysis. Biogeosciences 2018;15:1933-46.

Iqbal A, He L, Ali I, Ullah S, Khan A, Khan A, et al. Manure combined with chemical fertilizer increases rice productivity by improving soil health, post-anthesis biomass yield, and nitrogen metabolism. PLoS ONE 2020;15(10):e0238934.

Khush GS. Green revolution: Preparing for the 21st century. Genome 1999;42(4):646-55.

Kibblewhite MG, Ritz K, Swift MJ. Soil health in agricultural systems. Philosophical Transactions of the Royal Society Series B 2007;363(1492):685-701.

Moe K, Moh SM, Htwe AZ, KajiharaY, Yamakawa T. Effects of integrated organic and inorganicf on yield and growth parameters of rice varieties. Rice Science 2019;26(5):309-18.

Lehmann J, Kleber M. The contentious nature of soil organic matter. Nature 2015;528:60-8.

Leip A, Weiss F, Lesschen J, Westhoek H. The nitrogen footprint of food products in the European Union. Journal of Agricultural Science 2014;152:20-33.

Li S, Pu S, Deng F, Wang L, Hu H, Liao S, et al. Influence of optimized nitrogen management on the quality of medium hybrid rice under different ecological conditions. Chinese Journal of Eco-Agriculture 2019;27:1042-52.

Liang Y, Yang Y, Yang C, Shen Q, Zhou L, Yang L. Soil enzymatic activity and growth of rice and barley as influenced by organic matter in an anthropogenic soil. Geoderma 2003; 115:149-60.

Linquist BA, Phengsouvanna V, Sengxue P. Benefits of organic residues and chemical fertilizer to productivity of rain-fed lowland rice and to soil nutrient balances. Nutrient Cycling in Agroecosystem 2007;79:59-72.

Mackill DJ, Ismail AM, Singh US, Labios RV, Paris TR. Development and rapid adoption of submergence-tolerant (Sub1) rice varieties. Advances in Agronomy 2012;115:299-352.

Moscatelli MC, Lagomarsino A, Marinari, S, Angelis, De P, Grego S. Soil microbial indices as bio indicators of environmental changes in a poplar plantation. Ecological Indicators 2005; 5:171-9.

Nadeem F, Farooq M. Application of micronutrients in rice-wheat cropping system of South Asia. Rice Science 2019;26(6): 356-71.

Naher UA, Ahmed MN, Sarkar MIU, Biswas JC, Panhwar QA. Fertilizer management strategies for sustainable rice production. In: Chandran S, Unni MR, Thomas S, editors. Organic Farming: Global Perspective and Methods. Woodhead Publishing Series in Food Science, Technology and Nutrition; 2019. p. 251-67.

Naresh RK, Gupta RK, Shukla AK, Tomar SS. Enhancing carbon sequestration potential and nutrient release dynamics under conservation agriculture in the Indo-Gangetic Plains, India: A review. Journal of Pharmacognosy and Phytochemistry 2018;7(2):326-46.

Ngatia LW, Moriasi D, Grace III JM, Fu R, Gardner CS, Taylor RW. Land use change affects soil organic carbon: An indicator of soil health. In: Otsuki T, editor. Environmental Health. Intech; 2021. p. 1-15.

Page L, Miller RH, Keeney DR. Methods of Soil Analysis Part 2. Wisconsin, USA: Soil Science Society America, Inc; 1982.

Pal DK, Wani SP, Sahrawat KL. Carbon Sequestration in Indian soils: Present status and the potential. Proceeding of the National Academy of Sciences India Section B: Biological Sciences 2015;85(2):337-58.

Rose GH, Temminghoff EJM, Hoffland E. Nitrogen mineralisation: Review and meta-analysis of the predictive value of soil tests. European Journal of Soil Science 2011;62:162-73.

Shukla AK, Behera SK. All india coordinated research project on micro- and secondary nutrients and pollutant elements in soils and plants. Research Achievements and Future Thrusts Indian Journal of Fertilisers 2019;15(5):522-43.

Singh RB, Kumar P, Woodhead T. Smallholder Farmers in India: Food Security and Agricultural Policy. Bangkok, Thailand: FAO: RAP Publication 2002/03; 2002.

Singh RB. Environmental consequences of agricultural development: A case study from the green revolution state of Haryana, India. Agriculture, Ecosystems and Environment 2000;82(1-3):97-103.

Walkley A, Black I. An examination of Degtjareff method for determining soil organic matter and a proposed modification of the chromic acid titration method. Soil Science 1937;37:29-37.

Effect of Fungus-Growing Termite on Soil CO_2 Emission at Termitaria Scale in Dry Evergreen Forest, Thailand

Warin Boonriam[1], Pongthep Suwanwaree[2*], Sasitorn Hasin[3], Phuvasa Chanonmuang[4], Taksin Archawakom[5], and Akinori Yamada[6,7]

[1]*Faculty of Environment and Resource Studies, Mahidol University, Nakhon Pathom 73170, Thailand*
[2]*School of Biology, Institute of Science, Suranaree University of Technology, Nakhon Ratchasima 30000, Thailand*
[3]*Innovation of Environmental Management, College of Innovative Management, Valaya Alongkorn Rajabhat University under the Royal Patronage, Pathum Thani 13180, Thailand*
[4]*Expert Centre of Innovation Clean Energy and Environment, Thailand Institute of Scientific and Technological Research, Pathum Thani 12120, Thailand*
[5]*Sakaerat Environmental Research Station, Nakhon Ratchasima 30370, Thailand*
[6]*Department of Biological Sciences, Tokyo Institute of Technology, Tokyo 152-8550, Japan*
[7]*Graduate School of Fisheries and Environmental Sciences, Nagasaki University, Nagasaki 852-8521, Japan*

ARTICLE INFO

Received: 24 Mar 2021
Received in revised: 10 Jul 2021
Accepted: 20 Jul 2021
Published online: 10 Sep 2021
DOI: 10.32526/ennrj/19/202100048

Keywords:
CO_2 efflux/ *Macrotermes carbonarius*/ Termite mound/ Soil respiration/ Spatial variation/ Dry evergreen forest

*** Corresponding author:**
E-mail: pongthep@sut.ac.th

ABSTRACT

Termites are one of the major contributors to high spatial variability in soil respiration. Although epigeal termite mounds are considered as a point of high CO_2 effluxes, the patterns of mound CO_2 effluxes are different, especially the mound of fungus-growing termites in a tropical forest. This study quantified the effects of a fungus-growing termite (*Macrotermes carbonarius*) associated with soil CO_2 emission by considering their nesting pattern in dry evergreen forest, Thailand. A total of six mounds of *M. carbonarius* were measured for CO_2 efflux rates on their mounds and surrounding soils in dry and wet seasons. Also, measurement points were investigated for the active underground passages at the top 10% of among efflux rates. The mean rate of CO_2 emission from termitaria of *M. carbonarius* was 7.66 µmol $CO_2/m^2/s$, consisting of 2.94 and 9.11 µmol $CO_2/m^2/s$ from their above mound and underground passages (the rate reached up to 50.00 µmol $CO_2/m^2/s$), respectively. While the CO_2 emission rate from the surrounding soil alone was 6.86 µmol $CO_2/m^2/s$. The results showed that the termitaria of *M. carbonarius* contributed 8.4% to soil respiration at the termitaria scale. The study suggests that fungus-growing termites cause a local and strong variation in soil respiration through underground passages radiating out from the mounds in dry evergreen forest.

1. INTRODUCTION

Carbon dioxide (CO_2) emission from soils (soil respiration) is an important of the carbon balance in terrestrial ecosystems. Soil respiration contributes 50-95% of the total ecosystem respiration (Janssens et al., 2001; Chambers et al., 2004) as well as the second largest terrestrial carbon emission in the forest ecosystems (Solomon et al., 2007). Soil respiration comes from CO_2 production of all living organisms in the soil, including plant roots, soil microbes, and animals (Lavelle and Spain, 2001; Luo and Zhou, 2006). Tropical forests contribute to over a third of net primary productivity in global terrestrial ecosystems (Field, 1998; Roy and Saugier, 2001; Field and Raupach, 2004). According to Bonan (2008) reported that about 45% of global terrestrial carbon stocks were contributed by tropical forests. Consequently, tropical forests could strongly influence future CO_2 concentration in atmosphere.

High variability in soil respiration from tropical forests has been discussed. Although soil microorganisms and roots constitute the dominant contributors of soil respiration, the rate of soil respiration has been shown to change and fluctuate at an unexpectedly large scale (10-90%) (Hanson et al., 2000). It is difficult to explain by known environmental factors, such as soil water content and temperature. According to Ohashi et al. (2007) and

Citation: Boonriam W, Suwanwaree P, Hasin S, Chanonmuang P, Archawakom T, Yamada A. Effect of fungus-growing termite on CO_2 emission from soil at termitaria scales in a seasonal tropical forest, Thailand. Environ. Nat. Resour. J. 2021;19(6):503-513. (https://doi.org/10.32526/ennrj/19/202100048)

Ohashi et al. (2017), extremely higher rates of soil respiration as hot spots (>10 µmol $CO_2/m^2/s$) were observed in the tropical forest of Southeast Asia and suggested that soil macrofauna were the main causes in a tropical forest. Thus, the phenomena were proposed to be attributed to un-revealed activities of soil animals, especially social insects such as termites, because it is well known that termites are superabundant soil animals in seasonal tropical forests (Yamada et al., 2003; Yamada et al., 2005).

Termites play an important role in litter decomposition processes as much as half of the primary litter production (Matsumoto and Abe, 1979; Bignell and Eggleton, 2000; Coleman et al., 2004). They have caused interest in their respiratory gas exchanges associated with soil respiration at niche differentiation. Mound building termites, especially fungus-growing termites (Macrotermitinae) cultivate symbiotic fungi on fungus gardens (fungus combs) that consist of plant litter materials built by using their partially digested faeces (Korb, 2003). A termite colony built the nest ranges from small belowground chambers to large aboveground mounds with the underground passages for its foraging behavior, called termitaria. In tropical savanna, several studies reported that a part of the epigeal termite mound emitted higher CO_2 than its surrounding soils (Konate et al., 2003; Brümmer et al., 2009; Risch et al., 2012). In the tropical forest, according to Lopes de Gerenyu et al. (2015) reported that termite mounds contributed up to 10% of the total soil respiration in southern Vietnam. On the other hand, there was no significant effect of termite mounds on soil CO_2 emission in the tropical rainforest, China (Song et al., 2013). However, the mounds have a complex architecture that allows for the constant environment in temperature and humidity. To evaluate how much CO_2 efflux by underground passages from the mound where could lead to high spatial heterogeneity of soil respiration in the tropical forests.

To date, there is no compelling evidence to support the effect of termites on soil respiration in seasonal tropical forests. Here, this study focuses on the effect of termites on soil respiration by considering their nesting pattern. Numerous termite nests have underground passages expanding from the nest center to up to several tens meters. Not only the nest itself but also their surrounding area has been affected by termite activities. Consequently, the observation was conducted in termitaria of the fungus-growing termites in order to depict the effects of termites on soil respiration at a large scale, and the results can be applied to tropical forest ecosystems.

2. METHODOLOGY

2.1 Study site

A field study was conducted in the dry evergreen forest (DEF) at Sakaerat Environmental Research Station (SERS) (14°30′N, 101°56′E; approximately 500 m above sea level) in Nakhon Ratchasima Province, northeastern Thailand (Figure 1). According to SERS meteorological station from 2005 to 2015, the mean annual rainfall was 1,083.8 mm with monthly rainfall less than 40 mm during the dry season from November to March and the wet season lasting from May to October. The averages of relative humidity and the annual temperature were 83.8% and 26.7ºC (9.1-38.9ºC), respectively. The DEF covers an area of 29.5 km^2, where the dominant tree species are *Hopea ferrea* and *Hopea odorata* with canopy trees generally reaching 23 to 40 m high (Kanzaki et al., 1995).

2.2 Field experiments design

Six mounds of *M. carbonarius* were randomly determined for the mound CO_2 emission with a distance greater than 10 m between each mound. The mounds were chosen at different places in the DEF according to the vegetation, elevation. Mound sizes were measured for the height (base to the top) and circular length of the bottom. A plot (10 m × 10 m) was set up to cover each mound and its surrounding soil. Each plot was divided into 100 grids (1 m × 1 m in each grid). PVC collars were placed on a mound randomly at 5 to 6 points and the center of the grids for 100 points in each mound plot (Figure 2). CO_2 emission rates were measured using a portable infrared gas analyzer (IRGA, EGM-4, PP Systems, Hitchin, UK) with a closed soil CO_2 efflux chamber (SRC-1, PP Systems) (diameter 10 cm) for 1 time per dry season from December 2014 to May 2015, and wet seasons from October 2015 to November 2015. After CO_2 measurement, the soil temperatures and soil moisture contents were measured immediately around each PVC collar at about 10 cm depth by using a digital thermometer waterproof probe (type H-1 and H-2, Shinwa Co., Ltd., Japan) and soil moisture sensor (SM150, Delta-T Devices Ltd., Cambridge, UK), respectively. The measurement was performed one day per plot with starting from 9:00 am until 6:00 pm (3 to 5 minutes per point) without rainfall.

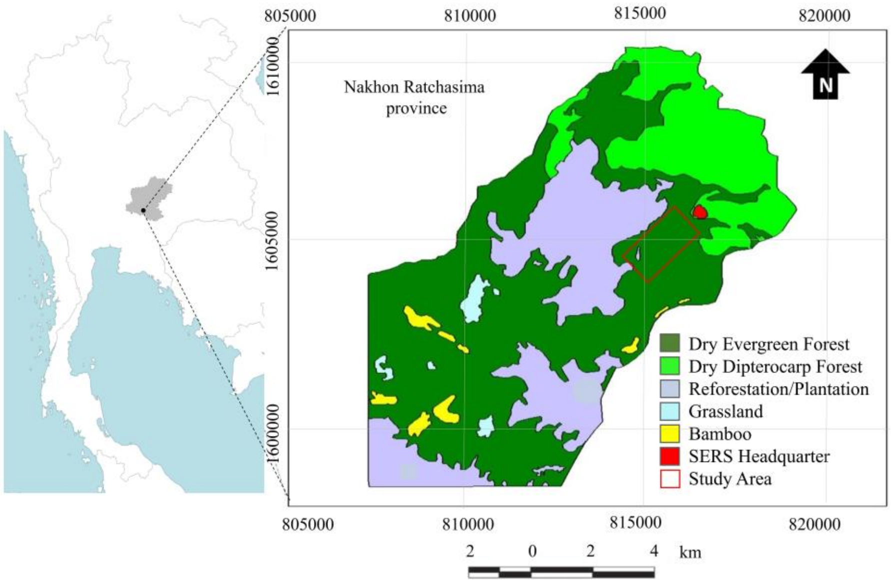

Figure 1. Study site in DEF at Sakaerat Environmental Research Station (SERS), Thailand. (SERS map modified from Trisurat, 2010)

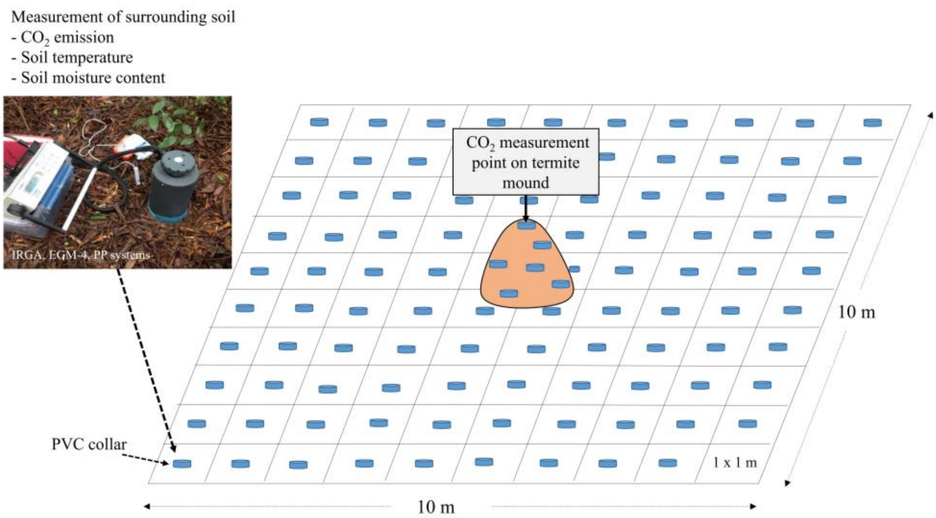

Figure 2. Experimental design for determine CO_2 emission and relative factors from the termitaria of *M. carbonarius*.

The high emission rate was determined at top 5% (>6 µmol $CO_2/m^2/s$ in dry season), and top 10% (>10 µmol $CO_2/m^2/s$ in wet season) of CO_2 emission rates. If the high rate was found on the measurement points in each plot (excepted on mound), this points was examined for active or inactive termitaria by excavating in the depth of 40 cm, such excavated underground passages will be soon repaired about 1 h. by termites. The depth and diameter of underground passages were measured. The distributions of the high rate efflux points were put on the map of the plot scale.

2.3 Statistical analysis

All the raw data were tested for normality by using the Kolmogorov-Smirnov test. Significant differences of CO_2 emission rates between the termite mounds and surrounding soils for the dry and wet seasons were detected by the univariate ANOVA with Tukey's HSD Post-hoc test. The relationship of CO_2 emissions between depth and diameter of underground passages from mounds of *M. carbonarius* was tested using linear regression analysis. All statistical calculations were performed in SPSS ver. 20.0.0 for Windows.

3. RESULTS

3.1 CO_2 efflux from termitaria of fungus-growing termite (*M. carbonarius*)

The total average of CO_2 emission rates from the termitaria of *M. carbonarius* and the surrounding soil was 7.10±4.74 µmol $CO_2/m^2/s$. There was a significant difference among the six plots (Table 1).

CO_2 emission rates from the mounds and surrounding soils were significantly different between dry and wet seasons (Table 2). The annual mean of CO_2 efflux rates from the mounds was 2.94±2.73 µmol $CO_2/m^2/s$ which was 2.5 times significantly lower than the surrounding soils (included the underground passages) of 7.36±4.72 µmol $CO_2/m^2/s$, with a wide range from 0.91 to 50.00 µmol $CO_2/m^2/s$ (Figure 3). CO_2 efflux from the surrounding soils was higher in the wet season than the dry season ($F=436.38$, $p<0.001$), while above mound CO_2 emissions itself were higher in the dry season (3.86±3.35 µmol $CO_2/m^2/s$) than wet season (2.06±1.52 µmol $CO_2/m^2/s$).

Table 1. CO_2 emission rates from six plots of *M. carbonarius* (mound and surrounding soil) with varying mound sizes in dry and wet seasons.

Plot	Mound area (m^2)	CO_2 emission (µmol $CO_2/m^2/s$±SD)			
		Dry season		Wet season	
		Mound (n=6)	Surrounding soil (n=100)	Mound (n=6)	Surrounding soil (n=100)
1	0.64	5.34	3.69	1.44	10.54
2	0.24	3.07	2.32	3.94	8.20
3	1.85.	2.48	5.43	1.67	12.24
4	1.61	1.90	7.11	1.06	9.85
5	3.85	6.97	7.66	2.03	10.14
6	2.55	3.41	4.39	2.20	8.87
Location average		3.86±3.35	5.10±4.06	2.06±1.52	9.97±4.24
Season average		5.03±4.03		9.17±4.49	
Total average	1.79	7.10±4.74			

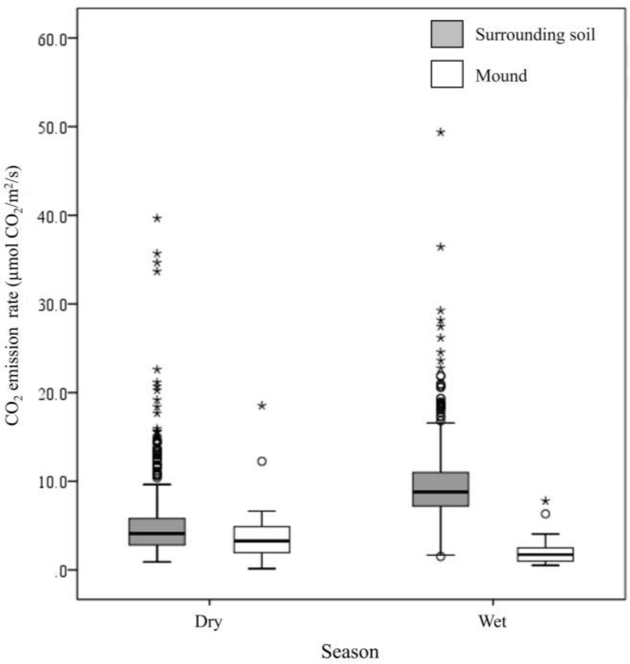

Figure 3. Box plots of distribution of seasonal variation in CO_2 emission rates from termitaria of *M. carbonarius* in dry and wet season. Box plots indicate the distribution by percentiles. The median is given by horizontal line in the box. A part of bottom and top of the box indicates 25th and 75th percentiles, respectively. The whiskers extend out to the maximum or minimum value of the data. Significant differences are indicated by asterisk on the curly bracket ($p=0.001$).

Table 2. Differences in CO_2 emission between the plot, area (mound and surrounding soil), and season.

Source of variation	CO_2 emission rate (µmol $CO_2/m^2/s$)		
	df	F	p
Plot	5	2.464	**0.031**
Season	1	9.027	**0.003**
Area	1	95.130	**0.001**
Plot × Season	5	2.595	**0.024**
Plot × Area	5	2.593	**0.024**
Season × Area	1	48.94	**0.001**
Plot × Season × Area	5	1.984	0.078

Statistically significant p values are in bold.

As extremely high CO_2 points, the top 5-10% of CO_2 emission rates were considered in each plot. A total number of high CO_2 points were found at 101 points among 1,200 measurement times. These points were examined which consisting of 3 types as active underground passage (Figure 4), lateral root, and normal soil. The termitaria as underground passages were found 69.31% of all the points, the remaining of 26.73% and 3.96% were roots (almost closed to the big tree) and the normal soils, respectively (Table 3). An area of termitaria as underground passages was calculated as 5.83 m^2 by the number of active underground passages (70) among measurement points (1,200) per plot area (100 m^2).

Figure 4. Active underground passages of *M. carbonarius* mound representing high CO_2 emission resources

Table 3. Examination of underground soils on measurement point of high CO_2 emission rate

Examination of underground soil*	Termitaria (underground passage)	Surrounding soil	
		Root	Normal soil
Number of high CO_2 emission source	70	27	4
Average of CO_2 emission rate (μmol $CO_2/m^2/s$)	15.97±9.20	18.11±5.90	16.99±2.83

*Underground passage=active underground passage from the mound of *M. carbonarius*, Root=lateral root/branch root, and normal soil=neither found.

Mean of CO_2 efflux rate (±SD) from the underground passages of *M. carbonarius* mounds was 15.97±9.20 μmol $CO_2/m^2/s$. Frequency distribution of CO_2 efflux rates from the soil around the mounds, and underground passages of the termite mounds is shown in Figure 5. CO_2 efflux rates from surrounding soil including the underground passages (7.36±4.72 μmol $CO_2/m^2/s$) was significantly higher than soil alone around the mound (6.86±3.92 μmol $CO_2/m^2/s$) ($p<0.001$), whereas CO_2 effluxes from the surrounding soils included the high CO_2 efflux rates from the flat roots and normal soils, which had mean values of 18.11 and 16.99 μmol $CO_2/m^2/s$, respectively.

3.2 Effect of termitaria (*M. carbonarius*) and surrounding soils on soil respiration

As mentioned above, the mean rate of CO_2 emission from the underground passages of *M. carbonarius*'s mound was immoderately high. In fact, this rate was not only from the activities of termites but also from the microbe activities by the gas passed through the nearby soils associated with underground tunnels. Thus, the mean CO_2 emission rate was 9.11 μmol $CO_2/m^2/s$ from only the underground passages (5.83 m^2) by excluded the mean CO_2 emission rate of surrounding soils (6.86 μmol $CO_2/m^2/s$). However, CO_2 emission rate from above the mound was only 2.94 μmol $CO_2/m^2/s$ with area of 1.79 m^2. The finding in the results showed that the average of CO_2 emission from the termitaria (mound and underground passage) of *M. carbonarius* was 7.66 μmol $CO_2/m^2/s$ with the total area of 7.62 m^2. Consequently, the fungus-growing termite (*M. carbonarius*) contributed 8.43% to soil respiration at the termitaria scale (100 m^2), consisting of the mounds and the underground passages of 0.76% and 7.67%, respectively (Figure 6). In addition, the relationship between underground passages of *M. carbonarius* and their CO_2 emission rates was determined. There was no significant difference in CO_2 efflux rates between depth and diameter of underground passages in the dry and wet seasons as an example in Figure 7.

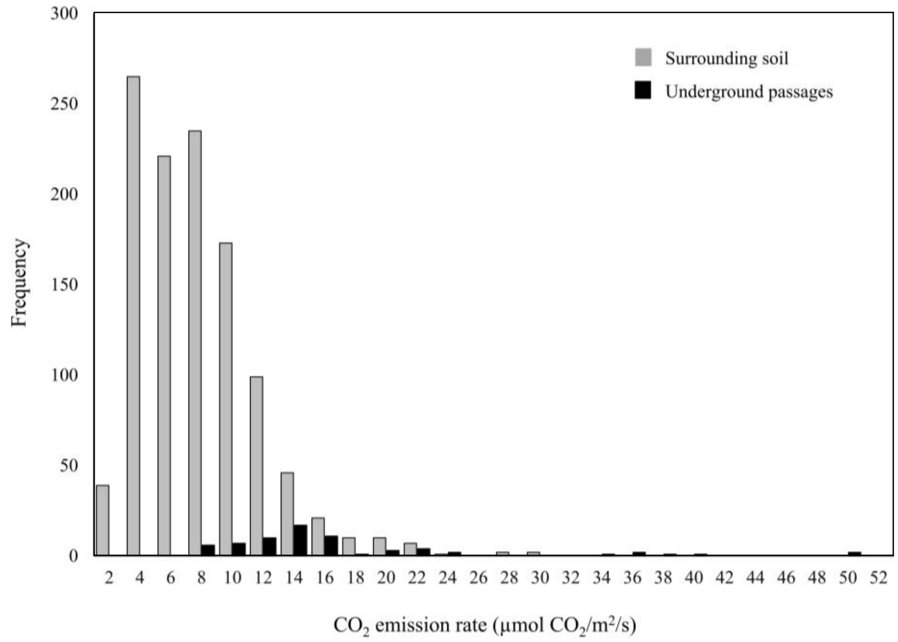

Figure 5. Frequency distribution of CO_2 emission rate from surrounding soil and underground passages (activities of termite+natural microbe) of *M. carbonarius* mounds

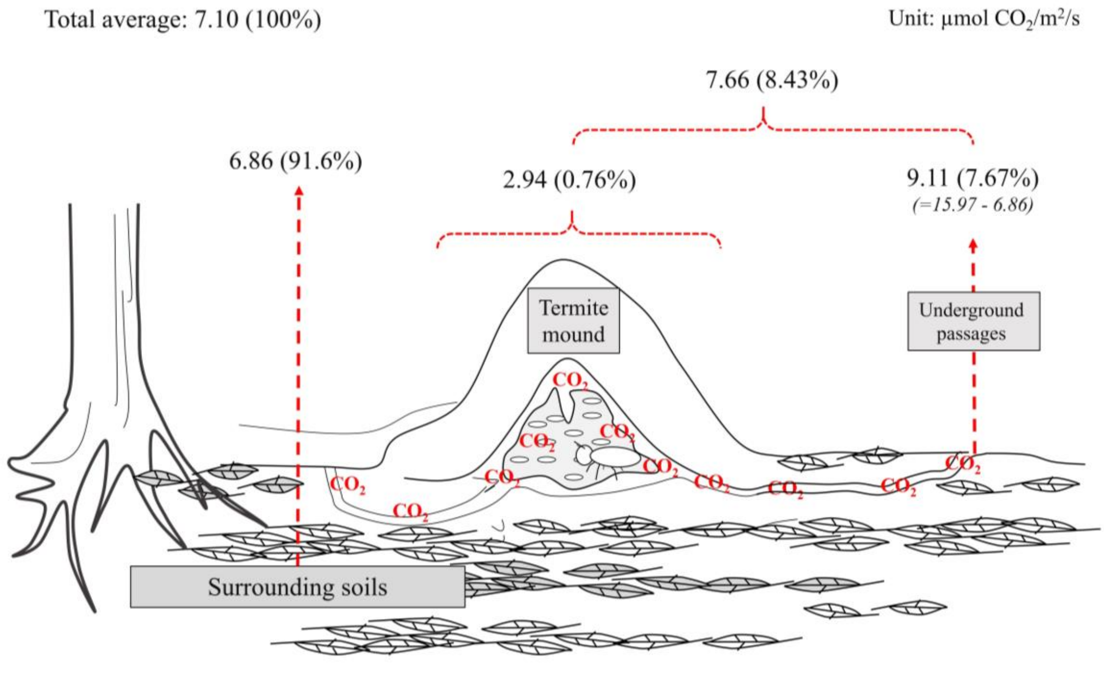

Figure 6. An aspect of contribution of *M. carbonarius*'s termitaria and surrounding soil on soil respiration at area scale 100 m^2

3.3 Changes in soil respiration with soil temperature and soil moisture content

The temporal variation in soil respiration, as well as soil temperature and moisture, showed large variation by the season. Annual respiration of surrounding soil was significantly positively correlated with soil temperature ($R=0.259$, $p<0.001$) and soil moisture content ($R=0.359$, $p<0.001$) (Figure 8). However, the rate of soil respiration tended to drop with soil temperature and moisture tended to high. As the result, there was ambiguity between the effects of soil temperature and soil moisture on the variability of soil respiration, because this result includes both temporal and spatial variation, especially hot spots from the underground passages.

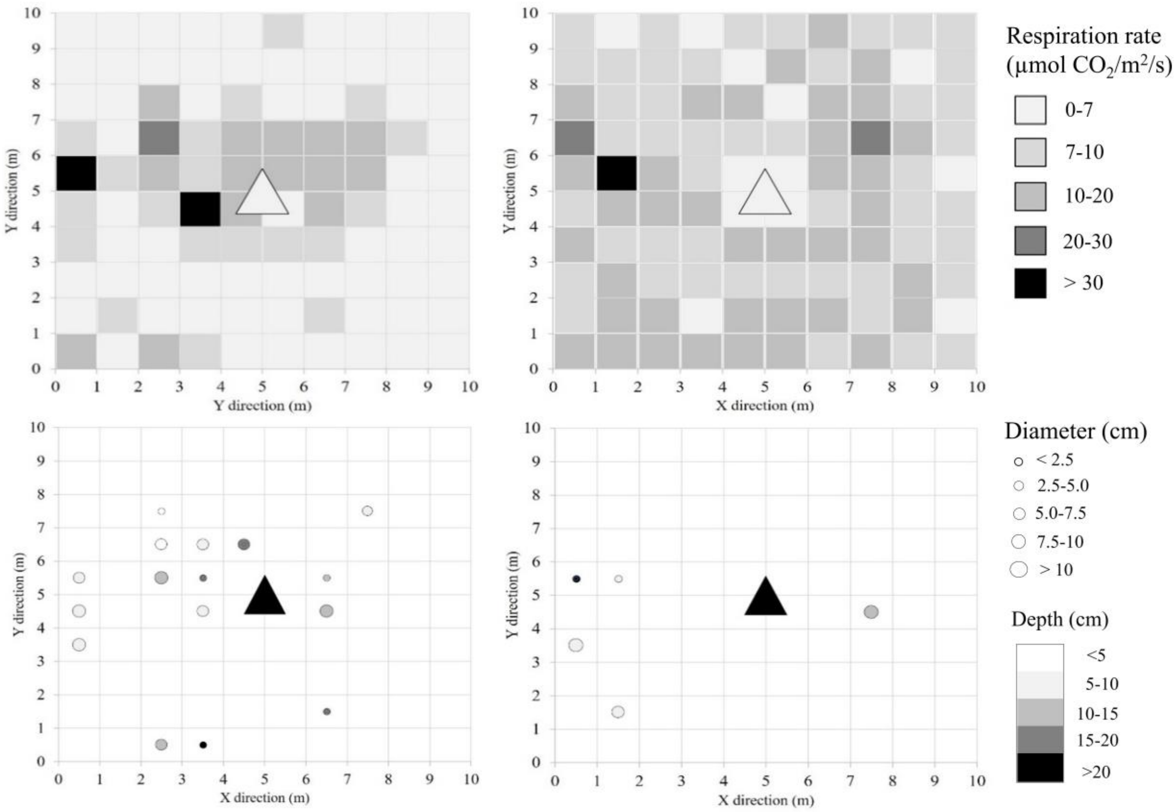

Figure 7. An example of distribution maps of CO_2 emission rate (top row) and underground passage (bottom row) with the diameter and depth from a mound (triangle) of *M. carbonarius* in dry season (left) and wet (right) seasons

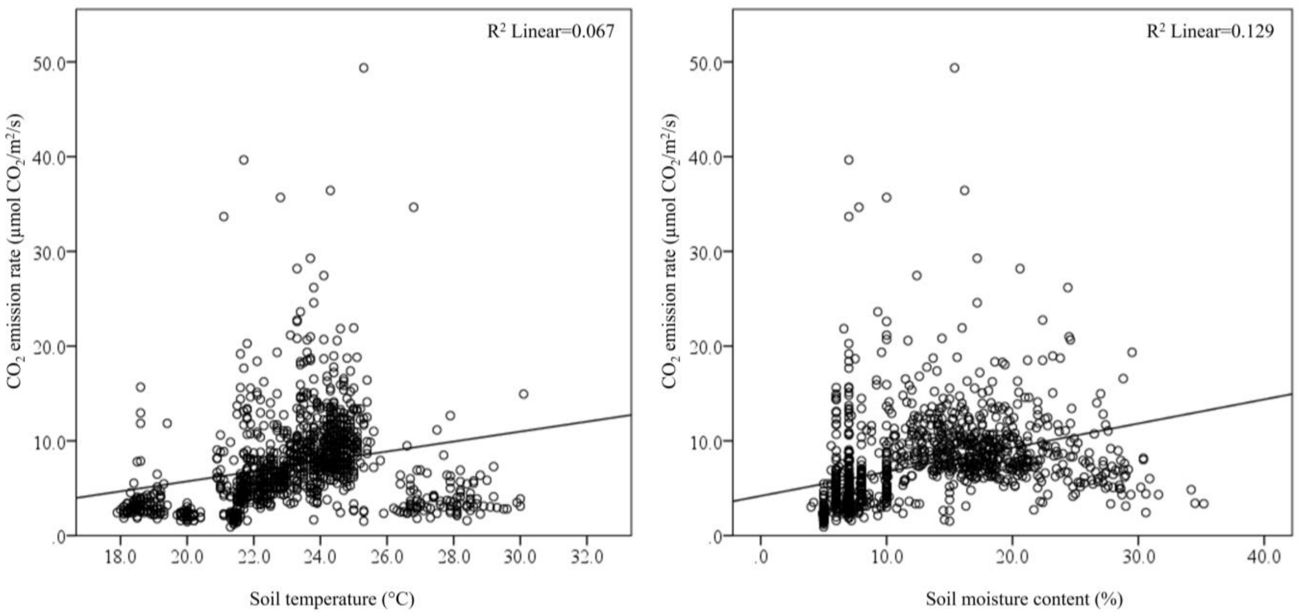

Figure 8. The relationship between soil respiration and soil temperature and moisture.

4. DISCUSSION

Our results showed that the mean of the frequency distribution of the respiration rates from surrounding soils alone (6.86 µmol $CO_2/m^2/s$) was determined as respiration rates from soil microbes, roots, and subterranean soil insects or animals at the termitaria scales (100 m^2/mound). In the same forest, the rate of soil respiration was widely fluctuations in both dry season (1.3-6.1 µmol $CO_2/m^2/s$) and wet season (3.6-14.5 µmol $CO_2/m^2/s$) where was considered by Hasin et al. (2014). The rate of the ground soil respiration in this study was similar to the rate of 6.57 µmol $CO_2/m^2/s$ in the same site (Boonriam et al., 2021) as well as the rates of 6.05 and 6.76 µmol $CO_2/m^2/s$ from DEF of northern Thailand which reported by Adachi et al. (2009) and Hashimoto et al. (2004) respectively. It seems that the CO_2 emission rate of this study has not much change over the years. In addition, the previous other studies had shown the rate of soil respiration in various tropical forests which were 6.45 µmol $CO_2/m^2/s$ in Amazon, Brazil (Sotta et al., 2004), 3.96-5.32 µmol $CO_2/m^2/s$ in Malaysia (Ohashi et al., 2007; Ohashi et al., 2017), and 4.28 µmol $CO_2/m^2/s$ in Vietnam (Avilov et al., 2019).

In this study, fungus-grower termite (*M. carbonarius*) has a crucial influence on soil respiration by the total rate of CO_2 emissions from their termitaria (7.66 µmol $CO_2/m^2/s$), especially CO_2 emissions from underground passages (9.11 µmol $CO_2/m^2/s$) at termitaria scale in this forest. As results of this study, CO_2 emission from above the mounds (2.94 µmol $CO_2/m^2/s$) were 2.5 and 3.1 times significantly lower than their surrounding soils (including underground passages) and only underground passages, respectively. Our result showed that the dispersal (transmission) of the CO_2 emission from the underground passages of *M. carbonarius*'s mounds were expressed as at top 5% (>6 µmol $CO_2/m^2/s$ in dry season), and top 10% (>10 µmol $CO_2/m^2/s$ in wet season) of CO_2 emission rates. There were extremely high at around the surrounding soils as much as the rate of hot spots in Malaysia-tropical rainforest that were suggested by Ohashi et al. (2007). Although Ohashi et al. (2017) determined that the CO_2 emission from the termite nest was higher than the surrounding soil in Malaysia-tropical rainforest, the rate was conducted from different types of nests comprising tree base (nests built on a tree base), epigeous and subterranean nests. On the other hand, Song et al. (2013) reported that the termite mound did not affect as hot spot to soil respiration in China-tropical rainforest with the range of 1.63 to 3.71 µmol $CO_2/m^2/s$. These mounds were either typical soil-feeding termites (non-fungus grower), or the fungus-growing termites that build a dome-shaped mound with thick walls and several branching underground passages (Inoue et al., 2001).

Mound-building termites construct the nests in sophisticated ways to achieve the thermoregulation and gas exchange (Noirot and Darlington, 2000; Korb, 2003). According to Inoue et al. (2001) conducted in the same DEF, Thailand, the study found that about 4-10 main underground passages radiating out from each *M. carbonarius*'s mound and build the dome-shaped mounds with a thick wall. The thickness of the mound wall was about 20-40 cm thick. Thus, it was difficult for passing gas through the wall. On the other hand, while the gas exchange was mostly released through the central mound in tropical savanna according to Konate et al. (2003), Brümmer et al. (2009), and Risch et al. (2012). For example in Konate et al. (2003) reported that the mounds of fungus-growing termites emitted about 10-19 µmol $CO_2/m^2/s$ compared to 5-10 µmol $CO_2/m^2/s$ from its surrounding soils. However, CO_2 emission from termite mounds in savannas contributes less than 1% to total soil respiration (Brümmer et al., 2009; Jamali et al., 2013). In relative hot environments as tropical savannas, fungus-growing termites (*Macrotermes* species.) built mounds like a cathedral shape to maintain the inside temperature and CO_2 concentration for fungus cultivation in the mounds at 30ºC and 0.2-1.0%, respectively (Korb and Linsenmair, 2001). In contrast, the mound architecture in tropical forest relatively cool environments has achieved to maintain the inside temperature (28-30ºC) and CO_2 concentration (1.0-1.5%) by building the dome-shaped structure with thick walls (Korb and Linsenmair, 2001). As our results, mound CO_2 emission of the fungus-growing termites in tropical forests is quite different from the tropical savannas by the nest pattern and ventilation.

Fungus-growing termite contributions to soil respiration were not only from individual termite activities but also from the nest material (fungus combs). Fungus combs have much higher biomass than termite individuals in mound (Konate et al., 2003; Yamada et al., 2005) and release a high rate of CO_2 emissions (Sugimoto et al., 2000). In the same forest, according to Yamada et al. (2005) estimated the fraction of respiration from annual aboveground litterfall, the total amount of respiration rate from fungus combs (7.2%) was six times higher than the population of fungus growers (1.2%), while non fungus-growing termites respired as 2.8% of carbon in the annual aboveground litterfall. Apparently, fungus-growing termite in a tropical forest has the potential of fungus combs to mound CO_2 emissions that mediated by termites as well as a previous study in savannas according to Konate et al. (2003). In addition, the fungus grower, especially *M. carbonarius* is widely distributed in Southeast Asia such as Thailand, Cambodia, Vietnam, and Malaysia (Roonwal, 1970).

In recent research, the density of *M. carbonarius* was recorded at 33 mounds/ha in the same forest of the DEF of northeast Thailand (Boonriam, 2016).

In general, soil CO_2 emission rate increased with increasing soil temperature and soil moisture content (Lloyd and Taylor, 1994; Xu and Qi, 2001; Qi et al., 2002; Reichstein et al., 2002). Nevertheless, this study results seem as if the values of soil temperature and soil moisture content were moving to high point, the soil respiration rates tend to drop. According to Boonriam et al. (2021) implied that soil respiration in the same forest was limited by soil moisture during the dry season, so the increase in soil temperature to a very high degree reduced soil moisture even more, which reduced soil respiration. In addition, precipitation variability can have an effect on soil respiration. A high soil moisture content creates a barrier on the surface of the soil atmosphere, which may inhibit the release of CO_2 from the soil. (Sotta et al., 2004; Wood et al., 2013).

In tropical forests, the soil CO_2 emission was mainly controlled by soil organic carbon and soil moisture (Pandey and Singh, 2018), while soil temperature was slightly related to soil respiration during the wet season (Intanil et al., 2018). However, CO_2 emission rates from the mounds of fungus-growing termites were significantly higher in the dry season than in the wet season resulting in this study. As the expected result, the respiration rate on the termite mound should be very low by little plant litters falling to the top, low microbial activity in the dry season, and the thickness of the mound wall as well. In this case, there was probably due to the relatively hot-dry environments that affected termites to maintain inside to optimal conditions by exchange gases through the thinnest part or dry cracked parts of the mound wall. Perhaps, according to Ashton et al. (2019) found that the termite abundance and activity (included *Macrotermes*) increased during the drought in the tropical forest. Therefore, termite mound needs to control the condition inside the mound to the optimal (Korb, 2003). In Asian zone, Ocko et al. (2017) noted that the active *Macrotermes* mound must be effectively ventilated to remove CO_2 and heat with diffusivity through their porous surface and underground passages by contribution of the diurnal wind.

For attractive features of earlier studies, CO_2 emissions from termite mounds have confirmed that mounds are important local hot spots, estimated to be between 0.05 and 0.27 µmol $CO_2/m^2/s$, representing reach up to 3% of the total estimated ecosystem respiration (Chambers et al., 2004; van Asperen et al., 2021). However, seasonal tropical forests have sometimes a fluctuation of the climate. Consequently, this contribution of mound CO_2 emission in terms of fungus-growing termites is one of the best approaches for evaluating soil biological activities in relation to carbon and energy flow in terrestrial ecosystems.

5. CONCLUSION

Overall, the study highlights the termitaria of fungus-growing termite (*M. carbonarius*) was contributed about 8.4% to the soil respiration at termitaria scale. The rate of CO_2 emissions from the mound alone was lower than their surrounding soil. However, the high CO_2 emissions from the surrounding soil were affected by the underground passage through from the nest/colony of the fungus-growing termite. Future information regarding the total soil CO_2 emission and the mound density on large scale as well as their environmental conditions are necessary for evaluating the contribution to the total soil respiration in Thai-tropical forest.

ACKNOWLEDGEMENTS

This work was mainly supported by the Japan Society for the Promotion of Science under Grant-in-Aid for Young Scientists (B) 25850104 (to AY). This study was also partly financially supported by both Suranaree University of Technology and Thailand Institute of Scientific and Technological Research (TISTR). We are thankful to SERS staff for their advice and support in this study.

REFERENCES

Adachi M, Ishida A, Bunyavejchewin S, Okuda T, Koizumi H. Spatial and temporal variation in soil respiration in a seasonally dry tropical forest, Thailand. Journal of Tropical Ecology 2009;25:531-9.

Ashton LA, Griffiths HM, Parr CL, Evans TA, Didham RK, Hasan F, et al. Termites mitigate the effects of drought in tropical rainforest. Science 2019;363(6423):174-7.

Avilov VK, Ivanov DG, Avilov KK, Kotlov IP, Thinh NV, Luu DP, et al. Hot spots of soil respiration in a seasonally dry tropical forest in southern Vietnam: A brief study of spatial distribution. Geography, Environment, Sustainability 2019; 12(2):173-82.

Bignell DE, Eggleton P. Termites in ecosystems. In: Abe T, Higashi M, Bignell DE, editors. Termites: Evolution, Sociality, Symbiosis, Ecology. Dordrecht: Kluwer Academic Press; 2000. p. 363-87.

Boonriam W. CO_2 Emission from Soil and Termitaria in Dry Evergreen Forest at Sakaerat Environmental Research Station [dissertation]. Suranaree University of Technology; 2016.

Boonriam W, Suwanwaree P, Hasin S, Archawakom T, Chanonmuang P, Yamada A. Seasonal changes in spatial variation of soil respiration in dry evergreen forest, Sakaerat Biosphere Reserve, Thailand. ScienceAsia 2021;47S:112-9.

Bonan GB. Forests and climate change: forcings, feedbacks, and the climate benefits of forests. Science 2008;320:1444-49.

Brümmer C, Papen H, Wassmann R, Brüggemann N. Fluxes of CH_4 and CO_2 from soil and termite mounds in south Sudanian savanna of Burkina Faso (West Africa). Global Biogeochemical Cycles 2009;23:GB1001.

Chambers JQ, Tribuzy ES, Toledo LC, Crispim BF, Higuchi N, Dos Santos J, et al. Respiration from a tropical forest ecosystem: Partitioning of sources and low carbon use efficiency. Ecological Applications 2004;14(4):72-88.

Coleman DC, Crossley DA, Hendrix PF. Fundamental of Soil Ecology. 2nd ed. United Kingdom: Elsevier Academic Press; 2004.

de Gerenyu VL, Anichkin A, Avilov V, Kuznetsov A, Kurganova I. Termites as a factor of spatial differentiation of CO_2 fluxes from the soils of monsoon tropical forests in southern Vietnam. Eurasian Soil Science 2015;48:208-17.

Field CB. Primary production of the biosphere: Integrating terrestrial and oceanic components. Science 1998;281:237-40.

Field CB, Raupach MR. The Global Carbon Cycle: Integrating Humans, Climate, and the Natural World. Washington DC: Island Press; 2004. p. 526.

Hanson PJ, Edwards NT, Garten CT, Andrews JA. Separating root and soil microbial contributions to soil respiration: A review of methods and observations. Biogeochemistry 2000;48:115-46.

Hashimoto S, Tanaka N, Suzuki M, Inoue A, Takizawa H, Kosaka I, et al. Soil respiration and soil CO_2 concentration in a tropical forest, Thailand. Journal Forestry Research 2004;9:75-9.

Hasin S, Ohashi M, Yamada A, Hashimoto Y, Tasen W, Kume T, et al. CO_2 efflux from subterranean nests of ant communities in a seasonal tropical forest, Thailand. Ecology and Evolution 2014;20(4):3929-39.

Inoue T, Kirtibutr N, Abe T. Underground passage system of *Macrotermes Carbonarius* (Isoptera, Termitidae) in a dry evergreen forest of northeast Thailand. Insectes Sociaux 2001;48:372-7.

Intanil P, Boonpoke A, Sanwangsri M, Hanpattanakit, P. Contribution of root respiration to soil respiration during rainy season in dry Dipterocarp Forest, Northern Thailand. Applied Environmental Research 2018;40(3):19-27.

Jamali H, Livesley SJ, Hutley LB, Fest B, Arndt SK. The relationships between termite mound CH_4/CO_2 emissions and internal concentration ratios are species specific. Biogeosciences 2013;10:2229-40.

Janssens IA, Kowalski AS, Ceulemans R. Forest floor CO_2 fluxes estimated by eddy covariance and chamber-based model. Agricultural and Forest Meteorology 2001;106:61-9.

Kanzaki M, Kagotani M, Kawasaki T, Yoda K, Sahunalu P, Dhammanonda P, et al. Forest structure and composition of tropical seasonal forests of Sakaerat Environmental Research Station and the effects of fire protection on a dry deciduous forest. In: Yoda K, Sahunalu P, Kanzaki K, editors. Elucidation of the Missing Sink in the Global Carbon Cycling-Focusing on the Dynamics of Tropical Seasonal Forests. Osaka: Osaka City University; 1995. p. 1-20.

Konate S, Roux XL, Verdier B, Lepage M. Effect of underground fungus-growing termites on carbon dioxide emission at the point and landscape-scales in African savanna. Functional Ecology 2003;17:305-14.

Korb J. Thermoregulation and ventilation of termite mounds. Naturwissenschaften 2003;90:212-9.

Korb J, Linsenmair KE. The causes of spatial patterning of mounds of a fungus-cultivating termite: Results from nearest neighbor analysis and ecological studies. Oecologia 2001;127:324-33.

Lavelle P, Spain A. Soil Ecology. Dordrecht: Kluwer Academic Press; 2001. p. 365-87.

Lloyd J, Taylor JA. On the temperature dependence of soil respiration. Functional Ecology 1994;8:315-23.

Luo Y, Zhou X. Soil Respiration and the Environment. United Kingdom: Elsevier; 2006. p. 3-7.

Matsumoto T, Abe T. The role of termites in an equatorial rain forest ecosystems of West Malaysia. II Leaf litter consumption of the forest floor. Oecologia 1979;38:261-74.

Noirot C, Darlington JPEC. Termite nests: architecture, regulation and defence. In: Abe T, Bignell DE, Higashi M, editors. Termites: Evolution, Sociality, Symbioses, Ecology. Dordrecht: Kluwer Academic Press; 2000. p. 121-39.

Ocko SA, King H, Andreen D, Bardunias P, Turner JS, Soar R, et al. Solar-powered ventilation of African termite mounds. Journal of Experimental Biology 2017;220(18):3260-9.

Ohashi M, Kume T, Yamane S, Suzuki M. Hot spots of soil respiration in an Asian tropical rainforest. Geophysical Research Letters 2007;34:L08705.

Ohashi M, Maekawa Y, Hashimato Y, Takematsu Y, Hasin S, Yamane S. CO_2 emission from subterranean nests of ants and termites in a tropical rainforest in Sarawak, Malaysia. Applied Soil Ecology 2017;117-118:147-55.

Pandey SK, Singh H. Effects of environmental factors on soil respiration in dry tropical deciduous forest. Tropical Ecology 2018;59(3):445-56.

Qi Y, Xu M, Wu J. Temperature sensitivity of soil respiration and its effects on ecosystem carbon budget: Nonlinearity begets surprises. Ecological Modeling 2002;153:131-42.

Reichstein M, Tenhunen JD, Ourcival JM, Rambal S, Dore S, Valentini R. Ecosystem respiration in two Mediterranean evergreen Holm Oak forests: Drought effects and decomposition dynamics. Functional Ecology 2002;16:27-39.

Risch AC, Anderson TM, Schutz M. Soil CO_2 emissions associated with termitaria in tropical savanna: Evidence for hot-spot compensation. Ecosystems 2012;15(7):1147-57.

Roonwal ML. Termites of the oriental region. In: Krishna K, Weesner FM, editors. Biology of Termites. Vol. 2. Academic Press; 1970. p. 315-91.

Roy J, Saugier B. Terrestrial primary production: definitions and milestones. In: Roy J, Mooney HA, Saugier B, editors. Terrestrial Global Productivity. San Diego, USA: CA Academic Press; 2001. p. 1-6.

Solomon S, Qin D, Manning M, Chen Z, Marquis M, Averyt KB, et al. Climate Change 2007: The Physical Science Basis, Contribution of Working Group I to the Fourth Assessment Report of the Intergovernmental Panel on Climate Change. United Kingdom: Cambridge University Press; 2007.

Song QH, Tan ZH, Zhang YP, Cao M, Sha LQ, Tang Y, et al. Spatial heterogeneity of respiration in a seasonal rainforest with complex terrain. iForest 2013;6:65-72.

Sotta ED, Meir P, Malhi Y, Nobre AD, Hodnett M, Grace J. Soil CO_2 efflux in a tropical forest in the central Amazon. Global Change Biology 2004;10:601-17.

Sugimoto A, Bignell DE, MacDonald JA. Global impact of termites on the carbon cycle and atmospheric trace gases. In: Abe TD, Bignell DE, Higashi M, editors. Termites: Evolution, Sociality, Symbioses, Ecology. Dordrecht: Kluwer Academic Press; 2000. p. 409-35.

Trisurat Y. Land use and forested landscape changes at Sakaerat Environmental Research Station in Nakhon Ratchasima Province, Thailand. Ekologia Bratislava 2010;29(1):99-109.

van Asperen H, Alves-Oliveira JR, Warneke T, Forsberg B, de Araújo AC, Notholt, J. The role of termite CH_4 emissions on the ecosystem scale: A case study in the Amazon rainforest. Biogeosciences 2021;18:2609-25.

Wood TE, Detto M, Silver WL. Sensitivity of soil respiration to variability in soil moisture and temperature in a humid tropical forest. PLoS ONE 2013;8(12):e80965.

Xu M, Qi Y. Soil-surface CO_2 efflux and its spatial and temporal variations in a young ponderosa pine plantation in northern California. Global Change Biology 2001;7:667-77.

Yamada A, Inoue T, Sugimoto A, Takematsu Y, Kumai T, Hyodo F, et al. Abundance and biomass of termites (Insecta: Isoptera) in dead wood in a dry evergreen forest of Thailand. Sociobiology 2003;42(3):569-85.

Yamada A, Inoue T, Wiwatwitaya D, Ohkuma M, Kudo T, Abe T, et al. Carbon mineralization by termites in tropical forests, with emphasis on fungus-combs. Ecological Research 2005;20:453-60.

Environment and Natural Resources Journal (EnNRJ)
Volume 19, Number 6, November - December 2021 ISSN: 1686-5456 (Print)
ISSN: 2408-2384 (Online)

LIST OF REVIEWERS IN 2021

Name	Affiliation	Country
Professor Dr. Agnes Romero Pesimo	Partido State University College of Arts and Sciences	Philippines
Professor Dr. Khaing Khaing Soe	University of Forestry and Environmental Science	Myanmar
Professor Dr. Marzuki Hj Ismail	University Malaysia Terengganu	Malaysia
Professor Dr. Ranjana U.K. Piyadasa	University of Colombo	Sri Lanka
Professor Dr. Tjandra Setiadi	Institut Teknologi Bandung Perpustakaan	Indonesia
Associate Professor Dr. Benjaphorn Prapagdee	Mahidol University	Thailand
Associate Professor Dr. Doan Van Hong Thien	Can Tho University	Vietnam
Associate Professor Dr. Eko Hanudin	Universitas Gadjah Mada	Indonesia
Associate Professor Dr. Quang Minh Vo	Can Tho University	Vietnam
Associate Professor Dr. Trairat Kungsanant	Prince of Songkla University	Thailand
Associate Professor Dr. Takehiko Kenzaka	Osaka Ohtani University	Japan
Assistant Professor Dr. Achara Ussawarujikulchai	Mahidol University	Thailand
Assistant Professor Dr. Attaphon Kaewvilai	King Mongkut’s University of Technology North Bangkok	Thailand
Assistant Professor Dr. Aungsiri Tipayarom	Silpakorn University (Sanamchandra Campus)	Thailand
Assistant Professor Dr. Chaiwiwat Vansarochana	Naresuan University	Thailand
Assistant Professor Dr. Nukoon Tawinteung	King Mongkut's Institute of Technology Ladkrabang	Thailand
Assistant Professor Dr. Paul Egwuonwu DIM	Federal University of Technology Minna	Nigeria
Assistant Professor Dr. Rattapon Onchang	Silpakorn University	Thailand
Assistant Professor Dr. Saranya Peerakietkhajorn	Prince of Songkla University	Thailand
Assistant Professor Dr. V. Mohan Raj	Sir Theagaraya College Chennai	India
Dr. Achmad Siddik Thoha	Universitas Sumatera Utara Medan	Indonesia
Dr. Adel Mashaan Rabee	University of Baghdad	Irag
Dr. Adrian N. Goodwin	17 Renwick Street, Alexandria	Australia
Dr. Ali Azizi	National Population Studies and Comprehensive Management Institute-Tehran	Iran
Dr. Allan Sriratana Tabucanon	Mahidol University	Thailand
Dr. Asthervina Widyastami Puspitasari	Brawijaya University	Indonesia
Dr. Athit Phetrak	Mahidol University	Thailand
Dr. Bhanumas Chantarasuwan	Thailand Institute of Scientific and Technological Research	Thailand
Dr. Chandrika Nanayakkara	University of Colombo	Sri Lanka
Dr. Chay Asdak	Universitas Padjadjaran	Indonesia
Dr. Chitsanuphong Pratum	Mahidol University	Thailand
Dr. Doungkamon Phihusut	Chulalongkorn University	Thailand
Dr. Fahruddin Fahruddin	Hasanuddin University	Indonesia
Dr. Gabriel Salako	Kwara State University	Nigeria
Dr. Ghadir A. El-Chaghaby	Agricultural Research Center	Egypt
Dr. Hazlina Ahamad Zakeri	Universiti Malaysia Terengganu	Malaysia

Name	Affiliation	Country
Dr. Jessie Samaniego	Department of Science and Technology-Philippine Nuclear Research Institute	Philippines
Dr. Jiraporn Yongpisanphop	King Mongkut’s University of Technology North Bangkok	Thailand
Dr. Jose Isagani B. Janairo	De La Salle University	Philippines
Dr. Kaveh Ostad-Ali-Askari,	Isfahan University of Technology	Iran
Dr. Kazuyuki Yagi	King Mongkut’s University of Technology Thonburi	Thailand
Dr. Lamthai Asanok	Maejo University	Thailand
Dr. Li Liang	Thammasat University	Thailand
Dr. María Menéndez-Miguélez	University of Oviedo	Spain
Dr. Marjorie D. delos Angeles	University of the Philippines Los Baños	Philippines
Dr. Mats Leifels	Technological University	Singapore
Dr. Merry Krisdawati	Balikpapan University	Indonesia
Dr. Mohammed Syedul Islam	International Islamic University Chittagong	Bangladesh
Dr. Mohd. Hafiz Rosli	University Putra Malaysia	Malaysia
Dr. Motoki Nishimori	Institute for Agro-Environmental Sciences	Japan
Dr. Narayanan Kannan	Universiti Putra Malaysia	Malaysia
Dr. Navaporn Karnjanasiranon	Mahidol University	Thailand
Dr. Nazir Ahmad	The Graduate School of Chinese Academy of Agricultural Sciences	China
Dr. Ngo Thanh Son	Consulting Center of Technological Sciences for Natural Resources and Environment	Vietnam
Dr. Nguyen Thanh Giao	Can Tho University	Vietnam
Dr. Ogunyemi Akinsanmi	Federal University of Agriculture	Nigeria
Dr. Ornprapa Robert	Silpakorn University	Thailand
Dr. Parth S. Mahapatra	Air Quality Analyst	Nepal
Dr. Piangjai Peerakiatkhajohn	Mahidol University	Thailand
Dr. Selvaraj Vasantha Kumar	Vellore Institute of Technology	India
Dr. Shazia Pervaiz	Environmental Protection Agency Punjab	Pakistan
Dr. Silvester B. Pratasik	Sam Ratulangi University	Indonesia
Dr. Smriti Gurung	Kathmandu University	Nepal
Dr. Songkrit Prapagdee	Chulalongkorn University	Thailand
Dr. Suchanya Wongrod	King Mongkut's University of Technology Thonburi	Thailand
Dr. Sucheela Polruang	Kasetsart University	Thailand
Dr. Sumeth Wongkiew	Chulalongkorn University	Thailand
Dr. Supphasin Thaweesak	Burapha University	Thailand
Dr. Sutheera Hermhuk	Maejo University	Thailand
Dr. Tatchai Pussayanavin	Ramkhamhaeng University	Thailand
Dr. Thomas Neal Stewart	Mahidol University	Thailand
Dr. Trairat Muangthong-on	King Mongkut's University of Technology Thonburi	Thailand
Dr. Tumpa Hazra	Jadavpur University	India
Dr. Witchaya Rongsayamanont	Mahidol University	Thailand
Dr. Yutthaphong Kheereemangkla	Kasetsart University	Thailand
Mr. Arthur J. Lagbas	Technological University of Philippines Department College of Science	Philippines
Mr. Sangay Gyeltshen	Independent Researcher	India

INSTRUCTION FOR AUTHORS

Publication and Peer-reviewing processes of Environment and Natural Resources Journal

Environment and Natural Resources Journal is a peer reviewed and open access journal that is published twice a year (January-June and July-December). Manuscripts should be submitted online at https://ph02.tci-thaijo.org/index.php/ennrj/about/submissions by registering and logging into this website. Submitted manuscripts should not have been published previously, nor be under consideration for publication elsewhere (except conference proceedings papers). A guide for authors and relevant information for the submission of manuscripts are provided in this section and also online at: https://ph02.tci-thaijo.org/index.php/ennrj/author. All manuscripts are refereed through a **double-blind peer-review** process.

Submitted manuscripts are reviewed by outside experts or editorial board members of **Environment and Natural Resources Journal**. This journal uses double-blind review, which means that both the reviewer and author identities are concealed from the reviewers, and vice versa, throughout the review process. Steps in the process are as follows:

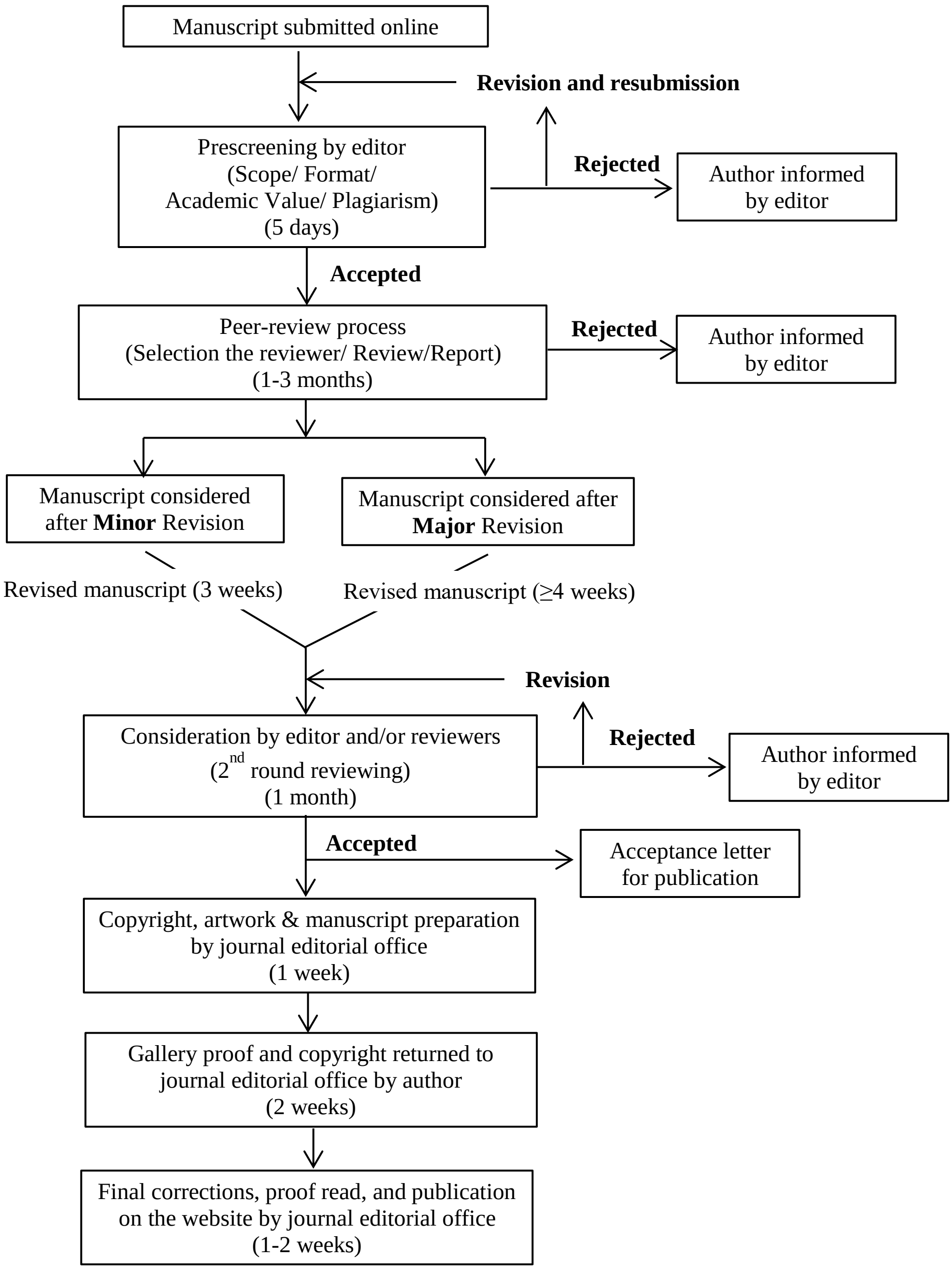

The Environment and Natural Resources Journal (EnNRJ) accepts 2 types of articles for consideration of publication as follows:

- *Original Research Article:* Manuscripts should not exceed 3,500 words (excluding references).
- *Review Article (by invitation):* This type of article focuses on the in-depth critical review of a special aspect in the environment and also provides a synthesis and critical evaluation of the state of the knowledge of the subject. Manuscripts should not exceed 6,000 words (excluding references).

Submission of Manuscript

Cover letter: Key points to include:

- Statement that your paper has not been previously published and is not currently under consideration by another journal
- Brief description of the research you are reporting in your paper, why it is important, and why you think the readers of the journal would be interested in it
- Contact information for you and any co-authors
- Confirmation that you have no competing interests to disclose

Manuscript-full: Manuscript (A4) must be submitted in Microsoft Word Files (.doc or .docx). Please make any identifying information of name(s) of the author(s), affiliation(s) of the author(s). Each affiliation should be indicated with superscripted Arabic numerals immediately after an author's name and before the appropriate address. Specify the Department/School/Faculty, University, Province/State, and Country of each affiliation.

Manuscript-anonymized: Manuscript (A4) must be submitted in Microsoft Word Files (.doc or .docx). Please remove any identifying information, such as authors' names or affiliations, from your manuscript before submission and give all information about authors at title page section.

Reviewers suggestion *(mandatory)*: Please provide the names of 3 potential reviewers with the information about their affiliations and email addresses. *The recommended reviewers should not have any conflict of interest with the authors. Each of the reviewers must come from a different affiliation and must not have the same nationality as the authors.* Please note that the editorial board retains the sole right to decide whether or not the recommended potential reviewers will be selected.

Preparation of Manuscript

Manuscript should be prepared strictly as per guidelines given below. The manuscript (A4 size page) must be submitted in Microsoft Word (.doc or .docx) with Times New Roman 12 point font and a line spacing of 1.5. *The manuscript that is not in the correct format will be returned and the corresponding author may have to resubmit*. The submitted manuscript must have the following parts:

Title should be concise and no longer than necessary. Capitalize first letters of all important words, in Times New Roman 12 point bold.

Author(s) name and affiliation must be given, especially the first and last names of all authors, in Times New Roman 11 point bold.

Affiliation of all author(s) must be given in Times New Roman 11 point italic.

Abstract should indicate the significant findings with data. A good abstract should have only one paragraph and be limited to 250 words. Do not include a table, figure or reference.

Keywords should adequately index the subject matter and up to six keywords are allowed.

Text body normally includes the following sections: 1. Introduction 2. Methodology 3. Results and Discussion 4. Conclusions 5. Acknowledgements 6. References

Reference style must be given in Vancouver style. Please follow the format of the sample references and citations as shown in this Guide below.

Unit: The use of abbreviation must be in accordance with the SI Unit.

Format and Style

Paper Margins must be 2.54 cm on the left and the right. The bottom and the top margin of each page must be 1.9 cm.

Introduction is critically important. It should include precisely the aims of the study. It should be as concise as possible with no sub headings. The significance of problem and the essential background should be given.

Methodology should be sufficiently detailed to enable the experiments to be reproduced. The techniques and methodology adopted should be supported with standard references.

Headings in Methodology section and Results and Discussion section, no more than three levels of headings should be used. Main headings should be typed (in bold letters) and secondary headings (in bold and italic letters). Third level headings should be typed in normal and no bold, for example;

2. Methodology
2.1 Sub-heading
2.1.1 Sub-sub-heading

Results and Discussion can be either combined or separated. This section is simply to present the key points of your findings in figures and tables, and explain additional findings in the text; no interpretation of findings is required. The results section is purely descriptive.
Tables Tables look best if all the cells are not bordered; place horizontal borders only under the legend, the column headings and the bottom.
Figures should be submitted in color; make sure that they are clear and understandable. Please adjust the font size to 9-10, no bold letters needed, and the border width of the graphs must be 0.75 pt. *(Do not directly cut and paste them from MS Excel.)* Regardless of the application used, when your electronic artwork is finalized, please 'save as' or convert the images to TIFF (or JPG) and separately send them to EnNRJ. The images require a resolution of at least 300 dpi (dots per inch). If a label needed in a figure, its font must be “Times New Roman” and its size needs to be adjusted to fit the figure without borderlines.

All Figure(s) and Table(s) should be embedded in the text file.

Conclusions should include the summary of the key findings, and key take-home message. This should not be too long or repetitive, but is worth having so that your argument is not left unfinished. Importantly, don’t start any new thoughts in your conclusion.

Acknowledgements should include the names of those who contributed substantially to the work described in the manuscript but do not fulfill the requirements for authorship. It should also include any sponsor or funding agency that supported the work.

References should be cited in the text by the surname of the author(s), and the year. This journal uses the author-date method of citation: the last name of the author and date of publication are inserted in the text in the appropriate place. If there are more than two authors, “et al.” after the first author’ name must be added. Examples: (Frits, 1976; Pandey and Shukla, 2003; Kungsuwas et al., 1996). If the author’s name is part of the sentence, only the date is placed in parentheses: “Frits (1976) argued that . . .”

Please be ensured that every reference cited in the text is also present in the reference list (and vice versa).

In the list of references at the end of the manuscript, full and complete references must be given in the following style and punctuation, arranged alphabetically by first author’s surname. Examples of references as listed in the References section are given below.

Book
Tyree MT, Zimmermann MH. Xylem Structure and the Ascent of Sap. Heidelberg, Germany: Springer; 2002.

Chapter in a book
Kungsuwan A, Ittipong B, Chandrkrachang S. Preservative effect of chitosan on fish products. In: Steven WF, Rao MS, Chandrkachang S, editors. Chitin and Chitosan: Environmental and Friendly and Versatile Biomaterials. Bangkok: Asian Institute of Technology; 1996. p. 193-9.

Journal article
Muenmee S, Chiemchaisri W, Chiemchaisri C. Microbial consortium involving biological methane oxidation in relation to the biodegradation of waste plastics in a solid waste disposal open dump site. International Biodeterioration and Biodegradation 2015;102:172-81.

Published in conference proceedings
Wiwattanakantang P, To-im J. Tourist satisfaction on sustainable tourism development, amphawa floating marketSamut songkhram, Thailand. Proceedings of the 1st Environment and Natural Resources International Conference; 2014 Nov 6-7; The Sukosol hotel, Bangkok: Thailand; 2014.

Ph.D./Master thesis

Shrestha MK. Relative Ungulate Abundance in a Fragmented Landscape: Implications for Tiger Conservation [dissertation]. Saint Paul, University of Minnesota; 2004.

Website

Orzel C. Wind and temperature: why doesn't windy equal hot? [Internet]. 2010 [cited 2016 Jun 20]. Available from: http://scienceblogs.com/principles/2010/08/17/wind-and-temperature-why-doesn/.

Report organization:

Intergovernmental Panel on Climate Change (IPCC). IPCC Guidelines for National Greenhouse Gas Inventories: Volume 1-5. Hayama, Japan: Institute for Global Environmental Strategies; 2006.

Remark

* *Please be note that manuscripts should usually contain at least 15 references and some of them must be up-to-date research articles.*

* *Please strictly check all references cited in text, they should be added in the list of references. Our Journal does not publish papers with incomplete citations.*

Copyright transfer

The copyright to the published article is transferred to Environment and Natural Resources Journal (EnNRJ) which is organized by Faculty of Environment and Resource Studies, Mahidol University. The accepted article cannot be published until the Journal Editorial Officer has received the appropriate signed copyright transfer.

Online First Articles

The article will be published online after receipt of the corrected proofs. This is the official first publication citable with the Digital Object Identifier (DOI). After release of the printed version, the paper can also be cited by issue and page numbers. DOI may be used to cite and link to electronic documents. The DOI consists of a unique alpha-numeric character string which is assigned to a document by the publisher upon the initial electronic publication. The assigned DOI never changes.

Mahidol University
Wisdom of the Land

Research and Academic Service Section, Faculty of Environment and Resource Studies, Mahidol University
999 Phutthamonthon 4 Rd, Salaya, Nakhon Pathom 73170, Phone +662 441-5000 ext. 2108 Fax. +662 441 9509-10
E-mail: ennrjournal@gmail.com Website: https://www.tci-thaijo.org/index.php/ennrj

Crossref

Google Scholar